KERNFORSCHUNGSZENTRUM

KARLSRUHE

November 1975                                        KFK 2183

Institut für Angewandte Kernphysik


PROGRESS REPORT
of the
Teilinstitut Nukleare Festkörperphysik
(1.6.1974 — 31.5.1975)


L. Pintschovius
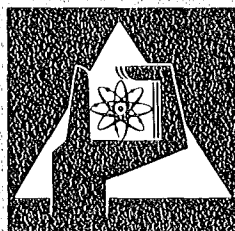

GESELLSCHAFT
FÜR
KERNFORSCHUNG M.B.H.

KARLSRUHE

GESELLSCHAFT FÜR KERNFORSCHUNG M. B. H.

KARLSRUHE

KERNFORSCHUNGSZENTRUM    KARLSRUHE


KFK 2183

Institut für Angewandte Kernphysik


P R O G R E S S    R E P O R T


of the

Teilinstitut Nukleare Festkörperphysik


(1.6.1974 - 31.5.1975)


Editor: L. Pintschovius

This progress report of the Teilinstitut Nukleare Festkörperphysik covers the period from 1st June 1974 - 31st May 1975. The arrangement has been chosen to emphasis the main areas of research in which the institute is presently involved.
These areas are Dynamics of Solids and Liquids, Electronic Structure and Magnetism of Solids and Development of Materials. Some of the technical developments relevant to these topics are also included.

Dieser Progress-Report des Teilinstituts Nukleare Festkörperphysik erfaßt den Zeitraum vom 1. Juni 1974 - 31. Mai 1975. Die Darstellung betont die Hauptforschungsgebiete, auf denen das Institut zur Zeit tätig ist. Diese sind: Dynamik von Festkörpern und Flüssigkeiten, Elektronenstruktur und Magnetismus von Festkörpern und die Entwicklung neuer Materialien. Einige technische Entwicklungen, die für die Forschungsarbeiten wichtig sind, wurden ebenfalls in den Bericht aufgenommen.

In dem vorliegenden Bericht gibt das Teilinstitut IAK I "Nukleare Fest-
körperphysik" einen Überblick über die wissenschaftlichen Arbeiten in
dem Zeitraum vom 1. Juni 1974 bis 31. Mai 1975. Das Forschungsprogramm
des Instituts hat derzeit folgende drei Hauptrichtungen:

- Untersuchungen zur Struktur und Dynamik von kondensierter
  Materie

- Untersuchungen der elektronischen und magnetischen Eigen-
  schaften von Festkörpern

- Herstellung neuer Materialien mittels Ionenimplantation,
  Kathodenzerstäubung und simultanem Aufdampfen.

Mit den Methoden der Neutronenspektroskopie werden am Forschungsreaktor
FR2 in Karlsruhe und am Hochflußreaktor in Grenoble Experimente zur Be-
stimmung der Phononendispersion und Phononenzustandsdichten von Festkörpern
sowie der Streugesetze von Flüssigkeiten durchgeführt. Zur Zeit stehen Un-
tersuchungen an supraleitenden Materialien im Vordergrund. Hierdurch soll
ein Beitrag zum besseren Verständnis der Wechselwirkung zwischen gitter-
dynamischen und supraleitenden Eigenschaften von Festkörpern geleistet
werden. Von besonderem Interesse ist ferner das Studium der Dynamik von
eindimensionalen metallischen Systemen.

Bei den Untersuchungen von elektronischen und magnetischen Eigenschaften
von Festkörpern werden die Methoden der $^{61}$Ni-Mößbauerspektroskopie und
der Neutronenstreuung eingesetzt, um Information über Hyperfeinfelder,
Spindichteverteilungen und magnetische Anregungen zu erhalten. Es wird
hier die Möglichkeit genutzt, die sehr kurzlebigen $^{61}$Ni-Quellen am
Zyklotron des Kernforschungszentrums herzustellen. Daher werden zur Zeit
vorwiegend Verbindungen und Legierungen des Nickels untersucht.

Die Methoden der Ionenimplantation, Kathodenzerstäubung und des simul-
tanen Aufdampfens werden derzeit ausschließlich zur Herstellung von
Supraleitern und zur gezielten Veränderung ihrer supraleitenden Eigen-

schaften eingesetzt. Im Rahmen dieses Programms werden auch Fragen der Strahlenschädigung untersucht. Als wichtiges Hilfsmittel für die Charakterisierung der hergestellten Materialien dient die He-Rückstreutechnik. Diese Arbeiten werden am Van-de-Graaff Beschleuniger des Institutes durchgeführt.

Die experimentellen Arbeiten werden durch eine kleine Theoriegruppe unterstützt, die sich zur Zeit vorwiegend mit Fragen der Elektron-Phonon Wechselwirkung sowie der Dynamik von Festkörpern und Flüssigkeiten beschäftigt.

Im Berichtszeitraum hat sich die Zusammenarbeit mit externen Forschungsgruppen wesentlich verstärkt. Dies betrifft insbesondere das Gebiet der Neutronenspektroskopie. Es zeigt sich, daß durch die Einrichtung des Hochflußreaktors in Grenoble die Neutronenstreuung als Meßmethode in der Festkörperforschung immer mehr an Bedeutung gewinnt. Dies bedingt eine verstärkte Nutzung des FR2 zur Vorbereitung von Experimenten für den HFR-Grenoble sowie zu einer Entlastung, wenn die Experimente auch an einem Reaktor mittleren Flusses durchgeführt werden können.

Das Teilinstitut IAK I hatte im Berichtsjahr 26 wissenschaftliche und technische Mitarbeiter. Ein Mitarbeiter ist für die Betreuung von Gastgruppen bei der Nutzung der beiden zum FR2 gehörenden Strukturspektrometer zuständig. Der größte Teil dieser Arbeiten erfolgt außerhalb des Forschungsprogramms des IAK I und wird daher in dem vorliegenden Bericht nicht berücksichtigt. Dagegen wird über Arbeiten von Mitarbeitern der technisch wissenschaftlichen Infrastruktur des Gesamtinstitutes berichtet, sofern sie das Forschungsprogramm des Teilinstituts IAK I betreffen.

Von den Arbeiten, die bereits veröffentlicht bzw. zur Veröffentlichung eingereicht sind, werden nur Kurzfassungen oder Literaturhinweise angegeben. Erste Ergebnisse von laufenden Arbeiten werden dagegen etwas ausführlicher beschrieben.

# C O N T E N S

# 1. INVESTIGATIONS ON THE DYNAMICS OF SOLIDS AND LIQUIDS

## 1.1. INVESTIGATIONS ON THE PHONON DISPERSIONS

### 1.1.1. Phonon Dispersion of MnO

V. Wagner, Physikalisches Institut der Universität Würzburg
und ILL Grenoble

W. Kress, MPI für Festkörperforschung, Stuttgart

W. Reichardt

Measurements of Haywood and Collins /1/ seemed to indicate that the phonon dispersion of MnO is quite different from those of the closely related compounds CoO and NiO and that the shell model is not applicable to this material. As this would have serious consequences concerning the lattice dynamical models for the transition metal oxides we have started measurements of the phonon dispersion of MnO on the triple axis spectrometer TAS 1 at the FR2. The sample is a single crystal of about 6 $cm^3$ grown by Crystal Tec with the flame fusion technique.

The results obtained so far at 296K are shown in fig. 1. The arrows mark the IR data of Plendl et al /2/. The curves are the result of a fit with a 7 parameter shell model, where only the negative ion was allowed to be polarisable. The overall fit is quite good. Discrepancies occur mainly for the LA branch in the [111] direction indicating that the polarisibility of the Mn-ion cannot be neglected. However as the investigations have not been completed it does not seem reasonable to use more elaborate models. Nevertheless we can already conclude that the measured phonons of MnO can be well described within the framework of a simple shell model.
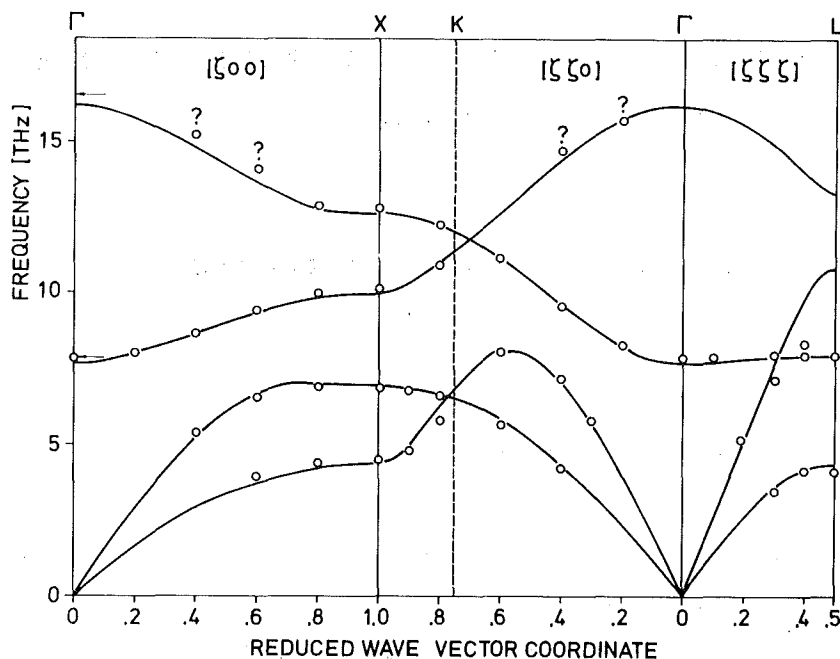
Fig. 1   Phonon dispersion of MnO at room temperature

References

/1/   B.C. Haywood and M.F. Collins, J. Phys. C 4, 1299 (1971)

/2/   J.N. Plendl, L.C. Mansur, S.S. Mitra and I.F. Chang, Solid State
      Commun. 7, 109 (1969)

1.1.2,   Lattice Dynamics of Strontium Oxide [+]

K.H. Rieder and R. Migoni, Max-Planck-Institut für Festkörperforschung,
Stuttgart, Federal Republic of Germany

B. Renker

Abstract

The phonon dispersion relations of SrO at $300^\circ K$ for the $|\zeta 00|$, $|\zeta\zeta 0|$ and
$|\zeta\zeta\zeta|$ directions of propagation have been measured using inelastic neutron
scattering. A shell model with seven parameters gives a good overall
description of the phonon dispersion relations. The phonon frequency

distribution calculated with this model yields a temperature dependence of the characteristic Debye temperature which is in satisfactory agreement with results derived from specific heat measurements. The second order Raman spectrum of SrO is discussed on the basis of the neutron data and a calculated two-phonon-density-of-states.

## 1.1.3. Lattice Dynamics of NiO

*W. Reichardt*

*V. Wagner, Phys. Institut der Universität Würzburg und ILL Grenoble*

*W. Kress, MPI für Festkörperforschung, Stuttgart*

The investigations of the phonon dispersion of NiO /1/ at room temperature have been continued by measurements of the optic branches in the symmetry directions $\Delta$, $\Sigma$ and $\Lambda$ on the triple axis spectrometer IN1 at the HFR Grenoble.

The experimental data are well reproduced within the framework of a shell model. It was found that both ions are highly polarizable. In the model the overlap polarization was taken into account by a positive shell charge $y_1$ of the $Ni^{2+}$ ion. Table 1 list the parameters of a model with 7 open parameters where $Y_1$ was set equal to $- Y_2$ and the ionic charge Z was assumed to be 2e. Releasing these restrictions did not improve the fit significantly.

| $A_{12}$ | $B_{12}$ | $A_{22}$ | $B_{22}$ | $Y_1$ | $Y_2$ | $k_1$ | $k_2$ | Z |
|---|---|---|---|---|---|---|---|---|
| $35.93\frac{e^2}{v}$ | $-5.34\frac{e^2}{v}$ | $-3.08\frac{e^2}{v}$ | $0.35\frac{e^2}{v}$ | $+3.13e$ | $-3.13e$ | $99.16\frac{e^2}{v}$ | $82.70\frac{e^2}{v}$ | $2e$ |

Table 1: Shell model parameters of NiO

## References

/1/ W. Reichardt, Progress Report, KFK 2054, 3 (1974)

### 1.1.4. Lattice Dynamics of Non-stoichiometric Niobium Carbide

*L. Pintschovius and W. Reichardt*

The dispersion relations of the acoustic phonons of $NbC_{.89}$ have been investigated on the TAS 1- and TOF3 - spectrometers at the FR2 at Karlsruhe. The sample is a single crystal of $0.6 \ cm^3$ grown by B. Scheerer using the floating zone method. The stoichiometry was checked by chemical analysis, measurement of the lattice parameters and of the superconducting transition temperature $(T_c \sim 4 \ K)$.

Stoichiometric NbC $(T_c=12 \ K)$ as well as other superconducting transition metal carbides show strong anomalies in their dispersion relations /1/. For $NbC_{.89}$ we have found less pronounced anomalies at the same points in q-space as in the case of $NbC_{.98}$. Fig. 1 shows a comparison of the dispersion relations in $|\zeta\zeta\zeta|$-direction for $NbC_{.98}$, $NbC_{.89}$ and $NbC_{.76}$ $(T_c=0)$.
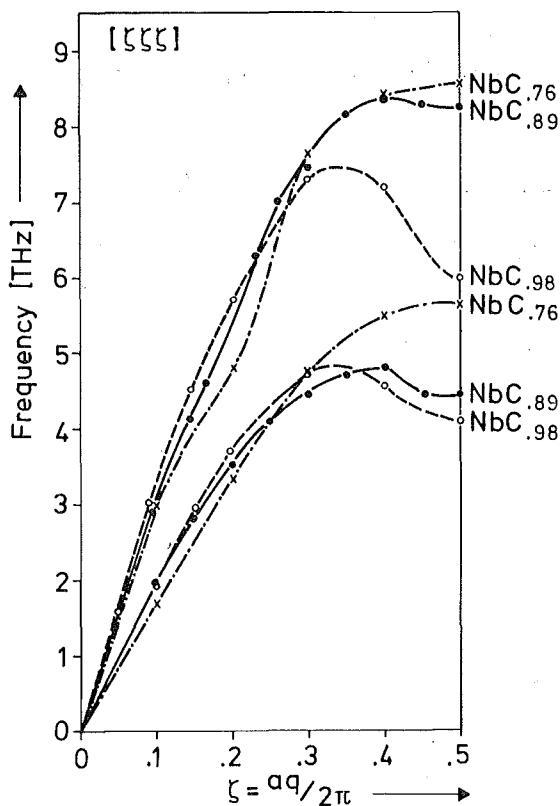


Fig. 1 Phonon dispersion of $NbC_x$ in $|\zeta\zeta\zeta|$ direction

In the region of the anomalies most phonon lines were considerably broadened. Furthermore the intensity distributions were not only dependent on the reduced wave number but also on the momentum transfer.

The double-shell model of Weber /2/ was used to analyze the data. Fig. 2 shows the experimental values and the results of a least squares fit. The dashed lines indicate the widths of the neutron groups in the regions of the anomalies.

It is intended to complete these investigations at the HFR at Grenoble.
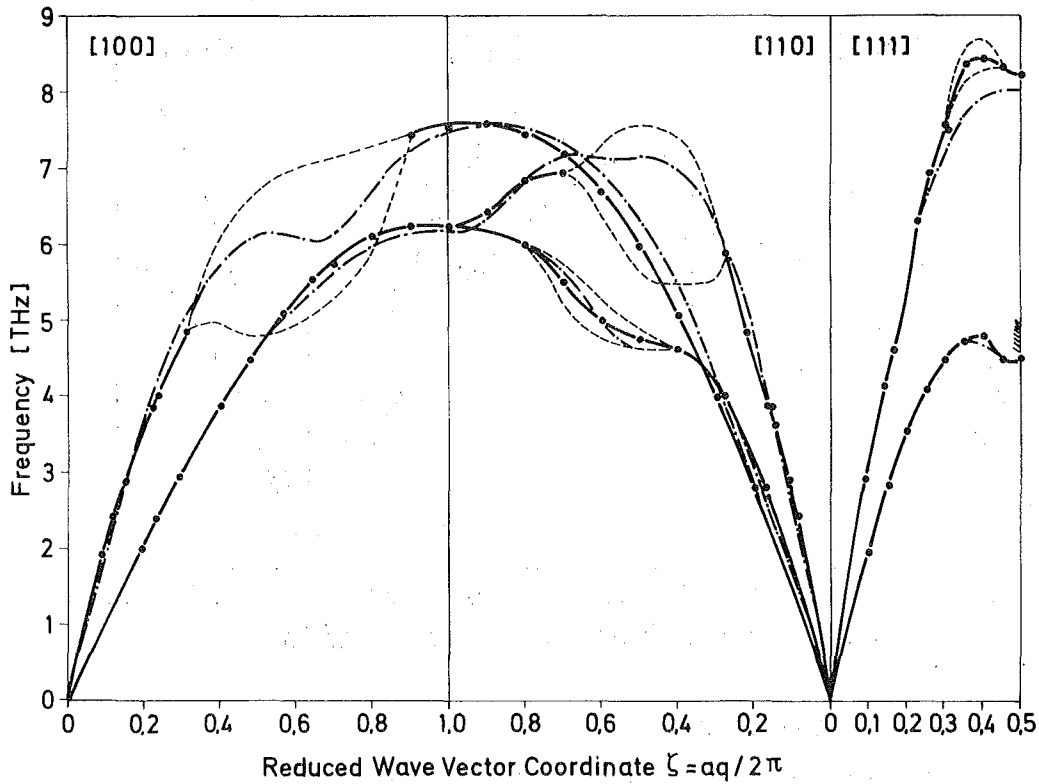


Fig. 2  Phonon dispersion of NbC$_{.89}$ at room temperature

———•——— guide to the eye

—·——·——·— fit with double shell model

References

/1/  H.G. Smith and W. Gläser, Phys. Rev. Lett. 25 (1970), 1611
/2/  W. Weber, Phys. Rev. B 8 (1973), 5082

1.1.5, Phonon Dispersion of TiC

*L. Pintschovius and W. Reichardt*

TiC is a non-superconducting representative of the transition metal carbides. The dispersion relations of its acoustic phonons have been measured on the triple-axis spectrometer TAS 1 at the FR2. Two samples of approximately $0.6 \ cm^3$ are available grown by B. Scheerer using the floating zone technique. By chemical analysis the compositions of the two samples have been determined to be $TiC_{.95}$ and $TiC_{.89}$.



Fig. 1 Phonon dispersion of TiC

Full circles: $TiC_{.95}$ , Open circles: $TiC_{.89}$

——•——•—— guide to the eye

—— —— —— —— fit with shell model

————•———— slopes determined from the ultrasonic data

Fig. 1 shows the results of our measurements on $TiC_{.95}$ and of former measurements on $TiC_{.89}$ by Drexel, Currat and Reichardt /1/ at the HFR Grenoble. The good agreement indicates that the phonon frequencies depend much less on the stoichiometry as in the case of $NbC_x$. Additional measurements

on TiC$_{.89}$ at Karlsruhe proved that there are only slight differences between the slopes at the $\Gamma$-point for the two samples (o...3%).

The elastic constants derived from our measurements agree satisfactorily with those determined by ultrasonic methods on TiC$_{.91}$ /2/.

A fit with an eight parameter shell model is included in fig. 1.

The measurements will be continued at the HFR Grenoble.

References

/1/ W. Drexel, R. Currat and W. Reichardt, Progress Report of the ILL Grenoble, 53 (1973)

/2/ R. Chang, L.J. Graham, J. Appl. Phys. 37, 3778 (1966)

1.1.6. Neutron Scattering Study of Lattice Vibrations in Ice Ih

B. Renker

G.I. Parisot, ILL Grenoble

In ice Ih the molecules are orientationaly disordered. Simplified dynamical models which succeeded to explain the translational spectrum up to 220 cm$^{-1}$ fail to describe the experimental results in the higher part up to 300 cm$^{-1}$.

Within the hexagonal plane we have studied polarisation vectors and structure factors for phonons in this frequency region and the lowest librational modes. Although the phonon peaks appear broadened we measure two branches at 220 and 284 cm$^{-1}$ and the influence of a structure factor.

Thus it becomes clear that: a) there is no crossing between translational and librational modes, b) the phonon branches are flat and the frequencies up to $\sim$290 cm$^{-1}$ cannot be explained by wiggles of the lower branch as suggested by some models, c) inspite of the disorder of the $H_2O$ molecules there exist collective excitations up to $\sim$290 cm$^{-1}$ and the higher translational excitations cannot be explained by a spread in frequencies due to an irregularity in the force constants caused by disorder of the static and transition dipole moments.

1.1.7.  Lattice Dynamics of HCP-Thallium

W. Reichardt

V. Wagner, Physikalisches Institut der Universität Würzburg
und ILL Grenoble

Investigations on the phonon dispersion of hexagonal Thallium in the $\Sigma$- and
$\Delta$ direction have been performed by Worlton and Schmunck /1/. However, the
phonon density of states F (h$\omega$) calculated by these authors from a Born von
Kàrmàn model fitted to the experimental data is in serious disagreement with
the Eliashberg function $\alpha^2$F(h$\omega$) determined by Dynes /2/ from tunneling experiments.
In order to provide a reliable phonon density of states for a comparison with
the tunneling data we have extended the measurements of Worlton and Schmunck
and remeasured some of their results. These measurements were performed on
the spectrometers TOF3 at the FR2 and IN3 at the HFR-Grenoble. In general the
phonon frequencies determined from our measurements are somewhat lower than
those of ref /1/.
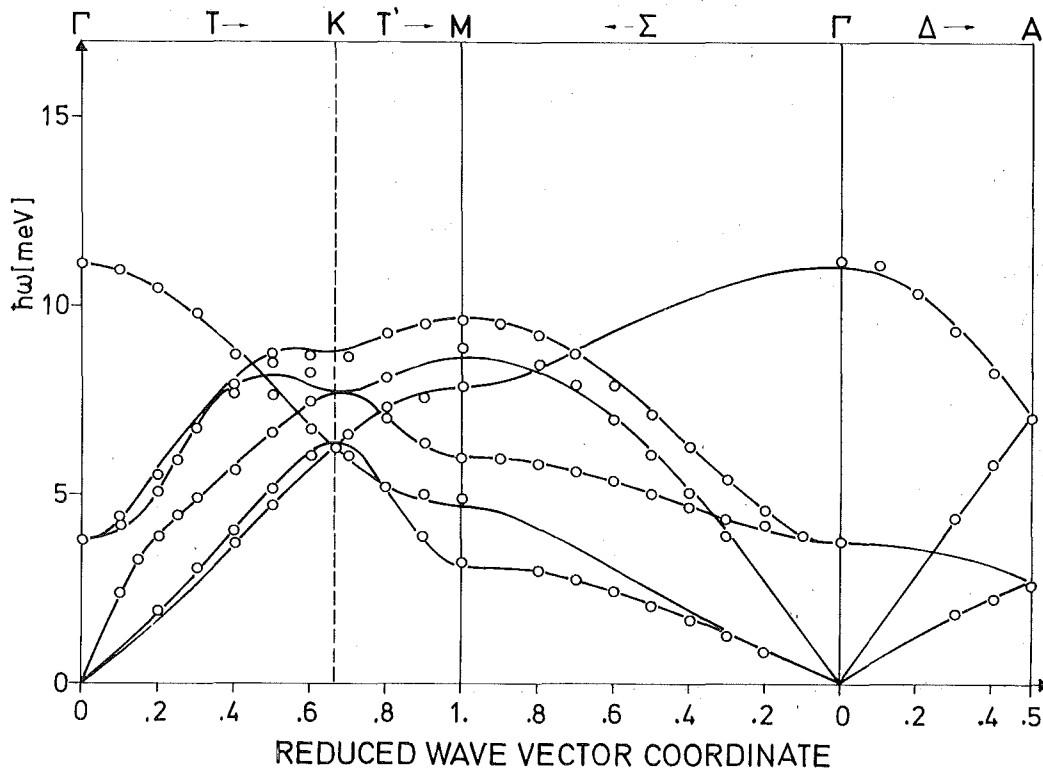


Fig. 1  Phonon dispersion of HCP-Thallium

Fig. 1 shows results for 140 K in the $\Sigma$-, T- and $\Delta$-directions. The curves are the result of a fit with a 4 nearest neighbours Born von Kàrmàn model where for the two nearest neighbours tensor forces and for the third and fourth neighbour axially symmetric forces were assumed. Some additional data in the P- and S direction, which are not shown in the figure, were included in the fit in order to be able to determine all four force constants of the first neighbour. A rather good fit can already be obtained with a four neighbour axially symmetric model. In Fig. 2 the phonon density of states calculated with this model is compared to the Eliashberg function $\alpha^2 F(\hbar\omega)$ of Dynes. There is very satisfactory agreement of the characteristic features of the two distributions.
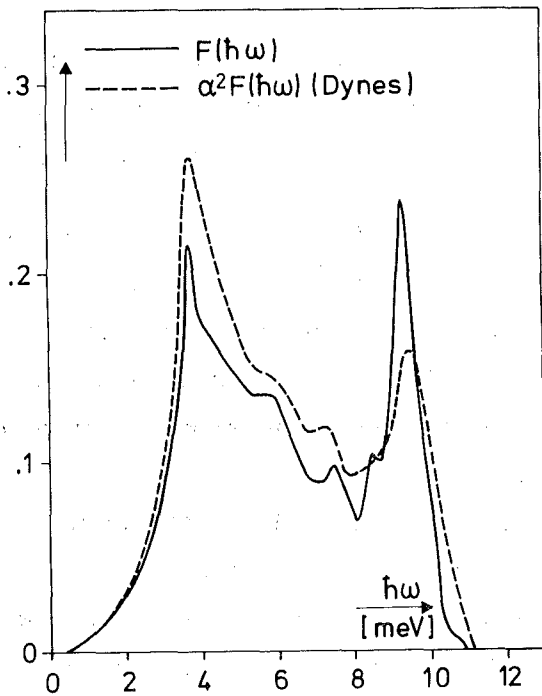


Fig. 2 Comparison of the calculated phonon density of states with the Eliashberg function $\alpha^2 F(\hbar\omega)$ of Dynes.

References:

/1/ T.G. Worlton and R.E. Schmunck, Phys. Rev. B3, 4115 (1971)
/2/ R.C. Dynes, Phys. Rev. B2, 644 (1970)

## 1.1.8. Stress-induced Changes in the Phonon Spectrum of Silicon

*J. Prechtel, J. Kalus, Technische Universität München*

*L. Pintschovius*

Measuring the stress-induced shifts and splittings of phonon energies, it is possible to determine the cubic (anharmonic) atomic force constants /1/. Experiments on Si are of interest for a) there are indications (for example the negative Grüneisen parameter) that anharmonicity might be important for Ge and Si /2/, b) there are several competing models for the lattice dynamics of diamond-type semiconductors.

First and second order Raman scattering gives us experimental data only for the Γ-point /3/ and for points at the edge of the B.Z. (because of experimental difficulties, until now only some data for the x-point are available. /4/ /5/).

To get informations about other symmetry points and about points within the B.Z., we are performing neutron inelastic scattering experiments. A 30-to hydraulic press has been built, which can be located on a spectrometer with its stress axis lying vertically or horizontally. First measurements have been done on the triple-axis spectrometer TAS1 at the FR2. The samples are weakly doped ($\sigma > 100 \Omega$cm) single crystals of silicon with the 111-direction parallel to the cylinder axis, diameters between 15 and 20 mm and length about 80 mm. Applying a stress of 10 K bar in the 111-direction, the energy of the 111-TA-phonon is lowered by $0.5 \pm 0.1\%$ accompanied by a broadening of the peak, which is a result of mode splitting and eventually of strain inhomogenities. In order to avoid the latter, larger crystals with a length more than ten times the diameter will be used.

To extract the anharmonic parameters like the mode-Grüneisen parameter for this and for other phonons, we prepare further experiments.

### References

/1/ A.J. Maradudin, Phys. Status Solidi **39**, 131 (1962)

/2/ H. Jex, Phys. Status Solidi **45**, 343 (1971)

/3/ E. Annastassakis et al., Solid State commun. **8**, 133 (1970)

/4/ W. Richter et al., Solid State Commun. **16**, 131-4 (1975)

/5/ J.F. Angress et al., J. Phys. C: Solid State Phys. **8**, 1136 (1975)

1.1.9. Lattice Dynamics of Sapphire (Corundum)[+]

Part I: Phonon Dispersion by Inelastic Neutron Scattering

*H. Bialas, H.J. Stolz*[++]

Part II: Calculations of the Phonon Dispersion

*W. Kappus*[+++]*, Institut für Angewandte Physik der Universität Heidelberg*

Abstract

By inelastic neutron scattering the phonon dispersion of sapphire ($\alpha$-$Al_2O_3$) has been measured along the two principal symmetry directions. Along the direction of threefold symmetry 20 different phonon modes are to be expected. From these 4 quasilongitudinal modes $\Lambda_1$ and $\Lambda_2$ respectively and 5 quasi-transverse $\Lambda_3$ modes could be identified making use of the selection rules for the structure factor. The highest measured phonon frequencies range up to 26 THz.

Theoretical models of the lattice dynamics of sapphire based on the assumption of rigid ions, have been fitted to measured phonons at the $\Gamma$-point of the Brillouin zone. Short range interactions were taken into account by assuming 2-body interactions between touching ions. Additional 3-body interactions could not improve the fit significantly. Calculated dispersion curves are presented and compared with inelastic neutron scattering data. A good agreement for branches along the trigonal axis can be stated.

## 1.1.10. Investigations of the Linear Conductor KCP

*R. Comés[a], R. Currat[b], H.J. Deiseroth[c], W. Gläser[d],*

*G. Heger, L. Pintschovius, B. Renker, G. Scheiber[e],*

*H. Schulz[c]*

a) Laboratoire de Physique des Solides associé au CNRS
   Université Paris-Sud, 91 405 Orsay (France)

b) Institut Max von Laue - Paul Langevin, Cedex No. 156,
   38 042 Grenoble (France)

c) Max-Planck-Institut für Festkörperforschung,
   D 7 Stuttgart (Germany)

d) present adress: Institut für Nukleare Festkörperphysik,
   Technische Universität München

e) Institut für Angewandte Physik der Universität
   D 75 Karlsruhe (Germany)

Previous work revealed the existence of a pronounced Kohn anomaly and a central peak in $K_2Pt(CN)_4Br_{.3} \cdot 3D_2O$ (KCP) for wave vectors with a component $2 k_F$ parallel to the chain direction. A transition to a three-dimensional state with a $2 k_F$ distortion along the c-direction takes place near 100 K. Recent measurements were concerned with a temperature dependent study of the soft phonons in the region of $2 k_F$. These results are collected in a paper the abstract of which is given below.

## Abstract

Besides the modifications of the longitudinal acoustic dispersion in the c direction, inelastic neutron scattering measurements of the 2 $k_F$ instability in KCP between room temperature and 60 K have revealed an additional excitation at a frequency of 0.6 THz for the wave vector 2 $k_F$. This excitation obviously corresponds to the additional structure earlier observed at low temperature by infrared and Raman scattering, but the extension in wave vector $2 k_F - 0.2 c^+ < q_c < 2k_F + 0.1 c^+$, the very small dispersion, and the fact

that, though much weaker than at low temperature, it is still observable
at room temperature, casts serious doubts on its interpretation in terms
of the pinned charge density wave (pinned Fröhlich mode). The existence
of a low freqency longitudinal optical phonon branch is more likely, despite
unexplained weak intensity of the corresponding phonons.

Further a detailed neutron diffraction study of the KCP crystal structure
was undertaken. The room temperature results are published with the
following abstract:

*On the Water Distribution in $K_2Pt(CN)_4Br_{0.3} \cdot 3D_2O$. A Single Crystal Neutron*
*Diffraction Structure Analysis*
*G. Heger, B. Renker, H.J. Deiseroth and H. Schulz, Mat. Res. Bull.* <u>*10*</u>, *217 (1975)*

## Abstract

A single crystal neutron diffraction analysis of the linear conductor
$K_2 Pt(CN)_4Br_{0.3} \cdot 3D_2O$ is reported. Complementary to former X-ray
investigations the distribution of the water molecules was studied and
three different types of $D_2O$ could be located. Besides the full and
reduced occupied two- and four-fold $D_2O$-positions, a third site nearby
the $Br^-$-position was clearly identified giving the picture of a filled
center of the unit cell occupied partially by $Br^-$ and $D_2O$. There is no
argument left for a crystallographically different second $Br^-$-site.

Low temperature measurements down to 31 K confirm the 295 K results and show
more precisely that water molecules in two different disordered orientations
fill the center of the unit cell.

In connection with the phase transition at 100 K a temperature dependent
study of the lattice parameters is of interest. Measuring results which
are shown in Fig. 1 show a smooth curve in the interesting region.
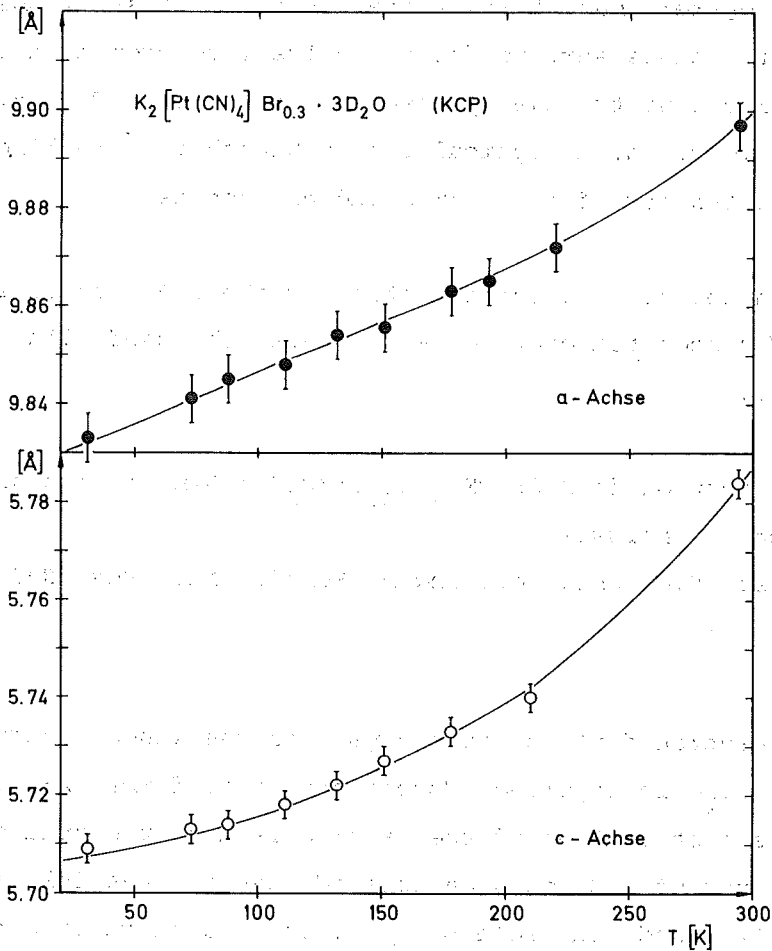
Fig. 1 Temperature dependence of the lattice parameters of KCP measured by neutron diffraction.

## 1.1.11. Phonon Dispersion of α-Arsenic

W. Reichardt

K.H. Rieder, MPI für Festkörperforschung, Stuttgart

Whereas extensive studies on the phonon dispersion of the group Vb elements Bi and Sb have been reported by several authors the information about the lattice dynamics of the isomorphic α-As to date was restricted to results of Raman scattering experiments /1/ and of the phonon density of states determined by neutron scattering from a polycrystalline sample /2/. As an extension of these investigations we have started measurements on the phonon dispersion at the FR2. The single crystal sample of about 3 cm$^3$ used in these experiments was grown by Miss G. Müller in the crystal

laboratory of Dr. E. Schönherr at the MPI-FKF.

So far we have performed measurements at 296 K in three directions lying
in the mirror plane ($\Gamma T, \Gamma L, \Gamma X$) and in the binary direction (Fig. 1).
The values for the optical branches at the $\Gamma$ point are in rather good
agreement with the Raman data of ref. /1/. Compared to the phonon dispersion
relations of Bi and Sb the following main differences can be observed:
The dips in the lower optical branches at small q-values are less pronounced.
Some of these branches drop below the $\Gamma$ point frequency when reaching the
zone boundary. Due to a much weaker bonding between the double layers
perpendicular to the trigonal axis the acoustic frequencies in the $\Gamma T$
direction are very low; for small q-values the LA branch crosses the TA
branch i.e. the longitudinal sound velocity is smaller than the transverse
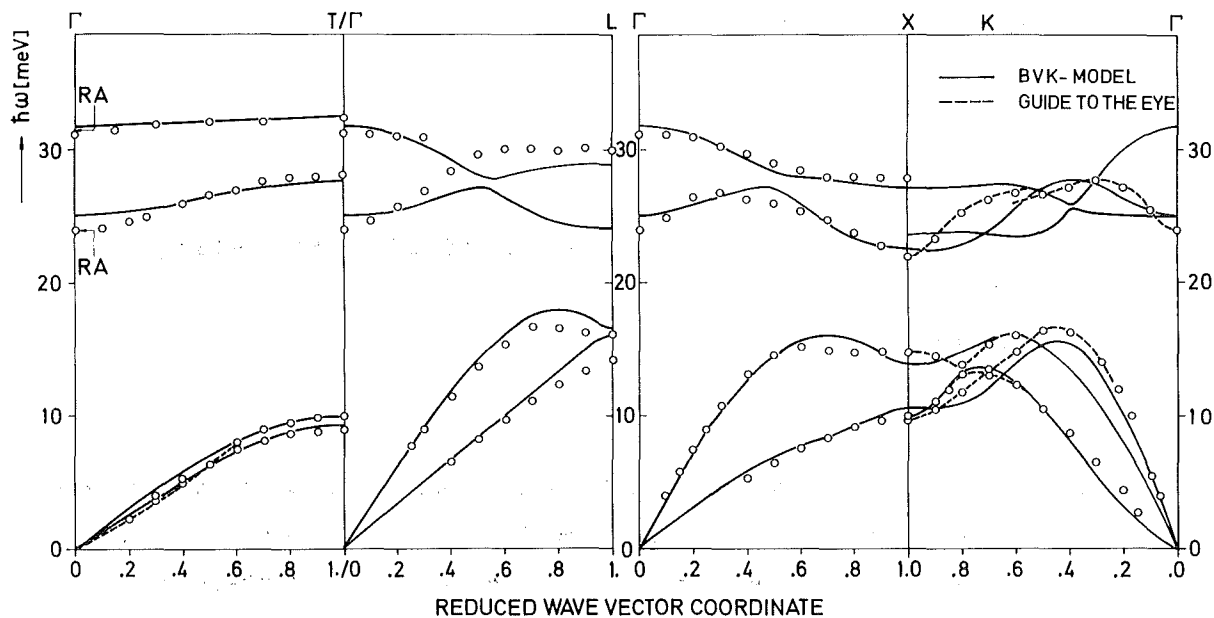


Fig. 1 Phonon dispersion of $\alpha$-arsenic

The bonding in the group Vb elements is partly covalent and partly metallic.
Thus the forces are long range and many neighbour shells in a Born v. Kàrmàn
model have to be taken into account. In order to keep the number of fit
parameters as low as possible we have used a mixed axially symmetric -
tensor force model with only two force constants for the farther distant
neighbours. We found that for a given number of parameters such a model
always gave a better fit than either a pure tensor force or a pure axially

symmetric model. The curves in fig. 1 were calculated using a model with
8 neighbours and 19 parameters. The transverse branches in the $\Gamma X$ and $\Gamma L$
directions polarised in the c direction have been omitted for clarity.
The model gives a reasonable overall description of the experimental
data but is not able to reproduce details of the dispersion curves as
for instance the dips in the lower optical branches at the $\Gamma$-point.

It is intended to continue these investigations with a main effort on
the development of improved lattice dynamical models for the A7-structure.

References

/1/   J.S. Lannin, J.M. Calleja and M. Cardona, Second Order Raman
      Scattering in the Groups Vb Semimetals: Bi, Sb and Sb; submitted for
      publication to Phys. Rev.
/2/   J. Salgado, KFK Report 1954 (1974)

1.1.12.   Phonon Dispersion Measurements of $Bi_{1-x}Sb_x$ Alloys

B. Hofmann

The lattice dynamics of the semimetals Bi and Sb are determined by covalent
bonding between nearest neighbour atoms and low concentrations of free
carriers which screen the bonding charges only over large distances.
By alloying a few percent of Sb into Bi the electronic band structure
is changed and becomes semiconducting ($x \geq 0.07$). Moreover, the periodicity
of the lattice is disturbed by mass defects.

Phonon dispersion measurements of $Bi_{1-x}Sb_x$ alloys are therefore of special
interest in order to reveal the influence of both effects on the lattice
dynamics. They complete the information already obtained by first order
Raman scattering /1/, /2/.

The $Bi_{1-x}Sb_x$ single crystals were grown by Bridgman's method (Tab. 1). They
were analysed with respect to their composition and crystalline perfection

by neutron diffraction techniques. The diffractometer at the R1 beam
tube was used with $\lambda$ = 1.5086 $\pm$ 0.0002 $\overset{o}{A}$ and a resolution of 0.15 %.
The lattice constants of the single crystals were determined by the method
described by Brockhouse et al. /3/. The Ge(551) reflection and the Bi (00 15)
reflection were used as standards.

Applying the linear relationship between the alloy parameter x and the
lattice constants $(a_H, c_H)$ /4/, the mean Sb concentration of the sample
could be determined with an accuracy of less than 5 %.

| Nr. | Mean Composition | Growing Method | Density $[\frac{g}{m^3}]$ | Volume[cm³] | Mosaic-Spread |
|-----|------------------|----------------|------------------|-------------|---------------|
| I | Bi | vert. zone | 9.805 | 4.5 | 0.1° |
| II | $Bi_{0.93}Sb_{0.07}$ | Bridgman | 9.57±0.05 | 4.08 | 0.5° |
| III | $Bi_{0.82}Sb_{0.18}$ | Bridgman | 9.37±0.05 | 7.56 | 0.6° |
| IV | $Bi_{0.88}Sb_{0.12}$ | horiz. zone | – | 25 (powder) | – |

Tab. 1   Data of the Bi and BiSb samples

The 2$\Theta$-scans of the alloy crystals are rather broad and show a peak structure
for sample II (fig. 1). A similar case has been reported by Zitter and Watson
/1/. According to Cucka and Barrett /4/ this indicates a large variation
in composition (extra scale in fig. 1). It is also possible that the broadening
is a grain effect due to micro-segregation.
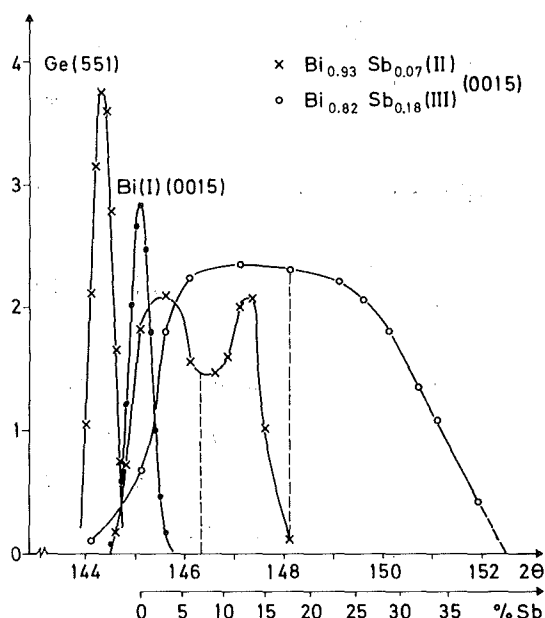


Fig. 1

2$\Theta$-scans of Ge(551), Bi(I) and
BiSb samples II and III(00 15).

Phonon measurements were performed on the triple axis spectrometer TAS 1
at the Karlsruhe FR2 reactor using the constant q-mode. The fixed primary
neutron energies were about 20 meV and 40 meV and the corresponding reso-
lutions were 6 % and 7 %, respectively.

In order to estimate the line broadening of the detected neutron groups,
line shapes have been calculated using a resolution program based on the
Cooper-Nathans formalism.

Fig. 2 shows the phonon dispersion of $Bi_{0.82}Sb_{0.18}$ (sample III) in the
symmetry direction $\Gamma T$ (trigonal axis). For comparison the dispersion of
pure Bi (I) was measured and is shown, too. Results of measurements of
$Bi_{0.93}Sb_{0.07}$ (II) have already been reported /5/.
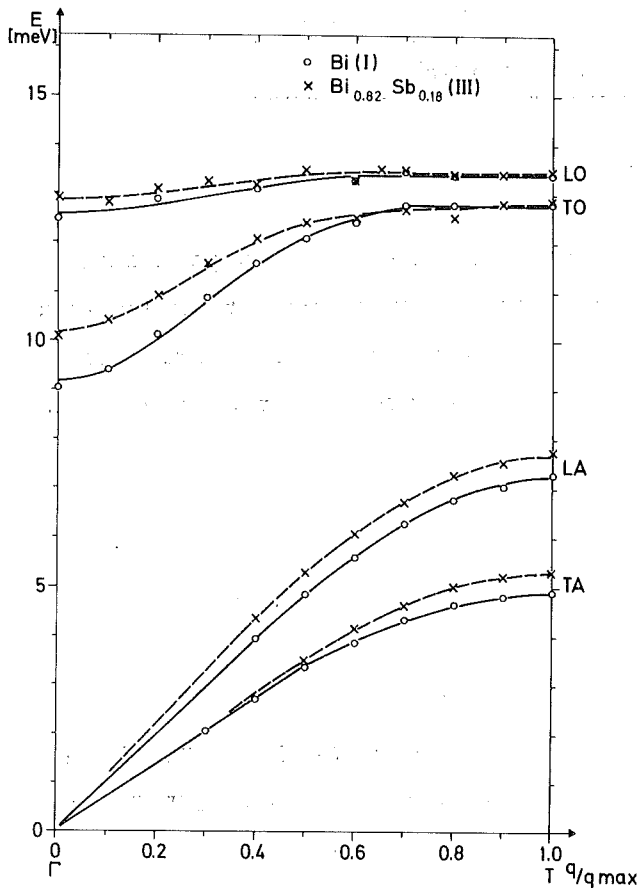


Fig. 2   Phonon dispersion in the
         trigonal direction ($\Gamma T$) for
         Bi(I) and $Bi_{0.82}Sb_{0.18}$ (III).
         ———,----- Theoretical curves
         calculated by linear B.v.K.
         models.
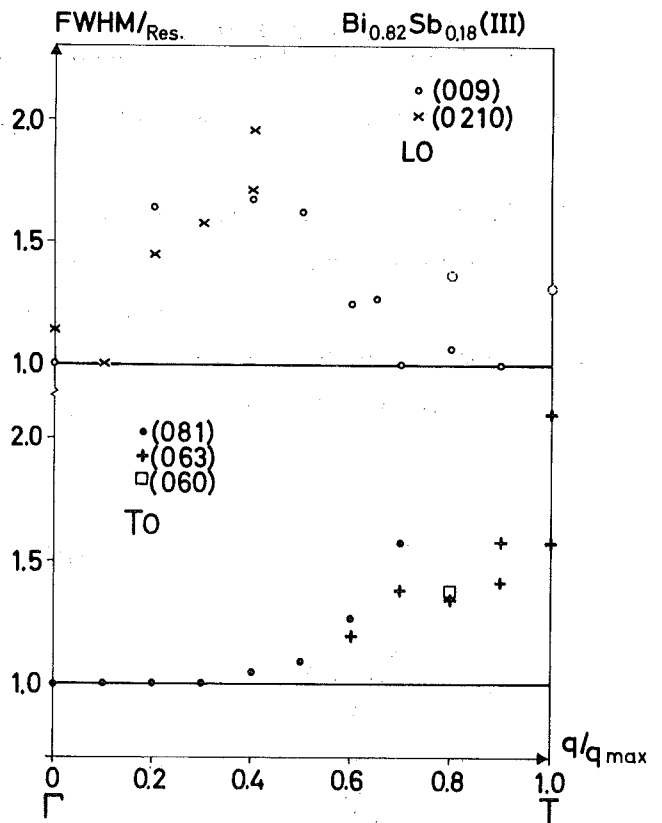
Fig. 3   Broadening of optical
         phonons measured at different
         points of the reciprocal
         lattice.

Compared to Bi the $Bi_{0.82}Sb_{0.18}$ branches are q-dependently shifted towards higher energies. This shift reaches a maximum for the zero wave vector TO phonon.

Additionally a q-dependent broadening of the phonon line width is found in the optical branches (fig. 3). The width of the TO phonons has a maximum at the zone boundary, whereas for the LO phonons the width is largest at $q = 0.4 \, q_{max}$.

This broadening may be caused by a neighbouring mode of the mixed type as described in Raman measurements /1/ or simply by the disturbed periodicity of the lattice.

There are two facts that favour the first assumption:

(i) The broadening increases with q. Taking into account the rather smooth dispersion of the main modes this means a q-dependent increase in intensity of the extra mode. This has already been found for localized modes of Al in Cu /6/.

(ii) Phonon density of state measurements /7/ show a shoulder in the energy region, where the extra mode is expected.

Comparing our results with those obtained by first order Raman scattering we find:

At zero wavevector our measurements do not show the so-called three mode behaviour (Bi-like, Sb-like and mixed modes), which is found in Raman experiments. The TO and LO phonons correspond to the Bi-like peaks of the Raman spectra. Their energies are shifted towards higher values depending on the mean Sb content of the alloy. This effect is also described by Lannin /2/. For q > 0 there are some hints for the existence of an extra optical mode, which may be identified with one of the mixed type.

The phonon dispersion of samples I, II, III in the $\Gamma$T direction can be well described by a linear B.v.K. model /8/, which takes into account interactions up to four neighbouring planes (fig. 2). Reduced masses, according to the Sb content were used in the calculations.

The dynamical model described by W. Mehringer /9/ has also been applied to the experimental data.

In order to estimate how the dispersions are determined by the electronic properties of the alloys, more elaborate models are going to be developed.

## References

/1/ R.N. Zitter, P.C. Watson, Phys. Rev. B2 10, 607 (1974)

/2/ J.S. Lannin, Raman Scattering of $Bi_{1-x}Sb_x$ alloys (to be published)

/3/ R.N. Brockhouse et al., Mat. Res. Bull. 2, 69 (1967)

/4/ P. Cucka, C.S. Barrett, Acta cryst. (Copenhagen) 15, 865 (1962)

/5/ B. Hofmann, Progress Report of the Teilinstitut Nukleare Festkörper-physik (1974)

/6/ R.M. Nicklow et al., IAEA Symp. Copenhagen, (1968)

/7/ F. Gompf, B. Hofmann and E. Schneider (this edition)

/8/ J.L. Yarnell et al., IBM Journal 7, (1964)

/9/ W. Mehringer (this edition)

## 1.1.13. A Simple Dynamical Model for Bi-Sb Alloys

### W. Mehringer

In a Bi crystal the atoms are arranged on planes perpendicular to the trigonal axis. Phonons propagating in the ΓT direction are therefore described as vibrations in which each plane of atoms moves as a rigid body. Thus only the problem of a linear chain has to be solved /1/.

In a hypothetical $Bi_{1-c}Sb_c$ crystal with long range periodicity also of the Sb atoms, the Bi and Sb atoms would move separately as rigid bodies for all phonon modes propagating in the ΓT-direction. We assume this kind of motion also for a random substitutional alloy in case of small values $c \lesssim 0.2$ of Sb concentrations.

The model is described in fig. 1. Conveniently, $m_{Sb} = m$ (Sb - atom) is used. Then $m_{Bi} = m$ (Bi-atoms) $\cdot (1 - c)/c$. Neglecting a possible change of the interplanar force constants $K_n$ of Bi, the force constants between Bi-planes of the alloy are obtained as $F_n = K_n (1 - c)/c$. To describe the interplanes Bi - Sb force constants $f_n$, a parameter Z is introduced according to $f_n = Z \cdot K_n$. This reduction factor, which we will assume

to be the same for both longitudinal and transverse polarization $(z^T = z^L)$, is expected to be $< 1$ due to the smaller size of the Sb atom as compared to the Bi atom. In addition intraplanar force constants $f_o^T$ and $f_o^L$ are introduced as disposable parameters.

As in this model the unit cell contains 4 particles, 4 dispersion curves are obtained for each polarisation. A part from TA (LA) and TO (LO) modes which correspond to the modes of pure Bi two additional modes appear with energies higher than the optical mode /3/ corresponding to localized modes of very low concentrations c).

The model was used to describe the experimental results of Hofmann /2/ for concentrations c = 0.07 and c = 0.18. From a fit to the measured dispersion curves the following parameters were determined:
$$z^T = z^L = 0.7, \quad f_o^T = 37 \cdot 10^3 \text{ dyn/cm}, \quad f_o^L = 24 \cdot 10^3 \text{ dyn/cm}.$$

A very rough estimation of $f_o$ can be made if we use the interatomic force constants of Bi instead of the unknown Sb-Bi interparticle force constants. The model of Brovman /3/ yields $f_o^T = 24 \cdot 10^3$ dyn/cm and $f_o^L = 10$ dyn/cm.
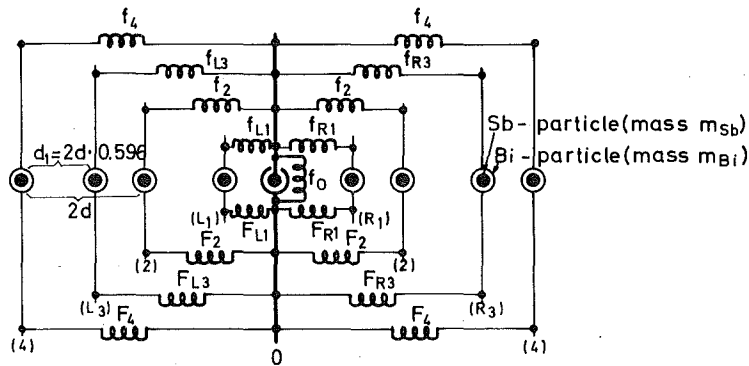


Fig. 2   Linear chain dynamical model for collective excitations of $Bi_{1-c}Sb_c$ alloys propagating in the trigonal direction. The planes perpendicular to this direction are indicated by symbols in brackets. The force constants $F_n$ ($f_n$) couple the Bi-(Sb-) particle of one plane to the Bi-particles of the neighbouring planes (and via $f_o$ to the Bi-particle of the same plane).

References
/1/   J.L. Yarnell, J.L. Warren, R.G. Wenzel and S.H. Koenig, IBM
      J. Res. Rev. 8, 234 (1964)
/2/   B. Hofmann, this report
/3/   E.G. Brovman, LA-TR68-33 (1967)

1.2    INVESTIGATIONS ON THE SCATTERING LAW OF SOLIDS
       AND LIQUIDS


1.2.1.  The Phonon Density of States of $V_3Ga$ and $V_3Ge$ at
        Different Temperatures


        *P. Schweiss*


In continuation of the investigations on the lattice dynamics of Vanadium-
based A-15 compounds the temperature dependence of the phonon frequency
distributions of $V_3Ga$ and $V_3Ge$ has been determined.


Fig. 1 and 2 show the results for these two compounds at 297 K and 77 K. They
were extracted from inelastic neutron scattering data by the extrapolation
method /1/. The spectra were measured with the multidetector time of flight
spectrometer TOF 1 at the FR2 using polycrystalline samples. The range of
scattering angles was from $35^{\circ}$ to $147^{\circ}$, the incoming energy was 65 meV,
only energy loss spectra were analysed. In both substances a softening of
phonon modes with decreasing temperature is observed similarly to the effect
found earlier in $V_3Si$ /2/. In $V_3Ga$ (composition 74.9 : 25.1, lattice
parameter $a_o$ = 4.816 Å, superconductive transition temperature $T_c$ = 13.9 K)
the squared frequency, averaged in the sense of McMillan /3/, is lowered
by 12 %. In $V_3Ge$ (sample "a" with composition 75.0 : 25.0, $a_o$ = 4.781 Å,
$T_c$ = 5.9K) this effect reaches 7 % only. This $V_3Ge$ sample contained only
about 70 % of the A-15 phase, the major part of the rest could be identified
as hexagonal $V_5Ge_3$. This is perhaps the reason why the shape of the density
of states is not very similar to that of $V_3Ga$, although the ratios of the
atomic masses are nearly identical.


Fig. 3 and 4 show the results of measurements with a $V_3Ge$ sample with
practically pure A-15 phase ("b" composition 75.4 : 24.6, $a_o$ = 4.782 Å,
$T_c$ = 6.2 K), performed on the spectrometer TOF 3 in a limited range of
scattering angles from 97 to 102 degrees. The influence of coherent effects
can not be excluded in this case. The shape of this spectrum resembles
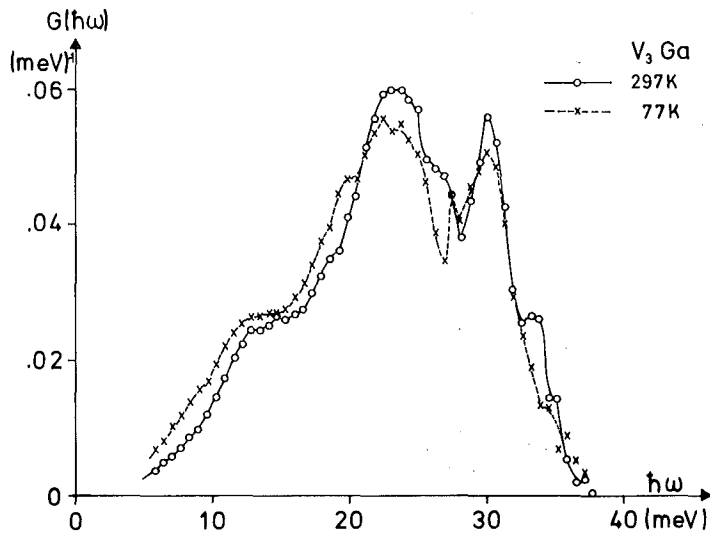
Fig. 1  Phonon density of states of $V_3Ga$ at 297 and 77 K

more the one of $V_3Ga$. The temperature effect is of about the same order in both samples of $V_3Ge$. The sample "b" was cooled to 4 K and a further decrease of the mean squared frequency by 2 % was observed.

Searching for a cubic to tetragonal transformation of these samples no splitting or broadening of the Bragg reflections after cooling to 4 K could be detected. The resolution of the two axis neutron spectrometer used in these investigations was $\Delta d/d = 2^{o}/oo$.

References

/1/  P.A. Egelstaff, "Inelastic Scattering of Neutrons in Solids and Liquids", IAEA, Wien (1961)

/2/  P. Schweiss, Progress Report of the IAK I, 12 (1974)

/3/  W.L. McMillan, Phys. Rev. 167, 331 (1968)
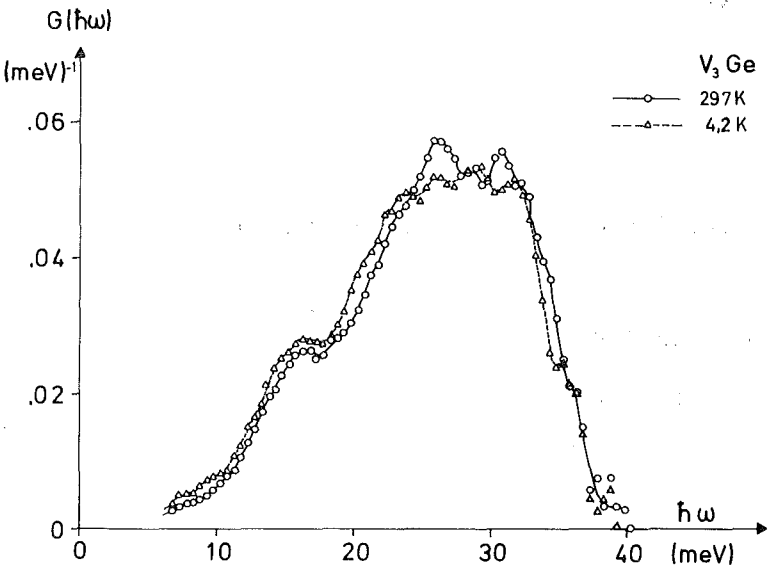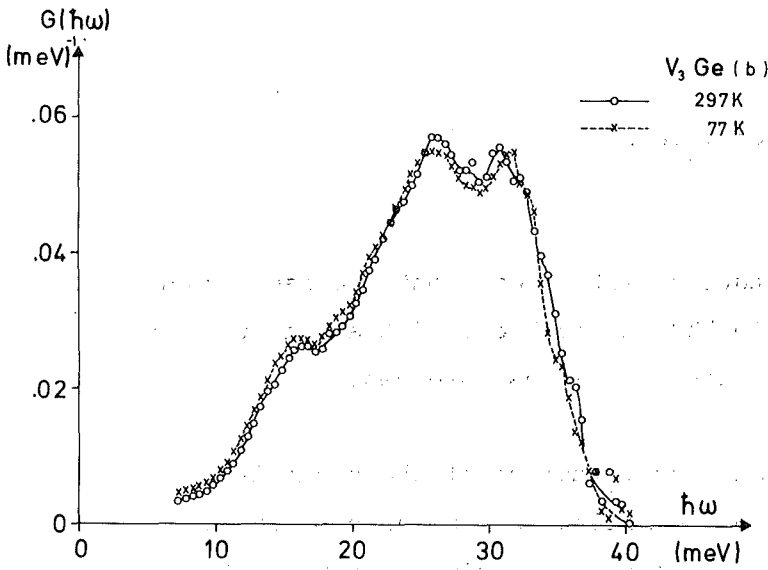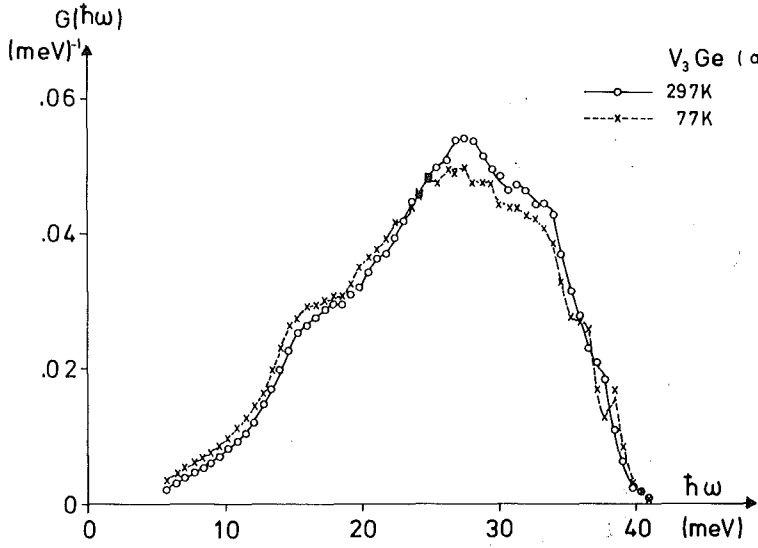
Fig. 2 - 4

Phonon density of states of

$V_3Ge$ (samples a and b) at different

temperatures

## 1.2.2. Temperature Dependence of the Phonon Density of States of $Nb_3Sn$

*E. Schneider, N. Nücker and W. Reichardt*

The scattering law measurements on polycrystalline $Nb_3Sn$ have been continued /1/ in order to study the temperature dependence of the phonon density of states.

At the HFR in Grenoble we performed two inelastic neutron scattering experiments at room temperature and at 5.5 K. Our results are shown in Fig. 1 together with the tunneling density determined by Shen /2/.
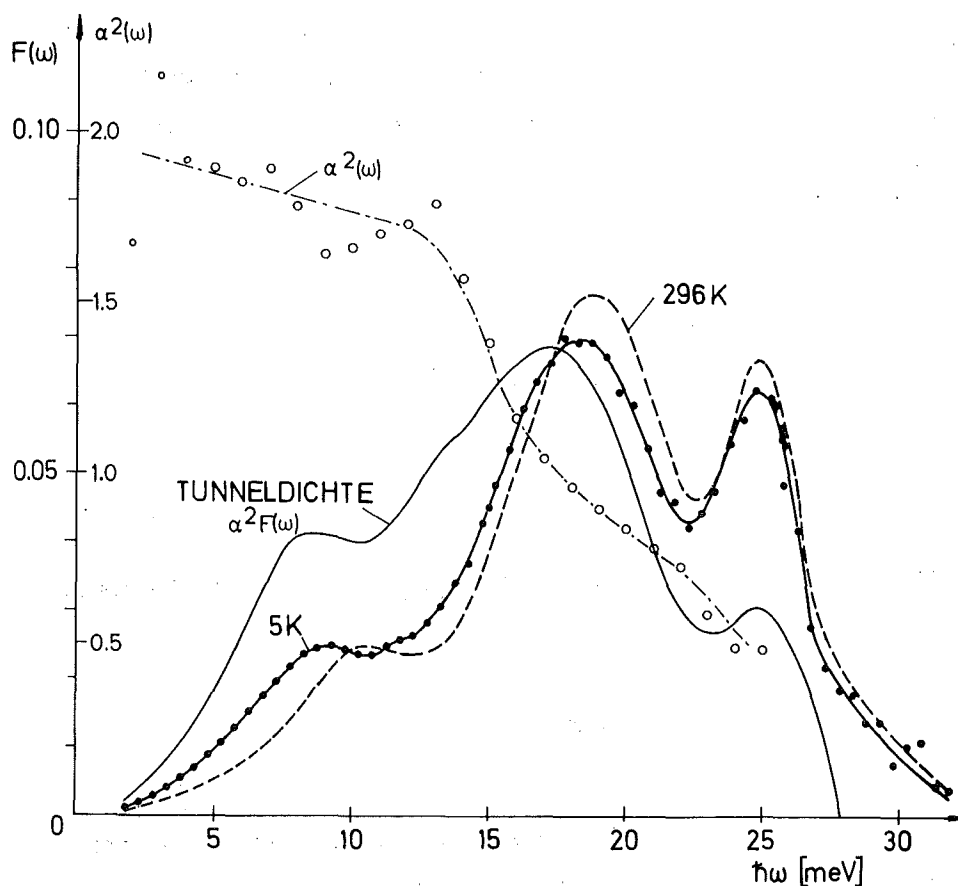


Fig. 1  Comparison of the tunneling density $\alpha^2F(\omega)$ with the phonon spectra at 296 K and 5 K of $Nb_3Sn$.

In the energy range below $\sim$25 meV we observe a considerable softening of the phonon frequencies on cooling. A measurement at 77 K showed that most of the softening occured already between room temperature and 77 K. The position of the peak near 25 meV remains essentially unchanged.

The comparison of the Eliashberg function $\alpha^2 F(\omega)$ with our phonon spectrum gives some information about the electron phonon coupling constant $\alpha^2(\omega)$. Though both curves have a pronounced structure (three peaked), their ratio $\alpha^2$ is a smooth function, which below 10 meV is relatively constant and decreases above 10 meV rather rapidly. This decrease may be caused by experimental difficulties in tunneling experiments with transition metals where the high frequency contributions are underestimated.

We have performed additional measurements on $Nb_3Sn$ with different experimental conditions concerning the primary energy and the range of scattering-angles at the FR2. These results are in very good agreement with the Grenoble data apart from resolution effects which are somewhat different for the various spectrometers.

### References

/1/ Progress Report, KFK 2054, 15 (1974)

/2/ L.S.L. Shen, Phys. Rev. Lett. 29, 1082 (1972)

1.2.3. **Phonon Density of States of $Nb_3Al$ at Room Temperature and at 4.2 K**

*E. Schneider and W. Reichardt*

The A15-compound $Nb_3Al$ is a favourable substance for inelastic neutron scattering experiments as the $\sigma/M$ - ratios of niobium and aluminium do not differ much, so that the scattered intensity can be directly related to the phonon density of states $F(\hbar\omega)$.

The results for $F(\hbar\omega)$ at 4.2 K and 296 K obtained from preparatory experiments performed on TOF 3 are shown in Fig. 1a. The primary energy was 72.37 meV. As

only a small range of scattering angles ($99.5^{\circ}$ to $104.5^{\circ}$) was used the influence of coherent effects in the experimental distributions cannot be excluded. Nevertheless a good idea on the temperature dependence of the phonon density of states can be obtained from these results.
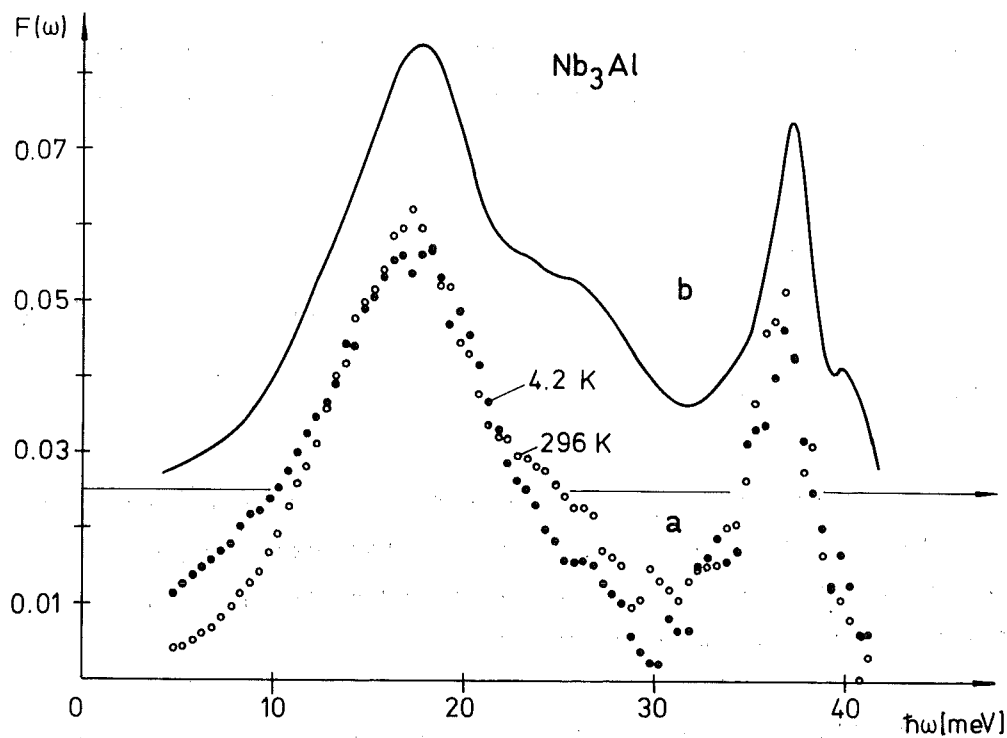


Fig. 1   a) Phonon density of states of $Nb_3Al$ at room temperature and at 4.2 K. Results from TOF 3

b) Room temperature data from TOF 1

The ratio of the areas of the peaks at 17 meV and at 36.5 meV is 3 : 1 indicating that the first one may be ascribed to the niobium vibrations, the latter to those of the lighter aluminium atoms.

Whereas the high energy peak is hardly affected by the variation of the sample temperature drastic changes occur in the range of the Nb-vibrations being most pronounced between 22 and 32 meV and below 12 meV.

Subsequent experiments were performed on TOF 1 ($E_o$ = 65 meV) with improved resolution and statistical accuracy as well as enlarged range of scattering angles ($35^{\circ} \leq \Theta \leq 147.4^{\circ}$) which guarantees a more reliable determination of the phonon density of states. The result of a room temperature measurement is shown in fig. 1b.

The corresponding curves of TOF 1 and TOF 3 are in fairly good agreement
which supports the reliability of the results on the temperature dependence
of F(hω) from our previous measurements. A similar experiment at 4.2 K is
presently carried out on TOF 1.

A structure analysis on a high resolution neutron diffractometer showed no
structural phase transition of our sample when cooled down from room
temperature to 4.2 K.

### 1.2.4. Direct Measurement of the Phonon Density of States for NbN

*F. Gompf and W. Reichardt*

On TOF 1, at the FR2 G(hω) of $NbN_{0.84}$ was determined at room temperature
with a primary energy of 65.0 meV. In energy loss the acoustic part of the
spectrum has been measured with higher accuracy and better resolution than
in the measurement done previously at TOF II /2/.

In fig. 1 we compare G(hω) for NbN (10VE) with NbC (9VE) also measured at
TOF 1 (see 1.2.6). There is a strong shift to lower frequencies for NbN
which most likely can be attributed to a strong increase of the anomalies
known from the dispersion curves of NbC
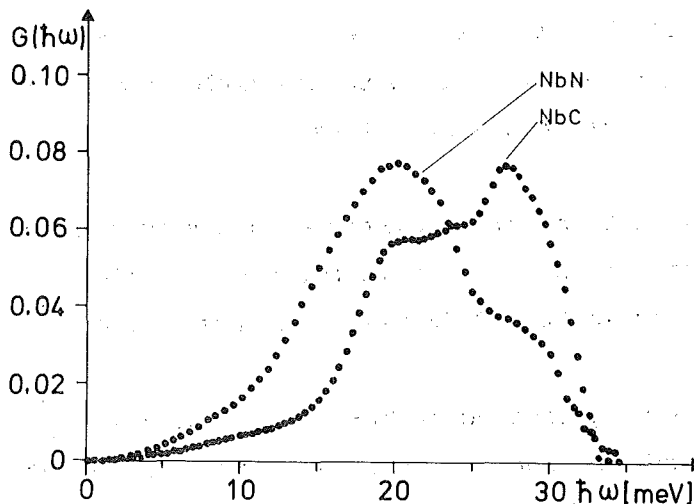


Fig. 1   Comparison of the acoustic part of the phonon density of states
for NbC and NbN

Under the assumption that the lattice dynamical models for the various
refractory materials differ from each other mainly by the parameters
for the super-shell, Weber /1/ has determined a model for a crystal
which is almost unstable at the L point and which may be applicable
to MoC or NbN. Histogram a) in fig. 2 has been calculated using Weber's
shell model parameters for NbC and the super-shell parameters for "NbN".
If compared to NbC this model shifts the upper cut-off of the distribution
towards lower frequencies in contrast to the experimental result. In order
to avoid the lowering of the zone boundary frequencies in some directions
we have reduced the coupling of the super-shell to the nearest neighbour
while simultaneously increasing the coupling to the second neighbour
in such a way that the depression of the phonon branches at the L point is
retained. The acoustic phonon density of states predicted by this model is
given by histogram b). Although the agreement with the experimental results
is far from being satisfactory the trend seems to be correct

## References

/1/  W. Weber, Phys. Rev. B8, 5082 (1973)

/2/  F. Gompf, W. Reichardt and J. Salgado, KFK 2054, 21 (1975)
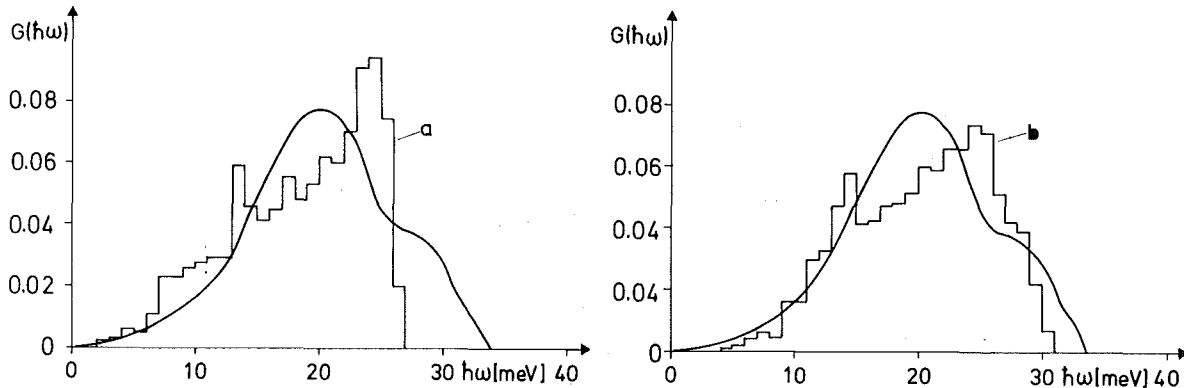
Fig. 2  Comparison of the measured phonon density of states for NbN with
two DSM calculations

## 1.2.5. Comparison of the Phonon Density of States of TiC with that of TiN

F. Gompf

$G(h\omega)$ of $TiC_{0.98}$ and $TiN_{0.92}$ were derived from scattering experiments at the
cold source of the FR2 with a primary energy of 5 meV. In this case it is not
important to have a large number of Brillouin zones within the sampling volume

since Ti is a predominantly incoherent neutron scatterer. This is underlined by Rieder et al. /1/ who measured TiN at the HFR Grenoble with a primary energy of 12.7 meV and found their G(hω) to be in good agreement with our results.

Fig. 1 shows a comparison of the acoustic part of the TiC - TiN spectra. The strong shift of the high temperature superconductor TiN towards smaller frequencies can readily be seen and can probably be attributed to strong anomalies in the dispersion relations simular to those found in NbC. The optical part of the TiC spectrum is about 20 % wider than that of TiN, it is shifted up by 6 meV and centers around 76.5 meV. In fig. 1 the non superconductor TiC is also compared with dispersion curves measured by Pintschovius et al. (see p. 6).
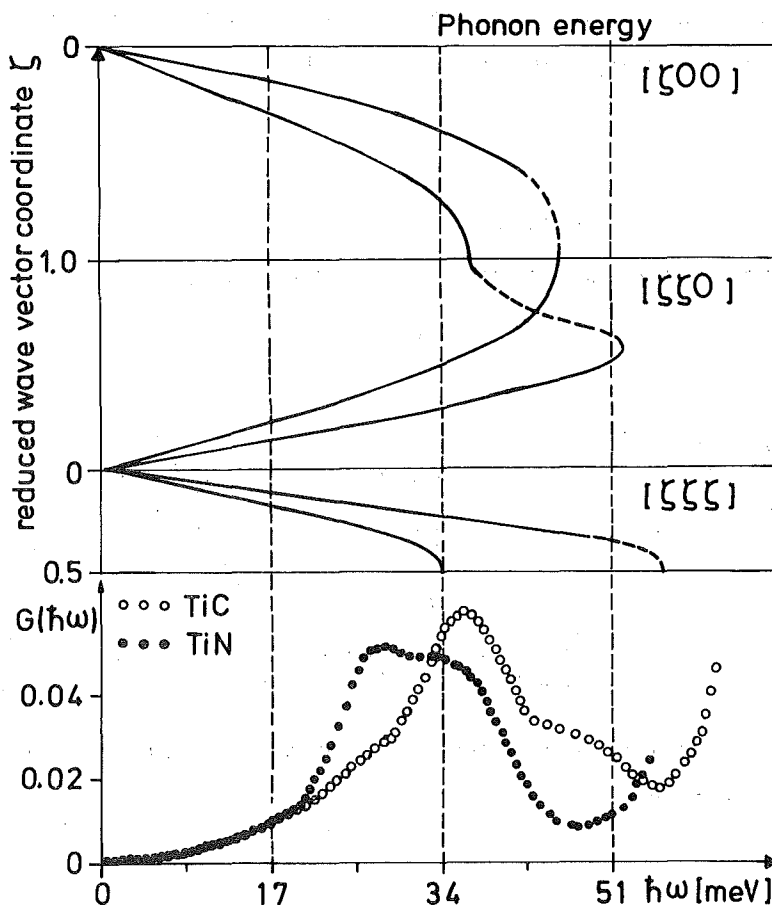


Fig. 1   Comparison of the acoustic part of the phonon spectra of TiC and TiN. The upper part shows the phonon dispersion of TiC.

References

/1/ K.H. Rieder and W. Drexel, Phys. Rev. Lett. 34, 148 (1975)

/2/ F. Gompf, J. Salgado and W. Reichardt, in Progress Report of the Teilinstitut Nukleare Festkörperphysik, KFK 2054, (1974)

1.2.6.  Comparison of the Phonon Density of States for NbC
with the Eliashberg Function and Model Calculations

*J. Geerk, F. Gompf, W. Reichardt and E. Schneider*

In continuation of our investigations on $NbC_{0.97}$ $G(\hbar\omega)$ has been determined using TOF 1 with a primary energy of 65 meV. In down scattering the acoustic part of the spectrum has been measured with better accuracy and higher resolution. The experiment was carried out at room temperature and at 4.2 K.

Since there are two different atoms in the unit cell of NbC only a generalized $G(\hbar\omega)$ can be derived from the scattering data. In order to convert $G(\hbar\omega)$ to the true phonon density of states $F(\hbar\omega)$ we calculated a correction factor $G(\hbar\omega)/F(\hbar\omega)$ using Weber's double shell model /1/. This correction factor is not very sensitive to details of the model and therefore is expected to be quite accurate. As can be seen from fig. 1b the corrections are rather small above 17 meV where the phonon density of states is mainly determined by the vibration of the Nb-atoms. Below this limit the increase of $G(\hbar\omega)/F(\hbar\omega)$ indicates that we have to correct for the C-contributions.
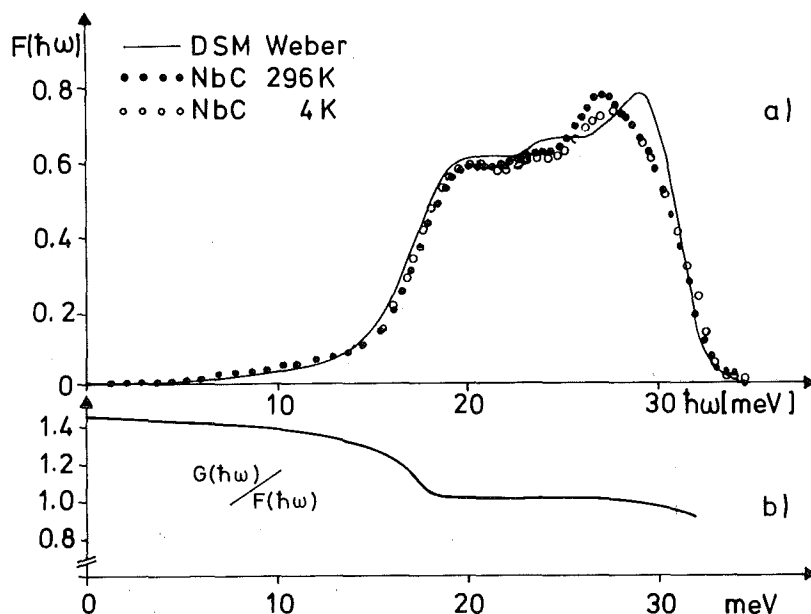


Fig. 1a  Phonon density of states of NbC

Fig. 1b  Correction factor $G(\hbar\omega)/F(\hbar\omega)$ to the generalized frequency distribution

As can be seen from fig. 1a there is a slight overall hardening of the phonon spectrum at 4.2 K compared to the room temperature results. If there is any softening at all of the phonon branches in the region of the anomalies this effect is too small to show up in the density of states. Fig. 1a also compares F($\hbar\omega$) with Weber's model calculation. The overall agreement seems satisfying. The main discrepancies occur in the high energy region of the distribution where the model predicts a rather pronounced peak at about 30 meV. In the experimental data the intensity of this peak (indicated by a shoulder in the distribution due to unsufficient experimental resolution) is reduced considerably whereas an additional peak shows up at 27 meV. As the model describes the experimental dispersion curves in the main symmetry directions very well these discrepancies must be due to off-symmetry phonons.
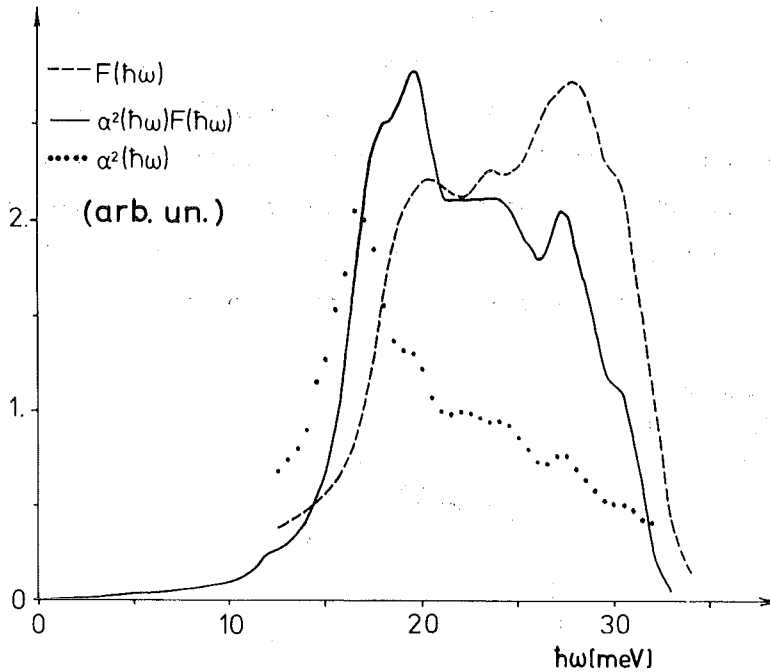


Fig. 2    Comparison of the phonon density of states F($\hbar\omega$) with the Eliashberg function $\alpha^2$($\hbar\omega$)F($\hbar\omega$)

In order to get some information on the electron-phonon coupling function $\alpha^2$($\hbar\omega$) the tunneling density of states $\alpha^2$($\hbar\omega$) F($\hbar\omega$) /2/ is compared with F(h ) in fig. 2.Good agreement is found for the cut off energies near 32 meV and the position of the peaks at 27 meV. Also the shoulder at 30 meV and the flat maximum at about 23 meV appears in both curves. However the steep rise of both spectra near 17 meV differs by more than 1 meV.

The ratio of $\alpha^2$($\hbar\omega$)/F($\hbar\omega$) and F($\hbar\omega$) representing the electron-phonon coupling function $\alpha^2$($\hbar\omega$) is also shown in fig. 2. Near 17 meV there is

a peak with a width of 3 meV, whereas outside of this region $\alpha^2(\hbar\omega)$ is a rather smooth function. The decrease in $\alpha^2(\hbar\omega)$ towards larger energies may be caused by experimental problems in the tunneling measurements. The unusual behaviour of $\alpha^2(\hbar\omega)$ around 17 meV might be explained by a stronger electron-phonon coupling in the region of the pronounced anomaly in the $|\zeta\zeta\zeta|$ transverse branch at the L-point. However it is not understood why other anomalies don't display effects of the same kind.

## References

/1/ W. Weber, Phys. Rev. B8, 5082

/2/ J. Geerk, Dissertation, Uni Karlsruhe, 1975

## 1.2.7.    The Phonon Density of States of Zr

*F. Gompf and W. Reichardt*

Zr crystallizes in the hexagonal closed packed structure. The dispersion relations of Zr have been measured by Bezdek et al. /1/ in two high symmetry directions $\Sigma$ and $\Delta$. They analyzed their data on the basis of a modified axially symmetric sixth nearest neighbour BvK model with 13 parameters. With this model they evaluated the phonon density of states $G(\hbar\omega)$.

We have directly determined $G(\hbar\omega)$ for Zr with a measurement on TOF 2 at the FR2. As the primary energy in this experiment was 5 meV the conditions for a reliable determination of the phonon density of states of a coherent scatterer were not fulfilled very well. However the systematic errors inherent in the method may be easily corrected for with sufficient accuracy if a reasonably good lattice dynamical model exists.

Fig. 1a gives a comparison of the phonon density of states determined from our experiment with that calculated from the MAS-model folded with the resolution of our spectrometer. As the authors do not give the value of the thirteenth model parameter we had to read the distribution from fig. 2 of their publication. The discrepancies between the two distributions are far outside the systematic errors of our experiment.
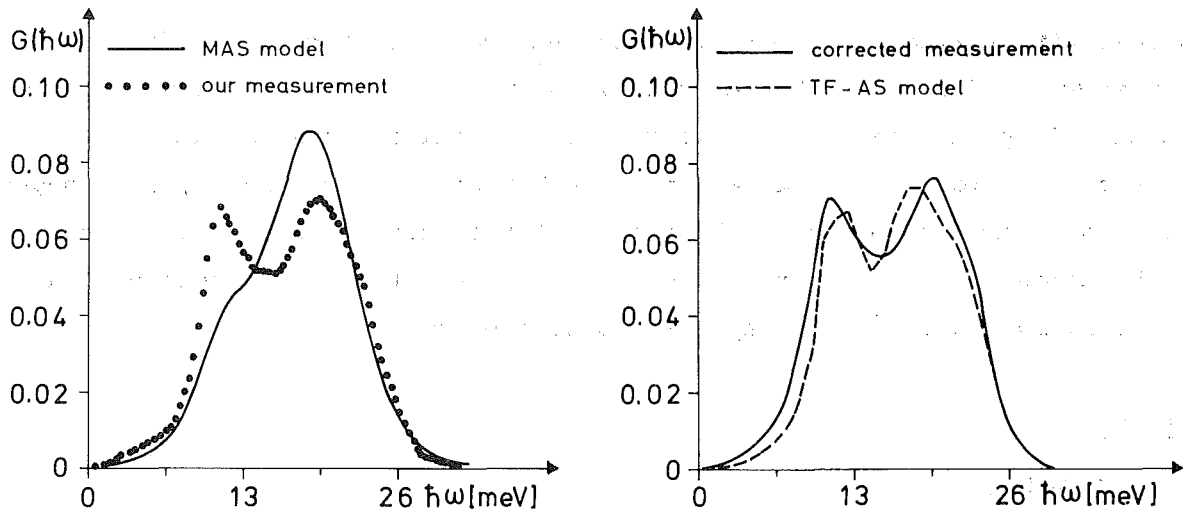
Fig. 1a,b   Comparison of experimentally determined phonon density of states
with model calculations

Although Bezdek's model may be sufficient for the determination of a quite
accurate correction we tried to improve the model for Zr by making use of
our experimental results. Fig. 1b shows $G(\hbar\omega)$ obtained from a mixed TF-AS
model with thirteen parameters fitted to Bezdek's phonon data while in
addition the lowest branch at the H point was pinned down to 11 meV, which
is the position of the lower peak in the measured distribution. Although
our model contains the same number of parameters as the MAS-model it gives
a somewhat better fit to the experimental phonon data in the $\Sigma$ and $\Delta$
direction while the agreement with the experimental phonon density of
states is considerable improved. The corrected experimental phonon density
of states obtained by using this model is also shown in Fig. 1b. The $\Theta_D$
versus T curves derived from the Bezdek's $G(\hbar\omega)$ as well as the one derived
from our results are shown in fig. 2 and compared with data calculated from
Burk's /2/ specific heat measurements.

References

/1/   H.F. Bezdek, R.E. Schmunck and L. Finegold, Phys. Stat. Sol. 42, 275 (1970)
/2/   D.L. Burk, J. Estermann and S.A. Friedberg, Z. phys. Chem., Frankfurt
        16, 183 (1958
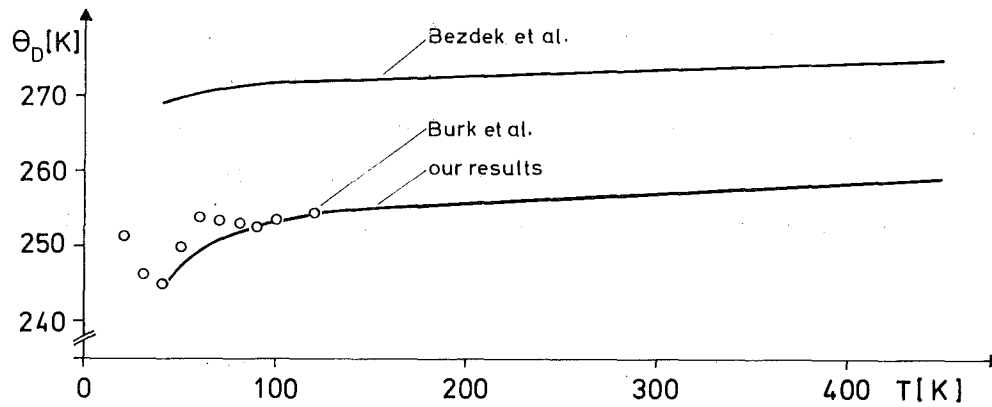
Fig. 2   The Debye temperature $\Theta_D$ as a function of the temperature T

## 1.2.8,   Comparison of the Phonon Density of States of Bi with that of the Alloy $Bi_{0.88}Sb_{0.12}$.

*F. Gompf, B. Hofmann and E. Schneider*

The phonon densities of states of $Bi_{0.88}Sb_{0.12}$ (sample IV, Tab. 1) and of pure Bi were measured on TOF 2 at the cold neutron source of the FR2 (fig. 1). The primary energy was 5 meV.

The alloy powder sample was prepared out of a 80 % single-crystalline rod, grown by horizontal zone levelling technique. It was annealed for ten days at $260^{\circ}C$, in order to reduce mechanical stresses. The Sb content was determined by lattice constant measurements and chemical analysis giving a value of 12 %.
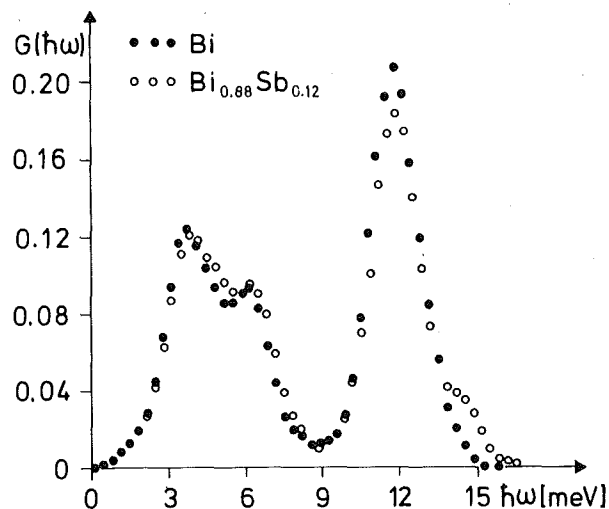


Fig. 1   Comparison of the phonon density of states of Bi and $Bi_{.88}Sb_{.12}$

Comparing the phonon spectra of Bi and $Bi_{0.88}Sb_{0.12}$, we find that the
acoustic peaks as well as the optic peaks coincide within the experimental
error. The important difference between both curves is a well defined
shoulder, which the alloy displays between 14 and 16 meV. Obviously it is caused
by the same mechanism, that causes the line-broadening in the single phonon
measurements, where the scattered neutron groups extend to that regions.

Calculations of the localized mode frequency of Sb in an unperturbed Bi
lattice /1/ using the Bi density of states give a value of 14.4 meV.

Fig. 2 shows the difference between the two distributions in this region. It
is compared with the resolution function of the spectrometer at 14.6 meV.
Shape and position of both curves are strong hints that this hump is caused
by a separate mode. The ratio of its area, corrected with σ/M for Sb, to
that of the rest of the optical peak yields 0.1, in good agreement with
the chemical composition. This result is expected for a localized vibration
of Sb in a Bi matrix.

References

/1/ R.J. Elliott, A.A. Maradudin, Inelastic Scattering of Neutrons
    (Proc. Symp. Bombay, 1964), 1 IAEA, Vienna, 231 (1965)
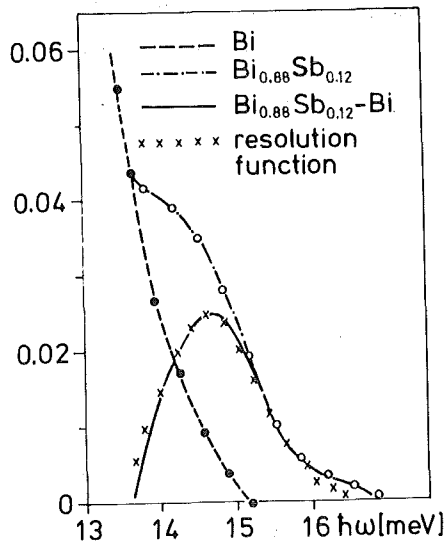


Fig. 2 Comparison of the high
energy part of the phonon
density of states of Bi and
$Bi_{.88}Sb_{.12}$

## 1.2.9.    The Phonon Density of States of Cubic Lanthanum

*N. Nücker*

The superconducting $T_c$ of Lanthanum rises under pressure from $T_c$ = 6 K
(fcc phase) to $T_c$ = 13 K at 200 Kbar /1/. Superconducting tunneling /2/
shows that this is accompanied with phonon softening.

We want to investigate the density of states of both fcc and dhcp Lanthanum
at different temperatures and pressures. Above 583 K Lanthanum has fcc structure,
which is metastable at lower temperatures. At room temperature Lanthanum
normally consists of a mixture of both fcc and dhcp structure. We prepared
pure dhcp Lanthanum by hammering it into small chips. An examination with a
two axis neutron powder diffractometer revealed the absence of the fcc
2 0 0 - reflex, which does not coincide with any of the dhcp reflexes.
Unfortunately later on we subjected this material to a three weeks heat
treatment at 545 K, which is below the transition temperature. Probably
due to impurities in the Lanthanum we got a mixture of fcc and dhcp phases.
In our attempts to prepare the fcc phase at room temperature we reached
concentrations of about 80 %.

We have performed a first measurement on pure fcc Lanthanum at 583 K with the
rotating crystal time-of-flight spectrometer at the cold source of the FR2.
From the scattering data the phonon density of states was derived (fig. 1).
In order to get an idea about the quality of our sampling experiment we did
a model calculation which is required for simulating the experiment on the
computer. With the assumption of central forces for the nearest neighbour
shell only we got a fairly good description of our measured data. The dashed
curve includesthe calculated correction of our distribution due to the
incomplete averaging. There is a remarkable similarity of this result to the
Eliashberg-function determined by Wühl et al. /2/ (dotted curve) although
these data have been obtained for the dhcp-phase. Our data don't show a
similar detailed structure, which is partly caused by an insufficient experimental
resolution. However, because of the rather high sample temperature $(T/\Theta_D \approx 4)$
a considerable smearing due to anharmonic effects has to be expected.

In our next experiments we will improve the resolution using a Fermi chopper instead of a rotating crystal.

References

/1/ M.B. Maple et al., Phys. Rev. Lett. 23, 1375 (1969)

/2/ H. Wühl et al., Phys. Rev. Lett. 31, 1393 (1973)
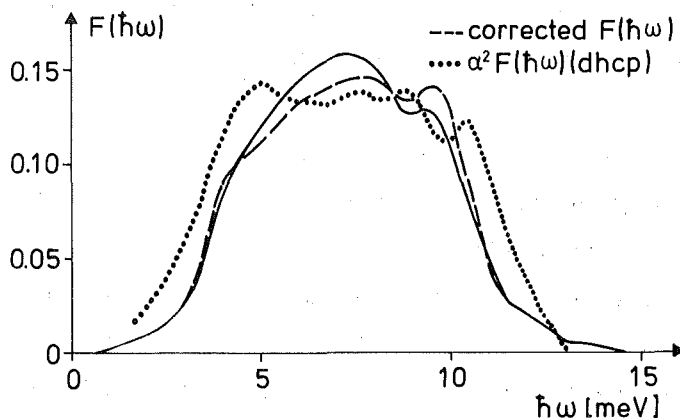


Fig. 1   Phonon density of states of fcc Lanthanum compared to a model spectrum and to the Eliashberg-function of dhcp-Lanthanum

1.2.10.     Phonon Density of States of the Two Phases of NiS

F. Gompf, G. Czjzek and J. Fink

G.I. Parisot, ILL Grenoble, France

J.M.D. Coey and R. Brusetti, CNRS Grenoble, France

The compound NiS with NiAs structure undergoes a first-order metal-to-semimetal transition at a temperature $T_t$ which depends strongly on the composition, varying from $T_t$ = 265 K for stoichiometric NiS to $T_t \sim$ 80 K for $Ni_{0.97}S$. For compositions $Ni_yS$ with $y \leq 0.965$ the material remains metallic at all temperatures.

Measurements of the specific heat /1/ and a study by [61]Ni-Mössbauer spectroscopy /2/ have indicated strong changes of the phonon frequency spectrum associated with this phase transition. Measurements of the phonon dispersion curves for some acoustic branches at room temperature and at 4 K /3/ have led to similar conclusions.

We have measured the phonon density of states using the spectrometer
TOF 1 with a primary neutron energy of 65 meV. The powder sample was
nearly stoichiometric NiS ($T_t \sim 260$ K). The phonon spectra $G(\hbar\omega)$ obtained
from measurements at 245 K (semimetallic phase) and at 269 K (metallic phase)
are shown in fig. 1a. The most pronounced differences between the phonon
spectra of the two phases are obviously in the low-frequency part of the
spectrum. The frequencies of the acoustic modes in particular are significantly
lower in the metallic phase than in the semimetallic one. In addition the sharp
drop near 25 meV of the spectrum taken at 245 K is considerably broadened at
269 K in the metallic phase. This result could indicate a stronger dispersion
of the optical modes in the metallic phase than in the semimetallic one.
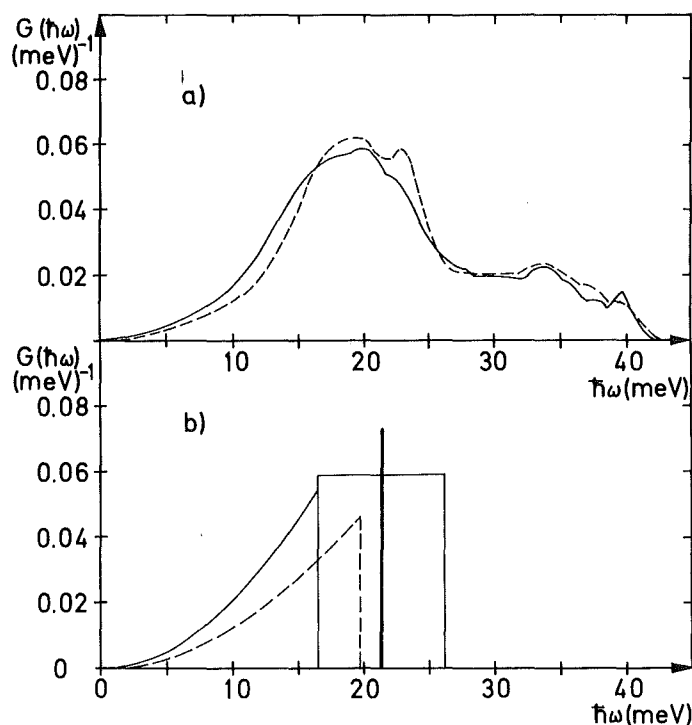


Fig. 1a/b   Phonon density of states of NiS. (a) determined by inelastic
neutron scattering: ———— at 269 K (metallic phase), — — — at 245 K
(semimetallic phase). (b) derived from the results of [61]Ni-Mössbauer
spectroscopy, analysed in terms of a Debye-plus-Einstein spectrum:
———— Debye spectrum of the metallic phase,
— — — Debye spectrum of the semimetallic phase. For both phases
the same Einstein-frequency, representing an average of optical-
mode vibrations of nickel ions, $\hbar\omega_E = 22.5$ meV was obtained.

Mössbauer spectroscopy with [61]Ni yields information on the partial density
of states $F_{Ni}(\hbar\omega)$ of nickel ions via the recoilless fraction $f(T)$ and the

second-order Doppler shift $\delta_{SOD}$ (T). The experimental data were analysed in terms of a Debye-spectrum for the acoustic modes and an Einstein term representing an average for the optical modes /2/. The results of this analysis, displayed in fig. 1b, agree quite well with those of the present work.

A comparison with results of specific heat measurements meets the difficulty that the spectrum determined by inelastic neutron scattering $G(h\omega) = N \mid (\frac{\sigma}{m})_{Ni} F_{Ni} (h\omega) + (\frac{\sigma}{m})_S F_S (h\omega) \mid$ is dominated by the contribution of nickel ions since the ratio of the weight factors $(\frac{\sigma}{m})_{Ni} / (\frac{\sigma}{m})_S$ has the value 8.2. We have tried to estimate the phonon contribution to the specific heat by a crude approximation, setting $r(h\omega) = F_{Ni} (h\omega) / F_S (h\omega) = m_{Ni}/m_S = 1.83$ for the acoustic modes /4/ up to $h\omega_D \simeq 17$ meV for the metallic phase, $h\omega_D \simeq 19$ meV for the semimetallic phase. In the region of optical modes, above this limit, we have assumed a decrease of $r(h\omega)$ which varies linearly with frequency up to the maximum frequency $h\omega_{max} = 42$ meV. To the phonon contribution to $c_v$ calculated in this way we have added the correction $c_p - c_v = a \cdot T$ with $a = 5$ mJ/mole $(K)^2$ as estimated by Coey and Brussetti, and for the metallic phase the electronic term $\gamma \cdot T$ with $\gamma = 6.2$ mJ/mole $(K)^2$ /1/. The result is shown in fig. 2 together with the specific heat curves measured for NiS and $Ni_{0.95}S$ /1/. In view of the uncertainty in the estimate of $r(h\omega)$ at all frequencies, the agreement is quite reasonable.
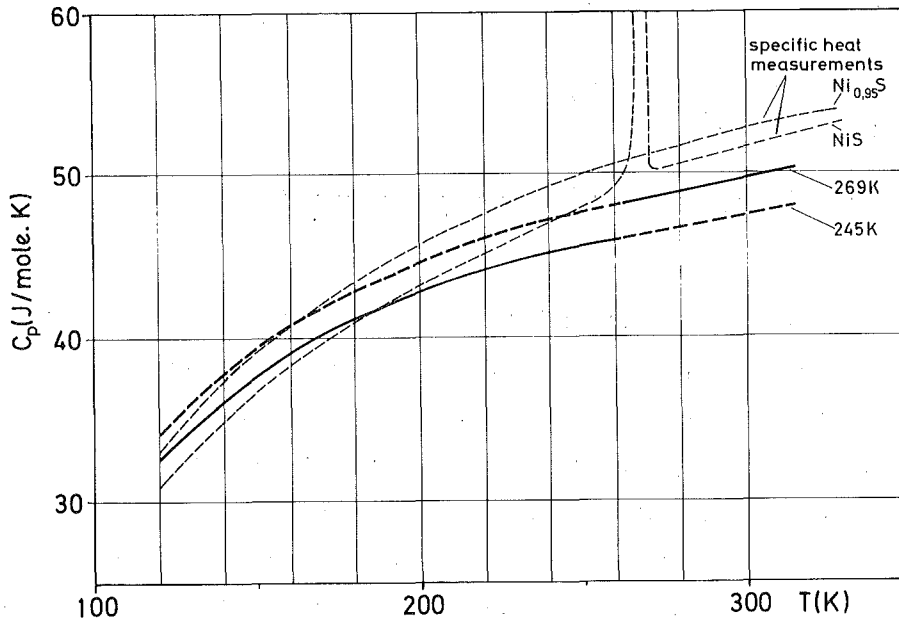


Fig. 2    Specific heat $C_p$(T) of NiS. Thin broken lines: Measured values of $C_p$(T) of NiS $(T_t \sim 265$ K) and of $Ni_{0.95}S$ (metallic at all temperatures). Heavy lines: Deduced from the phonon spectra of NiS $(T_t \sim 260$ K) measured at 245 K and 269 K, respectively.

The lattice contribution to the difference $\Delta c_v = c_v^{met.} - c_v^{semimet.}$ between the two phases at $T_t$ can be derived from our data with much higher degree of confidence as $r(\hbar\omega)$ can be expected to be essentially unaffected by the transition. The result is $\Delta c_v^{phon.}(260\ K) = (0.3 \pm 0.1)$ J/mole·K.

## References

/1/   J.M.D. Coey and R. Brusetti, Phys. Rev. B. 11, 671 (1975)

/2/   J. Fink, G. Czjzek, H. Schmidt, K. Ruebenbauer, J.M.D. Coey and
      R. Brusetti, J. de Physique Colloque 35, C6-675 (1974)

/3/   G.A. Briggs, C. Duffill, M.T. Hutchings, R.D. Lowde, N.S. Satya-Murthy,
      D.H. Saunderson, M.W. Stringfellow, W.B. Waeber and C.G. Windsor,
      in Neutron Inelastic Scattering, IAEA, Vienna, p. 669 (1972)

/4/   R.M. Housley and F. Hess, Phys. Rev. 146, 517 (1966)

## 1.2.11.   Phonon Density of States in Rubidium at 123 K and 294 K

*J.-B. Suck*

Phonon densities of states were determined from our measurements of the scattering law of polycrystalline Rubidium with TOF 2 at the cold source of the FR2 in Karlsruhe. The two temperatures chosen are about twice the Debye-temperature (62 K) and 18 degrees below the melting point. The former coincides with one of the temperatures of Copley's phonon measurements /1/. Besides the comparison of the 123 K-result with a model distribution, calculated with the force constants determined by Copley from his measurements, our interest was the agreement between results from different multiphonon corrections, the influence of the multiple scattering corrections on the frequency distributions and the applicability of our multiphonon corrections under extreme conditions as for Rubidium near its melting point (312 K) because of the large multiphonon contributions and anharmonicities.

The frequency distributions were determined from the detector sampling method following the way described in this report /2/ and the extrapolation method /3/ combined with a recalculation of $S(\alpha,\beta)/\alpha$ with LEAP. Both methods are based on an iterative correction for multiphonon contributions.

While these contributions in the 123 K measurement are largely removed except at energies above 6.2 meV, part of them remained in the 294 K-spectrum. Bearing in mind that only about 1/7 of the measured sum-spectrum was due to one phonon contribution this is not surprising. Besides this, anharmonic effects contribute to this distribution, which are not taken into account in our correction.

The results of both measurements are compared with the model-spectra in fig. 1 (123 K) and fig. 2 (294 K). For the latter model the force constants of Copley's 205 K-measurement were used, the first three of them extrapolated to room temperature. As the measured data were not corrected for resolution effects, the models were folded with the resolution function of the spectro-meter (see fig. 2 (294 K) and fig. 3 (123 K)).

The peak positions of both measured data sets and the rise of the 123 K-spectrum agree quite well with those of the folded distributions. The peaks of the distribution at 294 K are shifted to lower energies compared to the 123 K-spectrum. This shift is predicted by the model calculation, but the shape of the calculated distribution is not in agreement with the experimental result, even if the uncompleteness of the correction is taken into account.

The computer simulations of the experiments /5/ show that the deviation between the calculated phonon density of states and the measured distribution is largest at low frequencies. Especially between 1.5 and 3 meV the distribution is underestimated up to 10% (broken line in fig. 3). The calculated corrections are given for the data after multiple scattering corrections (points) in fig. 1 and 2 (broken line). This incomplete sampling is caused by the low primary energy ($E_o$ = 5.1 meV), because then only few Brillouin zones are covered by the momentum transfers corresponding to the small energy transfers. The data without multiple scattering, corrections (circles) do not show this effect so much, because elastic – inelastic scattering processes are not removed, which assist the sampling in the polycrystal. Further influences of the multiple scattering correction are seen in fig. 2, where the multiphonon contributions are reduced after this correction.

The extrapolation method did not converge for the 294 K-data, probably due to the anharmonic contributions to the scattering law. The results of the extrapolation of the 123 K-measurements are shown in fig. 3. They differ
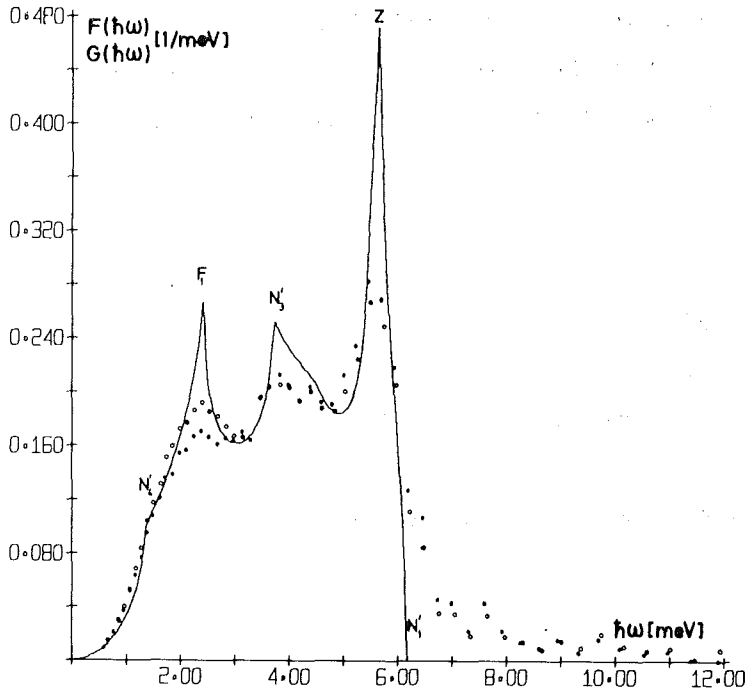
Fig. 1 Phonon density of states
        of Rb at 123 K

Circles:Experimental data

Points: Data after multiple
        scattering corrections

Line: Model-spectrum
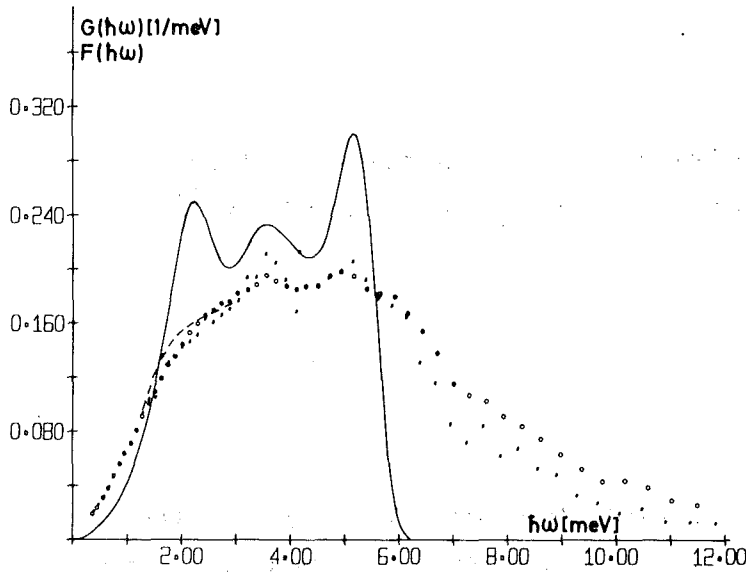


Fig. 2 Phonon density of states
        of Rb at 294 K

Circles:Experimental data

Points: Data after multiple
        scattering corrections

Full line: Model-spectrum folded
           with the resolution
           function

Broken line:Data after corrections
            for multiple scattering
            and incomplete sampling
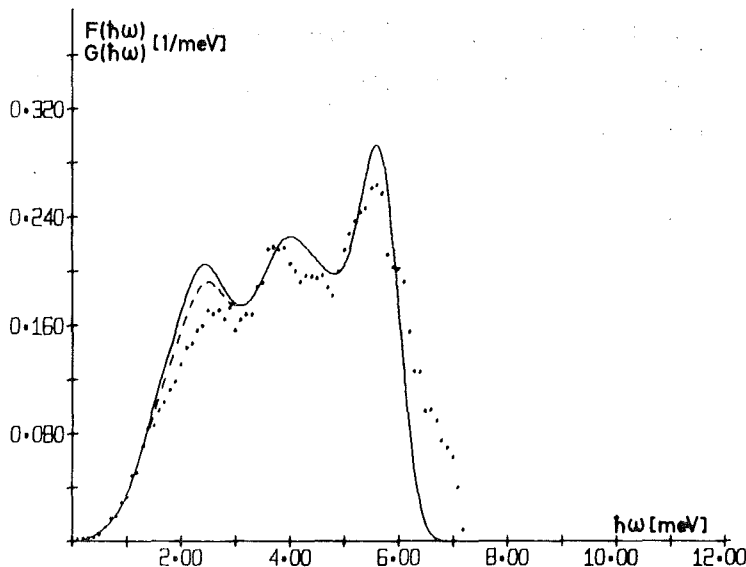


Fig. 3 Phonon density of states of
        Rb at 123 K

Points: Data after multiple
        scattering corrections

Full line: Model-spectrum folded
           with the resolution
           function

Broken line:Model-spectrum
            calculated by a
            computer simulation
            of the experiment

from the results obtained with the detector sampling method near the peak $F_1$, where the extrapolation is doubtful because of the strong coherent effects at low frequencies. However for larger energies the results of both methods agree quite well.

References

/1/ J.R.D. Copley, Can. J. Ph. 51, 657 (1973)

/2/ J.-B. Suck, W. Reichardt, this report (1975)

/3/ P.A. Egelstaff, P. Schofield, Nucl. Sci. Eng. 12, 260 (1962)

/4/ W. Abel, KFK 2054, 86 (1974)

/5/ J.-B. Suck, J. Salgado, W. Reichardt, KFK 2054, 88 (1974)

1.2.12. The Velocity Autocorrelation Function and the Effect of the Long-Range Interaction in Liquid Rubidium [+]

W. Schommers

Abstract

For liquid rubidium at $319^\circ$K moleculardynamics calculations using a realistic pair potential and a model system of 432 atoms have been performed. The cut-off radius for the potential was taken alternatively at 4.5 and 9.8 Å. The corresponding velocity autocorrelation functions and fourth moments of the scattering law were determined. The differences in the results for the two cut-off radii are attributed to long-range effects.

1.2.13.   Triplet Correlations in Disordered Systems:

A Study for Liquid Rubidium[+]

*R. Block and W. Schommers*

### Abstract

The triplet correlation function $g_3(r,s,t)$ for liquid rubidium is determined by molecular dynamics (M.D.). Calculations are based on a realistic pair-potential for a density $n = 0.0107 \,\overset{\circ}{A}^{-3}$ and a temperature $T = 319$ K. The results are compared with various models.

[+] J. Phys. C, **8**, 1997-2002 (1975)

1.2.14.     Frequency Spectrum and Scattering Law for Liquid Copper: A Molecular Dynamics Investigation

*W. Schommers*

Molecular dynamics is an important method of examining the dynamic properties of systems with strong anharmonic behaviour (eg. liquids), since anharmonicity is treated without approximations. For liquid copper molecular dynamics calculations were performed for the following model system: $N = 500$ atoms were arranged in a cubical box with the density $n = 0.0758 \,\overset{\circ}{A}^{-3}$. To avoid surface effects, periodical boundary conditions were imposed on the system. The interaction between the copper atoms is described by a pair potential /1/, which was determined from the pair correlation function without parameters using a selfconsistent method /2/. In contrast to the simple-metal pseudo-potential theory this method is applicable without modifications to metals with d-state resonances (eg. copper). For this system the classical Hamilton equations were solved by iteration to determine coordinates, velocities, and accelerations of all 500 atoms as a function of time. Starting from these data, the scattering law $S(k,\omega)$ and the frequency spectrum $f(\omega)$ were calculated for the liquid state at $T = 1375$ K.

The scattering law $S(k,\omega)$ was determined for several wave vectors $k$. Fig. 1 shows as a typical example the values for $k = 4$ $Å^{-1}$ compared with the respective data obtained for liquid copper in neutron scattering experiments /3/. Taking into account that no parameters were fitted, the agreement between the experimental data and the calculated values is quite good.
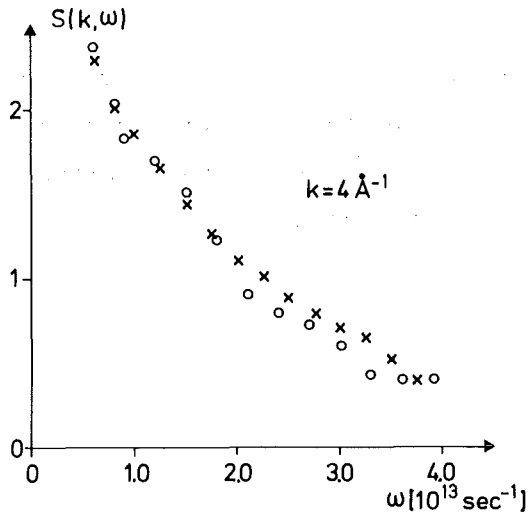


$^{\cdot}$Fig. 1  Scattering law for liquid copper

        o o o  molecular dynamics results

        x x x  experimental data /3/

The Fourier transform of the velocity autocorrelation function yields a frequency spectrum $f(\omega)$, which in the case of the harmonic solid is the frequency spectrum of the normal modes. $f(\omega)$ is therefore a valuable function in studying the change of the dynamic properties from the solid to the liquid state. Fig. 2 shows the molecular dynamics results for $f(\omega)$ for liquid copper at $T = 1375$ K. For comparison in fig. 2 the experimental data /3/, /4/ are given for solid copper at $T = 296$ K. From $f(\omega=o)$ we obtain for the diffusion constant a value of $D = 4.38 \cdot 10^{-5}$ $cm^2/sec$, which agrees quite well with the experimental value of $D = 4.25 \cdot 10^{-5}$ $cm^2/sec$ /5/.

References

/1/  W. Schommers: in KFK-report 2054, 40 (1974)

/2/  W. Schommers, Phys. Letters A43, 157 (1973)

/3/  S. Hagen, KFK-report 1774 (1973)

/4/  E.C. Svensson, B.N. Brockhouse, J.M. Rowe, Phys. Rev. 155, 619 (1967)

/5/  Henserson, Yang, Trans. Am. Inst. Min. Metall Engrs. 221, 72 (1961)
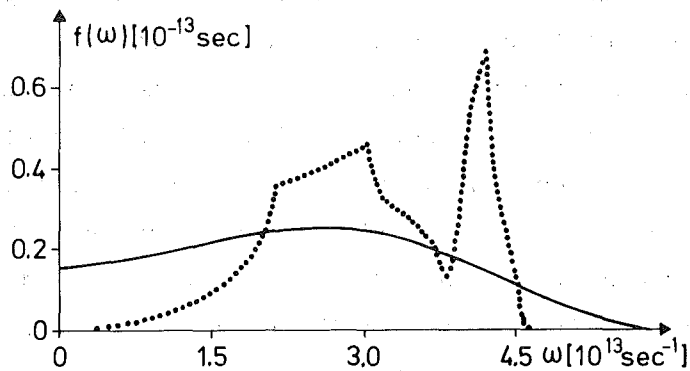
Fig. 2  Frequency spectra for liquid and solid copper

    —————— liquid copper at T=1375 K near the melting point ($T_m$=1356 K)

    · · · · · · solid copper at T=296 K

1.2.15.   An Approach by Classical Statistics to the Dynamics
         of Atomic Motion in Solids

       *W. Mehringer, Phys. Letters 53A, 197 (1975)*

Abstract

A statistical approach is presented which may be used to deal with all
kinds of problems related to vibrational atomic motion in solids within
the limits of classical mechanics. Applications considered are the hard
core solid in thermal equilibrium and the problem of collective excitations.

1.2.16.   Theoretical Investigation of the Liquid - Solid Phase
         Transition. A Study for Gallium

      *W. Schommers*

Liquid gallium is stable over an exceptionally large temperature range from
a supercooled state of at least 150 K to the boiling temperature of 2510 K.
The supercooled state of 150 K is far below the melting point ($T_m$=300 K) and
was observed in droplets of gallium less than 100 μm in  diameter by Bosio et al.
/1/. The following important questions arise: At which temperature $T_1$ is the

supercooled state still stable and which properties does liquid gallium show in the low temperature region? Is, for instance, a superfluid phase possible? In order to answer the first question Schneider et al. /2/, /3/ recently developed a theory of the liquid state which relates the stability of the liquid to the dynamics of its collective modes. In this development the stability limit $T_1$ of a supercooled system is given in the classical approximation $T_{1,cl}$. Neutron scattering experiments were carried out on liquid gallium over the temperature range 272 K - 370 K /4/ and 274 K - 325 K /5/, respectively. Attempts to fit the data to the expressions of Schneider et al. give values of $T_{1,cl}$ close to absolute zero.

We would like to show here that in the low temperature region a classical treatment of the problem is too imprecise. In short, the features of the investigation are: Within the mean field theory the density linear-response function $\chi(k,\omega)$ is given by

$$\chi(k,\omega) = \frac{\chi_o(k,\omega)}{1 - \upsilon^{eff}(k)\chi_o(k,\omega)}$$

where $\chi_o(k,\omega)$ is the density response function of a non interacting gas and $\upsilon^{eff}(k)$ is an effective potential which was determined by means of the second moment of the scattering law. In contrast to Schneider et al. both $\chi_o(k,\omega)$ and $\upsilon^{eff}(k)$ were calculated taking into account quantummechanical corrections. The collective mode frequencies $\omega_k$ are given by the poles of $\chi(k,\omega)$. The liquid-solid transition temperature $T_1$ is related to a soft-mode of wave-vector $k_o$ /2/, /3/ and was determined by

$$\lim_{\omega_{k_o} \to 0} T = T_1$$

$k_o$ corresponds to the principal peak in the structure factor $S(k)$. Following Schneider et al. it was assumed that the structure factor behaves like $T^{-1}$ near $k_o$. By varying a model-parameter we obtained different values for $T_1$. These and the corresponding classical limit $T_{1,cl}$ are given in Table 1.

Table   1

| $T_{1,cl}$ | $T_1$ |
|-----------|-------|
| 0 | 110 |
| 20 | 116 |
| 40 | 122 |
| 60 | 130 |
| 80 | 139 |
| 100 | 149 |
| 120 | 160 |
| 140 | 173 |

It can be seen that the quantummechanical corrections lead to large differences between $T_1$ and $T_{1,cl}$, especially at low temperatures. The correction to the experimental value ($T_{1,cl} = 27 \pm 20^{O}K$) of Page et al. /4/ is about 90 degrees.

It must be noted that the difference between $T_1$ and $T_{1,cl}$ is very sensitive to the temperature dependence of $S(k_o)$. Löffler /5/ fitted his experimental data to a $S(k_o)$ with logarithmic temperature dependence, resulting in a value $T_{1,cl} = 40^{O}K$. In this case the corresponding quantummechanical corrected value becomes $T_1 = 85^{O}K$. To obtain better results for $T_1$ more precise models for $\chi(k,\omega)$ and for the temperature dependence of $S(k_o)$ must be developed.

References

/1/  L. Bosio, A. Defrain, I. Epelboin, J. Phys. (Paris) 27, 61 (1966)

/2/  T. Schneider, R. Brout, H. Thomas, J. Feder, Phys. Rev. Letters
     25, 1423 (1970)

/3/  T. Schneider, Phys. Rev. A3, 2145 (1971)

/4/  D.I. Page, D.H. Saunderson, C.G. Windsor, J. Phys. C: Solid St. Phys.
     6, 212 (1973)

/5/  U. Löffler, KFK 1875, November 1973

1.2.17.    Vibrations  of  a  Linear  Amorphous  Solid

*W. Mehringer*

The dynamics of a linear amorphous solid of 20 particles has been investigated. Assuming a special form of nearest neighbour harmonic interaction the

applicability of the quasicrystalline approximation has been studied, which was derived in an improved form for the linear chain. Variations of both the strength of the interaction and the interparticle distance have been considered. From a comparison with the calculated maxima $\omega(k)$ of the one phonon part of the scattering function the limitations of the quasi-crystalline approximation could be shown. For large variations of the force constants the complete break-down of the plane wave phonon picture was found. The high-frequency modes then are represented by a motion of particles localized in regions of large force constants. The low-frequency modes may be considered as resonant modes, being characterized by the motion of clusters of particles, bound together by the large force constants and interacting via the small force constants.

# 2. ELECTRONIC STRUCTURE AND MAGNETISM OF SOLIDS

## 2.1. Investigations of Disordered Ni-Mn Alloys by Elastic Diffuse and Inelastic Neutron Scattering

*P. v. Blanckenhagen and Chr. v. Platen*

Magnetic and other physical properties of disordered Ni-Mn alloys depend on chemical and magnetic short range order. Recent neutron scattering measurements on polycrystalline samples could not be explained satisfactorily /1/. We have investigated the temperature dependence of the neutron intensity at small scattering angles. In our previous work we found that the increase of the intensity with decreasing scattering angle is caused by magnetic critical scattering /2/. The energy distribution of the neutrons scattered by an alloy with 15 % Mn was measured with a triple axis spectrometer at the cold source of the FR2 - reactor (the instrumental resolution was 45 $\mu$eV). A broadening due to critical fluctuations could be observed above and below the Curie temperature, e.g. $\Delta E = 66$ $\mu$eV at $Q = 0.065$ $\overset{o}{A}{}^{-1}$ and $T - T_c = 10^o$.

Cylindrical single crystals of Ni-Mn alloys containing 5 to 20 % Mn have been prepared to study the distribution of the diffuse nuclear and magnetic scattering intensity in reciprocal space. For crystals with 15 and 20 % Mn both contributions have a maximum at the super-lattice points for the $Ni_3Mn$ type ordering with an isotropic intensity distribution around these points (Fig. 1 (a)). The mean correlation length l, estimated from the line width of the diffuse intensity distributions, is different for the nuclear and the magnetic short range order (e.g. for 20 % Mn at room temperature: l (nucl) $\sim 10\overset{o}{A}$ and l (magn) $\sim 14$ $\overset{o}{A}$). For the alloys with lower Mn concentrations the diffuse intensity distributions are not isotropic around the 100 and 110 points.
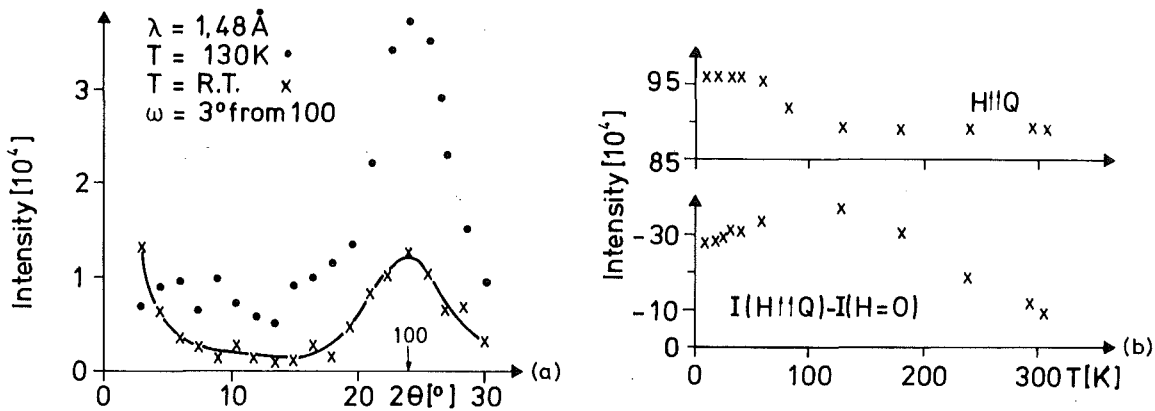
Fig. 1 Diffuse magnetic intensity scattered by a $Ni_{0.8}Mn_{0.2}$ single
crystal (20 at. % Mn)

a) angular dependence around 1 0 0  b) temperature dependence
$(2\theta = 24°)$

The diffuse magnetic intensity for $Ni_{0.8}Mn_{0.2}$ near 1 0 0 shows an
anomalous temperature dependence (Fig. 1 (b)). Similar to the tempera-
ture dependence of the magnetisation the intensity I (H↑↑Q) - I(H = 0) =ΔI
decreases at low temperatures. No significant change of the correlation
length with temperatures was observed for the ferromagnetic short range
order. The diffuse intensitiy measured with the applied magnetic field
(1.8 kG) parallel to the momentum transfer I(H↑↑Q) increases with de-
creasing temperature in the temperature region where the ferromagnetic
diffuse intensity I decreases. Further measurements at higher fields
and at other points of the reciprocal lattice are in progress to decide
whether this temperature dependence is caused by an antiferromagnetic
contribution to the magnetic short range order at low temperature.

Measurements of the magnon and phonon dispersion relations of these
alloys have been started. First results for $Ni_{0.9}Mn_{0.1}$ show a decrease
of the spin wave stiffness constant and of the energy of longitudinal
phonons in comparison to nickel.

References

/1/  J.W. Cable and H.R. Child, Phys. Rev. B10, 4607 (1974)

/2/  P. v. Blanckenhagen and Chr. v. Platen, in Progress Report of
the Teilinstitut Nukleare Festkörperphysik,  KFK 2054, p. 55 (1974)

/3/  J.S. Kouvel et al., J. de Phys. 20, 198 (1959)

## 2.2. Investigation on Structural and Magnetic Properties of the Intermetallic System $(Cr_{1-x}Fe_x)_{1+\delta}Sb$ $(0 \leq x \leq 1; \quad \delta \approx 0)$
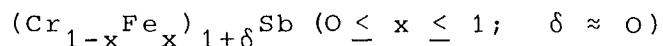
G. *Heger*

E. *Hellner, D. Mullen and W. Treutmann, FB Geowissenschaften der Universität Marburg*

The combined X-ray and neutron diffraction measurements on single crystals of several compositions have been continued. Until now for $x = 0.3$, $0.4$, $0.5$, $0.7$ all the structural details, including $\delta$-values and chromium to iron ratios, are available which have been partly published /1, 2/. In the concentration region of particular interest near $x = 0.5$ several crystals from different growings have been investigated. On the Cr-rich side of the system ($x = 0.3$, $0.4$) in addition to the neutron reflections due to nuclear Bragg scattering, we found magnetic scattering intensity contributions or peaks of purely magnetic origin at room temperature. The deduced magnetic ordering types are related to the antiferromagnetic structure of CrSb ($x = 0.0$) /3/ by a gradually twisting of the collinear aligned magnetic moments out of the hexagonal $\underline{c}$-direction. Neutron diffraction investigations at low temperatures (31 K) in the concentration range where ferromagnetic behaviour is expected, for $x = 0.7$, are in progress. So far no magnetic intensities could be detected.

### References

/1/ G. Heger, E. Hellner, D. Mullen, J. Nösselt, W. Treutmann,
in Progress Report of the Teilinstitut Nukleare Festkörperphysik,
Ges. f. Kernforschung Karlsruhe (KFK 2054), p. 58 (1974)

/2/ E. Hellner, G. Heger D. Mullen, W. Treutmann,
Mat. Res. Bull. 10, 91 (1975)

/3/ J. Takei, D.E. Cox, G. Shirane,
Phys. Rev. 129, 2008 (1963)

## 2.3.   Crystal Field Splitting in ErAl$_2$

*P. v. Blanckenhagen and Chr. v. Platen*

*H. Happel and K. Knorr, Physikalisches Institut der Universität*

*Frankfurt*

The REAl$_2$ (RE = rare Earth) intermetallic compounds crystallize in the MgCu$_2$ Laves phase /1/. Most of these compounds order ferromagnetically /2/. The saturation moments are generally less than those of the free trivalent ions /3/ suggesting that crystal field quenching is an important factor in these compounds.

Although there are a large number of measurements on this system and on the related pseudobinary compounds La$_{1-y}$RE$_y$Al$_2$ and Y$_{1-y}$RE$_y$Al$_2$ (/4/, /5/ and references therein), the crystalline electric field (CEF) parameters published by different authors scatter considerably. To clarify this discrepancy, a systematic investigation of the REAl$_2$ system by inelastic neutron scattering has been started. The result on ErAl$_2$ are reported here.

The rare earth ions are subject to a CEF of cubic point symmetry which can be given by two parameters A$_4$ and A$_6$ or - in the notation of /6/ by x and W. The effect of the CEF is to split the J-multipletts. These splittings can be directly observed by inelastic neutron scattering.

Measurements on a polycrystalline sample were performed with a time-of-flight spectrometer at the FR2. The energy of the incident neutron beam was 15 meV, the resolution (FWHM) at zero energy transfer was 1.2 meV. The sample temperatures were 18 K and 300 K, i.e. above the ferromagnetic ordering temperature which is at 14 K. The results are shown in Fig. 1. In comparison with neutron spectra of insulators or semi-metals like PrBi relatively broad lines were observed. At 18 K two transitions at the neutron energy loss spectrum and at 300 K one at the energy gain spectrum could be detected. A reasonable fit was only obtained with

$x = +0.28 \pm 0.03$ and $W = -0.027 \pm 0.005$ meV, corresponding to negative values for both CEF-parameters $A_4$ and $A_6$. This result is contrary to CEF parameters determined from magnetization measurements in the ferromagnetic phase and supports the idea that ferromagnetism in the $REAl_2$ system is not only due to CEF-effects and an isotropic exchange.
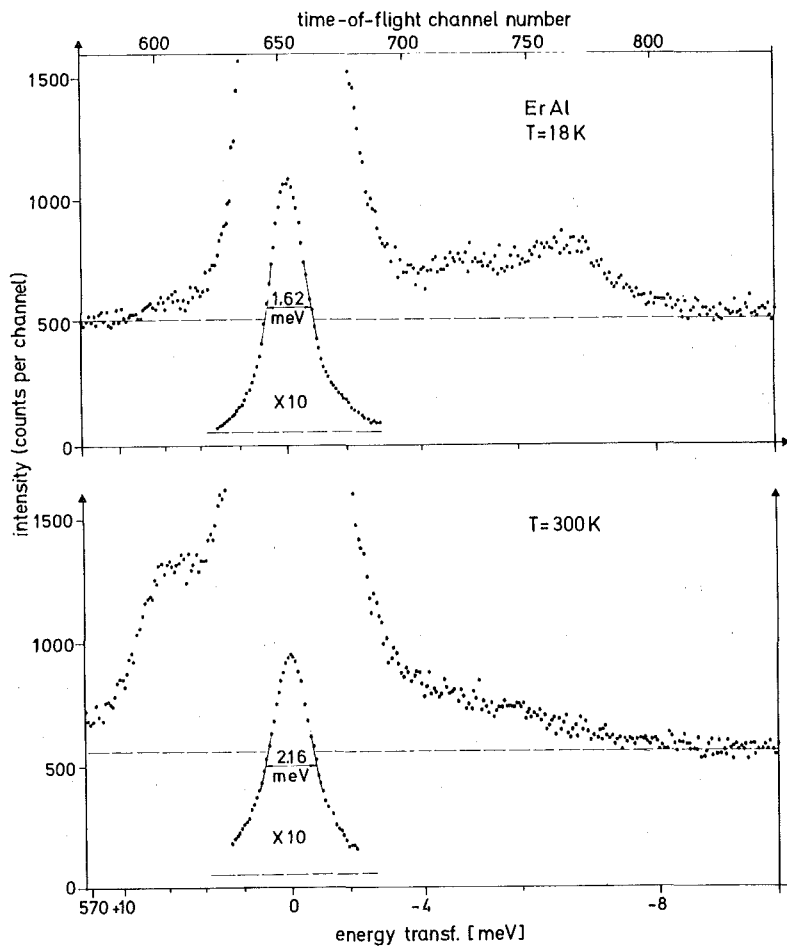


Fig. 1   Neutron time-of-flight spectra of $ErAl_2$ at 18 K and 300 K. The counting time was 55.5 hours and 60.5 hours, respectively. The incident energy was $E_o = 15$ meV.

## References

/1/   J. H. Wernick, S. Geller, Trans. AIME 218, 868 (1960)

/2/   H. J.Williams, J. H. Wernick, E. A. Nesbitt, R. C. Sherwood,
      J. Phys. Soc. Japan 17, Suppl. B1, 91 (1962)

/3/   N. Nereson, C. Olsen, G. Arnold, J. Appl. Phys. 37, 4575 (1966)

/4/   P. Bak, Excitations and Magnetic Properties of Rare-Earth $Al_2$
      Compounds, Risö Report no. 132 (1974)

/5/   H. Happel, Dissertation, Frankfurt am Main 1975

/6/   K. R. Lea, M. J. M. Leask, W. P. Wolf, J. Phys. Chem. Solids 23,
      1381 (1962)

## 2.4.   Single-Line Source Preparation for $^{155}$Gd-Mössbauer Spectroscopy

*J. Fink, K. Ruebenbauer, H. Schmidt and G. Czjzek*

*U. Berndt and C. Keller, Institut für Radiochemie*

An investigation of the coexistence of superconductivity and magnetism in $Gd_xCe_{1-x}Ru_2$ by $^{155}$Gd-Mössbauer spectroscopy has been started /1/. The source used was a dilute $^{154}$Sm in Al alloy cooled down to 43 K, giving a linewidth which is about three times larger than the natural one. Because of the poor resolution of the hyperfine splitting of $^{155}$Gd-Mössbauer spectra, especially with such a source, it was difficult to get quantitative information on the system $Gd_xCe_{1-x}Ru_2$. So it was decided to prepare a source with smaller linewidth.

Prowse et al. /2/ have shown that $^{155}$Eu dissolved in Pd is a rather narrow single-line source. Our preparation method is slightly different from that described in /2/. The starting material was 6 mC commercial $^{155}$EuCl$_3$ in 0.1 N HCl from New England Nuclear Corporation. This solution was converted to Eu $(NO_3)_3$ solution and then evaporated to dryness on a Pd foil. This coated foil was annealed in extremely pure hydrogen at 1300$^{\circ}$ C for 2 days. The $H_2O$ and $O_2$ content in the hydrogen gas was less than $10^{-4}$ vpm and $10^{-19}$ vpm, respectively. The details of the hydrogen purification have been described by Erdmann /3/. After annealing the sample was cooled down in extremely pure helium.

The source was tested at 4.2 and 1.3 K taking spectra with a $GdFe_2$ absorber at 4.2 K. The spectra were fitted with the full transmission integral. For the $GdFe_2$ absorber, the magnetic hyperfine interactions reported by Armon et al. /4/ and natural linewidth was used. For both source temperatures we got a source linewidth of 0.35 mm/sec. The additional line broadening compared to the natural linewidth of 0.25 mm/sec cannot be explained until now.

References

/1/  K. Ruebenbauer, G. Czjzek, J. Fink and H. Schmidt, in Progress Report
     of the Teilinstitut Nukleare Restkörperphysik, Ges. f. Kernforschung
     Karlsruhe, (KFK 2054), p. 52 (1974)
/2/  D.B. Prowse, A. Vas and J.D. Cashion, J. Phys. D: Appl. Phys. 6, 646 (1973)
/3/  B. Erdmann, KFK 1444, Oktober 1971
/4/  H. Armon, E.R. Bauminger and S. Ofer, Phys. Letters 43B, 380 (1973)

2.5.  An Investigation of $NiS_2$ by $^{61}$Ni-Mössbauer Spectroscopy:
      Influences of Vacancies and Copper Impurities

*J. Fink, G. Czjzek and H. Schmidt*

*G. Krill, M.F. Lapierre, F. Gautier and C. Robert, Laboratoire de
Structure Electronique des Solides, E.R.A. au CNRS No. 100,
Strasbourg (France)*

The pyrite structure compound $NiS_2$ can be prepared with variable composition $NiS_x$ in the range $1.91 \lesssim x \lesssim 2.1$. In $NiS_{1.91}$ the nickel sublattice is completely occupied and the deviation from stoichiometry is due to about 4.5% sulfur vacancies. With increasing x, the concentration of sulfur vacancies remains constant, whereas nickel vacancies appear with a concentration proportional to x /1/. Therefore we use the notation $Ni_{1-\delta}[\ ]_\delta S_{1.9}$ as an alternative to $NiS_x$, with $\delta = 1/2(x-1.9)$.

Significant changes of the physical properties (lattice parameter, electrical conductivity, magnetic susceptibility) with the introduction of nickel vacancies have been observed /1/. These changes are quite similar to those found when copper impurities were introduced in $NiS_{1.9}$.

We have studied the hyperfine interactions at $^{61}$Ni nuclei in samples $NiS_x$ with

x = 1.93, 1.94, 1.96, 2.00, 2.09 ($\pm$ 0.01 for all x) and in $Ni_{1-y}Cu_yS_{1.93}$ with

y = 0.05, 0.1($\pm$0.01) in the temperature range 1.3 K $\leq$ T $\leq$ 140 K by Mössbauer

spectroscopy. The results obtained for $NiS_{1.93}$ (whose properties are practically

identical to those of $NiS_{1.91}$) have been reported previously /2/. They serve

as reference for the evaluation of those effects which are associated with

defects.

From the $^{61}$Ni-hyperfine interactions (in fig. 1 we show the magnetic hyperfine

fields measured in some samples as a function of temperature) we can draw the

following conclusions:

(1) Although the bulk ferromagnetic moment observed in $NiS_{1.93}$ below 31 K drops

rapidly with increasing x, a magnetic phase transition occurs in all samples

near 31 K. The magnetic structure below this temperature remains essentially

the same in all samples. At 4 K we always find two sites with an intensity

ratio of 3 : 1 (low-field:high-field) as in $NiS_{1.93}$. The values of the hyperfine

fields and of the effective quadrupole coupling constants vary only slowly with x.
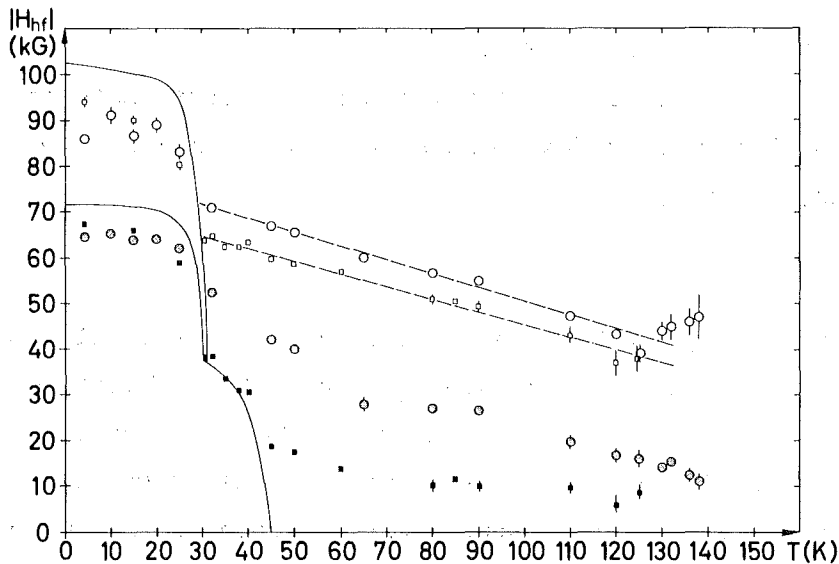


Fig. 1   Magnetic hyperfine fields at $^{61}$Ni nuclei in $NiS_x$. At all temperatures,
2 sites with different fields were found. The continuous lines trace
the hyperfine fields at $^{61}$Ni nuclei in $NiS_{1.93}$. The broken lines
emphasize the linear temperature dependence of the field at $\beta$-sites.

(2) For T > 31 K we observe two sites with different hyperfine fields in the samples containing nickel vacancies. The hyperfine field of the low-field site in $Ni_{1-\delta}[\ ]_{\delta}S_{1.9}$ with $\delta \leq 0.05$ is the same as in $NiS_{1.93}$ for 31 K $\leq$ T $\lesssim$ 40 K, but is does not go to zero at 45 K. Larger fields are obtained in $Ni_{0.91}[\ ]_{0.09}S_{1.9}$. The field associated with high-field sites ($\beta$-sites) does not depend on $\delta$ for $\delta \leq 0.05$. Again, larger values are found in $Ni_{0.91}[\ ]_{0.09}S_{1.9}$. The values of the $\beta$-site field drops linearly with temperature in the range 31 K $\leq$ T $\lesssim$ 125 K.

The fraction of the absorbed intensity due to $\beta$-sites, $c_{\beta}$, increases with $\delta$. The dependence of $c_{\beta}$ on $\delta$ agrees remarkably well with the concentration of nickel sites with at least one vacancy among the 12 nearest neighbours: $c(\delta) = 1 - (1 - \delta)^{12}$. In addition, we find in all samples a gradual decrease of $c_{\beta}$ with increasing temperature.

(3) Qualitatively similar results are obtained in the samples containing copper.

These results indicate that the changes of the physical properties occurring with the introduction of defects are inhomogeneously distributed. For low defect concentrations they may be ascribed to localized perturbations of the electronic structure (bound impurity states). With increasing defect concentrations the perturbations overlap and the transition to a metallic phase (occurring near $NiS_{2.00}$ in $NiS_x$, and near $Ni_{0.95}Cu_{0.05}S_{1.93}$) may be viewed as a percolation process.

### References

/1/  F. Gautier, G. Krill, M.F. Lapierre and C. Robert,
     J. Phys. C **6**, L 320 (1973)
/2/  G. Czjzek, J. Fink, H. Schmidt, G. Krill, F. Gautier, M.F. Lapierre
     and C. Robert
     J. de Physique Colloque **35**, C6-621 (1974).

## 2.6. An Investigation of Magnetic Structures and Phase Transitions in $NiS_{2-x}Se_x$ by [61]Ni-Mössbauer Spectroscopy

G. Czjzek, J. Fink and H. Schmidt

G. Krill, M.F. Lapierre, P. Panissod, F. Gautier, C. Robert, Laboratoire de Structure Electronique des Solides, E.R.A. au CNRS No. 100, Strasbourg (France)

The mixed compounds $NiS_{2-x}Se_x$, existing for the whole concentration range $0 \leq x \leq 2$ with pyrite structure, can be considered as a good test case for Mott's view of correlation-induced metal-insulator transitions. In $NiS_2$ correlation effects dominate, the material is a semiconductor and two magnetic phase transitions are observed. In $NiSe_2$ correlation effects are reduced due to stronger overlap between the Ni 3d-orbitals and the Se(4sp)-states, this compound is metallic and no magnetic order has been found at any temperature. The phase diagram of the mixtures $NiS_{2-x}Se_x$ was determined by Jarrett et al. /1/. They found the critical concentration for the metal-insulator transition at T = 0 K to be $x_{cr}$=0.47. According to these authors, the two magnetic phase transitions found in $NiS_2$ occur for all concentrations in the insulating phase (x < 0.47).

We have begun a systematic investigation of this system by combined measurements of macroscopic properties, such as magnetic susceptibility and electrical resistivity, NMR with [77]Se, and Mössbauer spectroscopy with [61]Ni. The results obtained by now lead to certain modifications of the phase diagram (fig. 1).
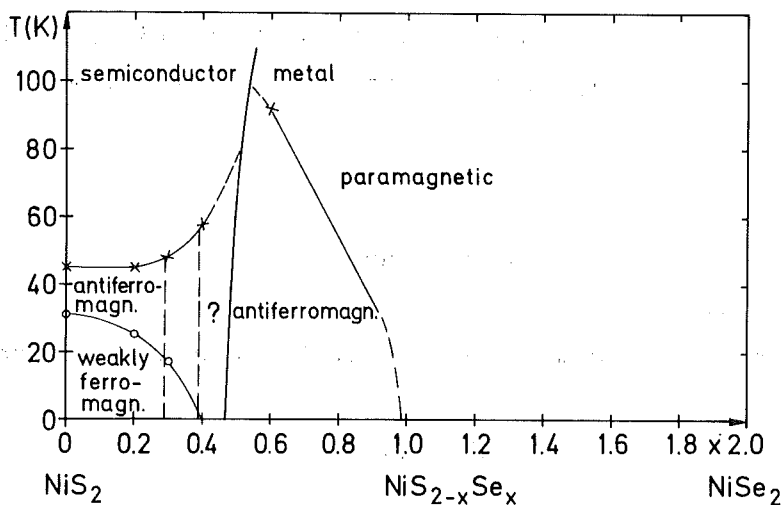


Fig. 1 Phase diagram of $NiS_{2-x}Se_x$ as determined in the present investigation

Firstly, we have observed the occurrence of antiferromagnetic order in the metallic region of the phase diagram for 0.47 < $x \lesssim$ 1.0 /2/. The transition to the paramagnetic state occurs for x = 0.6 at $T_N$ = (92 ± 2) K, as has been

determined independently by Mössbauer spectroscopy, susceptibility measurements and $^{77}$Se-NMR. By the latter two methods the concentration dependence of $T_N$ was determined to be linear up to x = O.9. At x = 1.0 no magnetic ordering could be detected. The Mössbauer spectra show that at least two nickel sites with different hyperfine fields exist in these materials. The hyperfine fields decrease approximately linearly with increasing x. For x = 0.9 we found about 65% of the absorbed intensity in an unsplit line, indicating the possible existance of a two-phase region between the antiferromagnetic and the paramagnetic metallic phase. A similar result was obtained by $^{77}$Se-NMR. In the region of concentrations where the materials are insulating we have found almost no changes of the magnetic transition temperatures and the hyperfine interactions between $NiS_2$ and $NiS_{1.8}Se_{0.8}$. For higher Se-concentrations the Néel temperature rises and the critical temperature for the transition from antiferromagnetic to weakly ferromagnetic ordering drops rapidly to zero. In $NiS_{1.6}Se_{0.4}$ no indication of this transition was found in the temperature dependence of the magnetic hyperfine fields which vary linearly from 1.3 K to 55 K (fig.2a). In this sample we also found a strong variation of the effective quadrupole coupling constant with temperature (fig. 2b). It appears likely that this can be interpreted in terms of a temperature-dependent change of the direction of the magnetic moments with respect to the local symmetry axis. These results make it presently questionable whether the magnetically ordered phase in this concentration region can be identified with the anti-ferromagnetic phase of $NiS_2$.
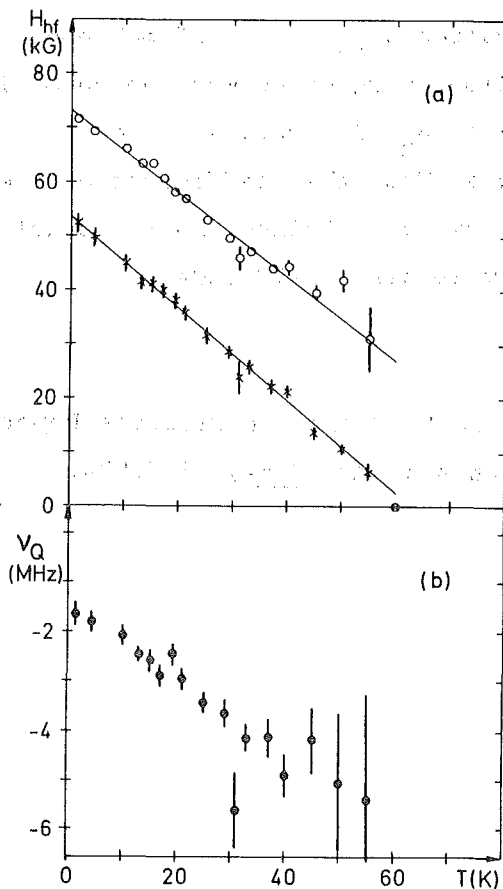


Fig. 2 Hyperfine interactions at $^{61}$Ni nuclei in $NiS_{1.6}Se_{0.4}$ (a) Magnetic hyperfine fields, x α-sites, O β-sites. (b) Electric quadrupole coupling constants No difference between α- and β-sites was found.

References

/1/ H.S. Jarret, R.J. Bouchard, J.L. Gillson, G.A. Jones, S.M. Marcus
and J.F. Weiher, Mat. Re. Bull. $\underline{8}$, 877 (1973)

/2/ F. Gautier, G. Krill, M.F. Lapierre, P. Panissod, C. Robert,
G. Czjzek, J. Fink and H. Schmidt, Phys. Letters $\underline{53A}$, 31 (1975)

## 2.7. Magnetic Interactions in $Na_2NiFeF_7$

*G. Heger, J. Fink, G. Czjzek and H. Schmidt*

*R. Geller, Institut für Kristallogrpahie der Universität Tübingen*

The investigations of the magnetic properties of Weberite structure compounds $Na_2NiM^{III}F_7$ ($M^{III}$ = Al, Fe, Cr) /1/ were continued. Mössbauer spectroscopy with $^{57}Fe$ and $^{61}Ni$ was employed to determine the temperature dependence of the iron and nickel sublattice magnetizations in the ferrimagnetic compound $Na_2NiFeF_7$. The curves of the magnetic hyperfine fields $H_{hf}^{Fe}$ (T) $/H_{hf}^{Fe}$(4.2 K) and $H_{hf}^{Ni}$ (T) $/H_{hf}$ (4.2 K) versus $T/T_N$ ($T_N$ = 85 ± 1 K) differ significantly from each other and from the corresponding curve of the bulk magnetization, M(T)/M(4.2 K). From an annalysis of these data in terms of molecular field theory we could derive the values $J_{Ni-Ni}$ = -1.26 meV and $J_{Ni-Fe}$ = -0.83 meV for the exchange interaction energies between neighbouring magnetic ions. At temperatures below $\sim$ 40 K the $H_{hf}$(T) – curves follow a $T^{3/2}$-law as expected for spin-wave excitations. From the coefficient of the $T^{3/2}$-term the value $8J_{Ni-Fe}-2J_{Ni-Ni}$ = -3.2 meV was obtained, in reasonable agreement with the results deduced from the molecular field model.

References

/1/ G. Czjzek, J. Fink, G. Heger, D. Babel and R. Geller in Progress Report
of the Teilinstitut Nukleare Festkörperphysik, KFK $\underline{2054}$, 56 (1974)

2.8. Investigations of the Structural and Dynamic Properties
of the Layered Molecule Crystal $(CH_3NH_3)_2 MnCl_4$

*G. Heger*

*D. Mullen, FB Geowissenschaften der Universität Marburg*

*K. Knorr, Institut für Kristallographie der Universität Tübingen*

*N. Lehner, K. Strobel and R. Geick, Physikalisches Institut der Universität Würzburg*

A main part of the experimental work by means of neutron diffraction and FIR spectroscopy deals with the second-order phase transition at 393.8 K. Most of the results will be published in two papers. Their abstracts are given below.

1. On the Second-Order Phase Transition in $(CH_3NH_3)_2 MnCl_4$.
   A Single Crystal Neutron Diffraction Study at 404 and 293 K.

G. Heger, D. Mullen and K. Knorr

Abstract

The crystal structure of $(CH_3NH_3)_2MnCl_4$ was determined by neutron diffraction at 404 and 293 K. The high temperature phase has a dis-ordered $K_2NiF_4$-type structure (I4/mmm) with $MnCl_6$-octahedra and $(CH_3NH_3)$-molecules tilted with respect to the $\underline{c}$-axis in four different orientations of equal probability. In the room temperature modification (Abma) one of these orientations predominates. Thus an ordered struc-ture results which can be seen as a "frozen" moment picture of the high temperature structure accompanied by a displacement of the $CH_3$-groups.

From the complete structure analyses (including the whole description of the $(CH_3NH_3)$-groups with the hydrogen atoms) a microscopic model of the second-order structural phase transition at 393.8 K is proposed. There are two possibilities to define an internal order parameter:

1. the predominance of one orientation of the tilted $(CH_3NH_3)_2MnCl_4$ molecules which can be described by an occupation probability

2. the displacement of the $CH_3$-groups.

A soft mode may be associated with this displacive behaviour.

2. Lattice Dynamics in Perovskite-Type Layer-Structures.

FIR-Studies of $(CH_3NH_3)_2$ $MnCl_4$ and $(CH_3NH_3)_2$ $FeCl_4$.

N. Lehner, K. Strobel, R. Geick and G. Heger

( submitted to J. Phys. C)

Abstract

In this paper, we present a detailed study of the crystal structures of $(CH_3NH_3)_2MnCl_4$ (=MAMC) above and below the phase transition at 394 K, which is essentially of the order-disorder type. In addition, the reflectivity of MAMC and MAFC (= $(CH_3NH_3)_2FeCl_4$) single crystals has been studied in the far infrared spectral region at several temperatures. By means of a Kramers-Kronig-Analysis, the frequencies of the long-wavelength infrared-active phonons were determined. Because of the considerable gap (300 - 900 $cm^{-1}$) between the frequencies of the organic ions, they can be treated as rigid bodies at far infrared frequencies. For the high temperature tetragonal modification, there are three strong and two weak ir-active modes for $\underline{E} \perp \underline{c}$. Our results can be compared to the results obtained for layer-structures of the $K_2NiF_4$-type. In this case three strong modes and only one weak are found, which are closely related to the three ir-active modes and the inactive mode in perovskite crystals. The second weak mode in MAMC and MAFC for $\underline{E} \perp \underline{c}$ is introduced by the rotational degrees of freedom of the organic molecules. Though with some difficulty, experimental data have also been obtained on MAMC for $\underline{E} \parallel \underline{c}$.

Further investigations concerning the crystal structure of the low temperature tetragonal phase ($P4_2/ncm$) have almost been finished. Inelastic neutron measurements are in preparation.

2.9.      Planar Dynamic Jahn-Teller Effects in $Cs_2PbCu(NO_2)_6$

G. Heger

D. Mullen, FB Geowissenschaften der Universität Marburg

D. Reinen, FB Chemie der Universität Marburg

As an example for a system with strong Jahn-Teller effects leading to structural phase transitions (collective Jahn-Teller effect) $Cs_2PbCu(NO_2)_6$

was studied by neutron diffraction on single crystals at 293 and 344 K in
order to determine the crystal structures. The results of the room tem-
perature investigation are to be published. The abstract is given below
including a drawing of the hexanitrocuprate(II) anion. Further crystallo-
graphic studies of the other modifications are in progress.

D. Mullen, G. Heger and D. Reinen

( Solid State Communications, in press )

## Abstract

We report a crystal structure analysis of the room temperature phase of
$Cs_2PbCu(NO_2)_6$. In the space group Fmmm (c/a < 1 (a ~ b)) the $Cu^{2+}$ ions
have a tetragonally compressed octahedral environment of N atoms. The
thermal ellipsoids of the nitro-groups in the (001)-plane indicate the
presence of a two-dimensionally dynamic Jahn-Teller effect (Fig. 1).
This result is interpreted in terms of a time-averaged picture of
tetragonally elongated octahedra in antiferrodistortive order.
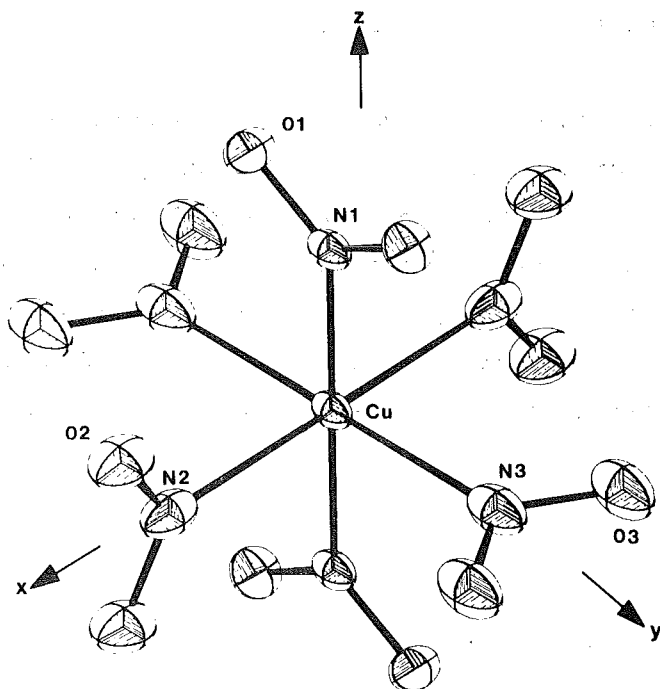
Fig. 1   The arrangement of the six nitro groups around the copper ion,
including the thermal ellipsoids.

## 2.10. Nuclear Magnetic Resonance Studies on Neutron Activated $^{20}$F Nuclei in $CaF_2$

H. Ackermann, D. Dubbers, F. Fujara, H. Grupp, P. Heitjans,

H.-J. Stöckmann and A. Winnacker, Physikalisches Institut der

Universität Heidelberg und ILL Grenoble

a) Structure of (n,γ) - Induced Lattice Defects

The present experiment deals with the observation of a well defined defect structure in the vicinity of neutron activated $^{20}$F (I = 2, $T_{1/2}$ = 11s) nuclei in $CaF_2$. The principle of the method is: Production of polarized $^{20}$F nuclei by polarized neutron capture, and detection of NMR transitions of the $^{20}$F nuclei via their asymmetric β-radiation:

$$^{19}F + n_{pol} \rightarrow {}^{20}F^*_{pol} \xrightarrow{\gamma's} {}^{20}F_{pol} \xrightarrow{\beta-} {}^{20}Ne^*_{pol} \xrightarrow{\gamma} {}^{20}Ne$$
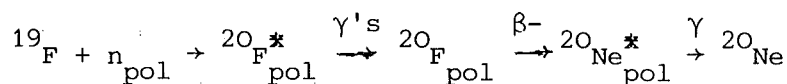
The capture-γ radiation imparts a mechanical recoil ($E_R \leq$ 1.2 keV) to the $^{20}$F nuclei and displaces them in the lattice.

$CaF_2$ has a cubic structure and one observes at room temperature (where the defects anneal quickly compared to $T_{1/2}$ = 11 s) a single, undisturbed NMR line. At temperatures below 75 K, however, the defects are stable and their electric field gradients q split the NMR line. This splitting can be observed, if only few defect types occur, as it is the case in $CaF_2$. But even then, the signals are weak and can only be detected using a broad frequency modulated radiofrequency field (see Fig. 1). This technique is described in detail in /1/.

Summary of the results:

1) Room temperature: undisturbed NMR line.

2) T = 10 ... 75 K: The NMR line broadens and 4 satellites appear. Their position corresponds to a quadrupolar interaction with $|e^2qQ/h|$ = (1.9 ± 0.1) MHz and $\theta (q,B_o)$ = (70 ± 3)$^o$.

3) The corresponding defect type is seen by ≈ 40 % of the $^{20}$F nuclei.

4) Observation of the $\beta^- (^{20}F) - \gamma (^{20}Ne)$ angular distribution: $e^2qQ$ is negative.
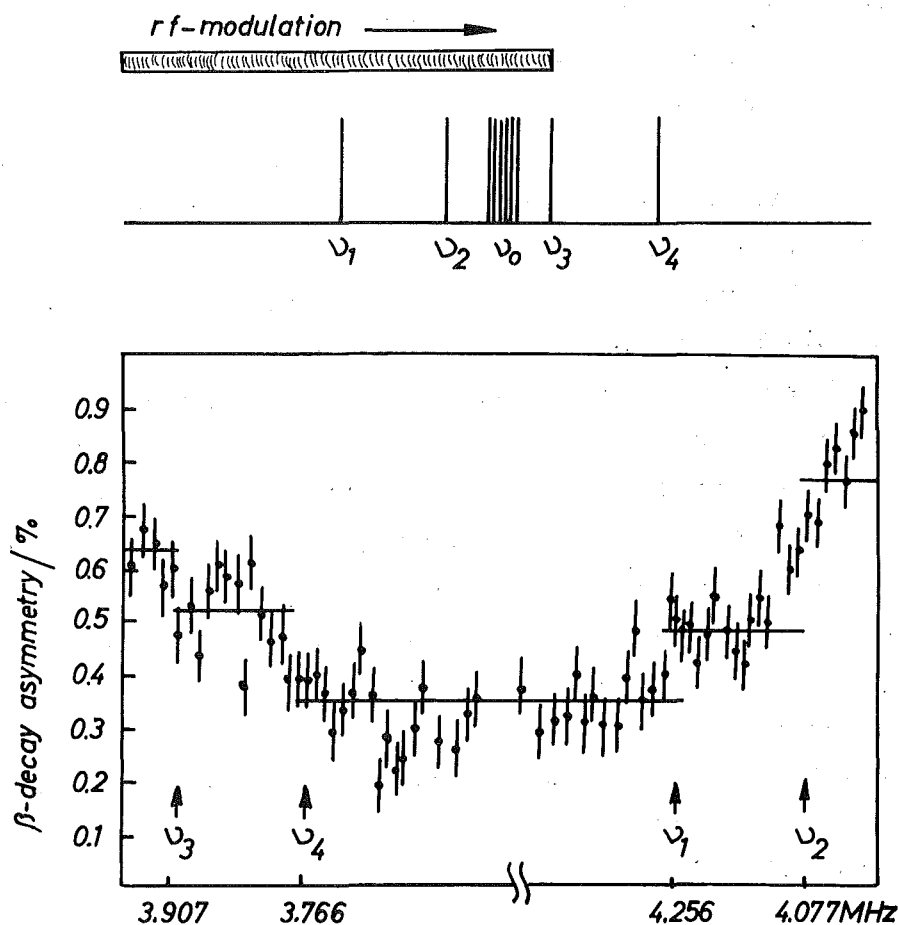
Fig. 1  A broad band modulated rf field is swept over the defect-field
split   NMR transitions. Whenever a transition enters or leaves
the band, a step in the nuclear polarization occurs. The solid
step curve is a least-square fit to the measured asymmetries. $B_o$
parallel to the crystallographic <111> direction, $B_o = 0.5$ T, T = 40 K.

Discussion: The $F^-$ sublattice of $CaF_2$ is simply cubic. Every second
elementary cube contains a body-centred $Ca^{++}$, whereas the other cubes
are empty. The observed defects consist of $^{19}F^-$ interstitials in these
empty lattice positions, whereas the $^{20}F$ probe nuclei occupy normal
lattice sites at the adjacent corners of the $E^-$ sublattice cubes.

b) Decoupling of the $^{20}F$-Magnetic Dipole Moment from Internal Magnetic
Fields: Strong Narrowing of Resonance Lines

In solids usually the NMR linewidth is determined by the dipolar coupling
of the observed nuclear magnetic moment to the magnetic moments of the
surrounding nuclei. It is well known /2/, however, that the contribution

of unlike neighbouring spins to the dipolar linewidth can be completely
eliminated by irradiation of a strong radiofrequency field at the NMR
frequency of that (unlike) spin species. In NMR-experiment on neutron-
activated nuclei the probe nuclei are so dilute that they are exclusively
surrounded by unlike nuclear spins. Thus it should be possible to produce
very narrow NMR lines of the probe nuclei by "decoupling" the surrounding
spins of the stable nuclei by application of a second, strong radiofrequency
field. A particularly favorable case is $CaF_2$ containing only $^{19}F$ with nonzero
nuclear spin, thus only one spin species has to be decoupled from the
observed $^{20}F$ probe nuclei. Fig. 2 shows the NMR lines of $^{20}F$ with and
without simultaneous irradiation of the $^{19}F$ NMR frequency. NMR lines
down to a width of 100 Hz have been observed, the linewidth only being
determined by inhomogeneities of the magnetic field. This opens up inter-
esting possibilities to resolve small splittings of NMR lines due to
electric field gradients of lattice defects. Experiments are in progress
to investigate defect fields created by the $(n,\gamma)$-capture process, or by
external pressure on single crystals. Precision measurements of ratios of
nuclear moments are also possible which is of interest for the evaluation
of hyperfine anomalies.
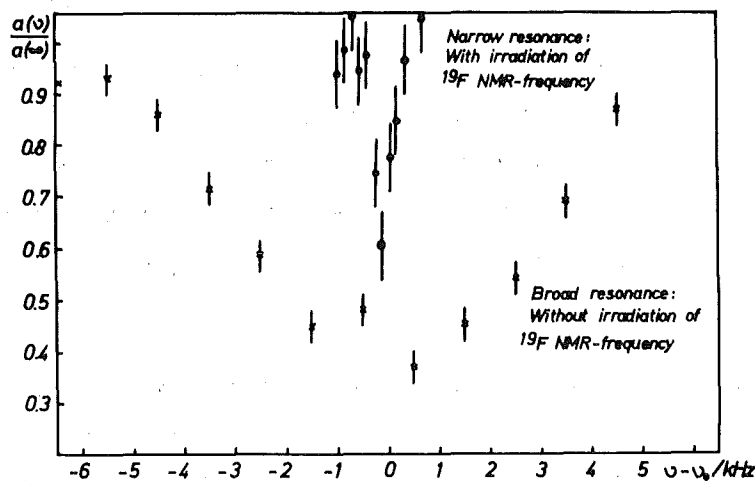


Fig. 2   NMR of $^{20}F$ with and without decoupling of the $^{19}F$ dipolar
fields

References

/1/ H.-J. Stöckmann, H. Ackermann, D. Dubbers, M. Grupp, P. Heitjans,
Z. Phys. 269, 47 (1974)

/2/ A. Abragam, The Principles of Nuclear Magnetism, Oxford University
Press , p. 570 (1961)

# 3. MATERIALS RESEARCH

## 3.1. Implantation and Diffusion of Carbon into Niobium Carbide Single Crystals: Influence on the Superconducting Transition Temperature

*J. Geerk and K.-G. Langguth*

Giorgi et al. /1/ found that the superconducting transition temperatures $T_c$ of niobium and tantalum carbides varies strongly with carbon content. Their major conclusion was, that the highest $T_c$ is reached for the stoichiometric composition and any deviation therefrom results in a lowering and eventual disappearance of $T_c$. Giorgi et al. /1/ obtained an almost stoichiometric carbide of niobium corresponding to the chemical notation $NbC_{0.98}$ with a $T_c$ of 11.1 K, which is to our knowledge the highest $T_c$ for niobium carbide reported so far in literature /2/.

For the production of niobium carbide layers of different compositions we used the methods of ion implantation and diffusion from evaporated layers on niobium carbide single crystals. Single crystals of size 5 x 2 x 2 mm of $NbC_{0.89}$ with a $T_c$ of 3.7 K were implanted at room temperature with $C^+$-ions at energies of 200 keV and 80 keV and fluences of $1.5 \times 10^{17}$ $cm^{-2}$ and $5 \times 10^{16}$ $cm^{-2}$, respectively. After implantation the single crystals were annealed by means of an electron beam oven mounted in a bakable UHV system. The ultimate pressure of the system was $2 \times 10^{-10}$ torr. During the annealing process the pressure increased to $2 \times 10^{-8}$ torr. The annealing time was 200 sec. The diffused niobium carbide layers were produced by first evaporating a 600 Å carbon layer onto the $NbC_{0.89}$ single crystal and then by heating the single crystal in the UHV oven.

The diffusion time was 200 sec. The sample temperature during annealing and diffusion was measured pyrometrically. The superconducting transition temperature was measured resistivily by a four probe arrangement. A well measureable voltage drop across the sample was obtained already with a DC-current of about 40 mA because of the rather high residual resistance (180 $\mu\Omega cm$) of the single crystals. Backscattering measurements using 2 MeV $\alpha$-particles were performed in order to analyze the samples. From the measured spectrum of $\alpha$-particles backscattered from niobium atoms

we were able to determine the approximate concentration profile of the carbon in the implanted layers.

Fig. 1 shows the transition temperature of the implanted single crystal versus annealing temperature after successive annealing steps. The vertical error bars indicate the width of the transition. After implantation $T_c$ of the implanted layers increases to about 7 K. Then with increasing annealing temperature, $T_c$ increases and reaches a maximum of 11.5 K. The backscattering measurements indicate, that a surface layer of a thickness of about 2000 Å with a carbon content very close to stoichiometry forms in the temperature range between 1050 °C and 1150 °C. At higher annealing temperature $T_c$ decreases rapidly because carbon diffuses from the high $T_c$ layer into the bulk crystal. The channeled backscattering spectrum of the as implanted sample shows a pronounced defect peak in the implanted layer. After annealing between 1050 °C and 1150 °C the defect peak disappears. The high $T_c$ surface layer causes only strong dechanneling of the incoming α-particles. This indicates that this layer is almost free from interstitial Nb atoms but still contains internal strain fields and / or interstitial carbon.
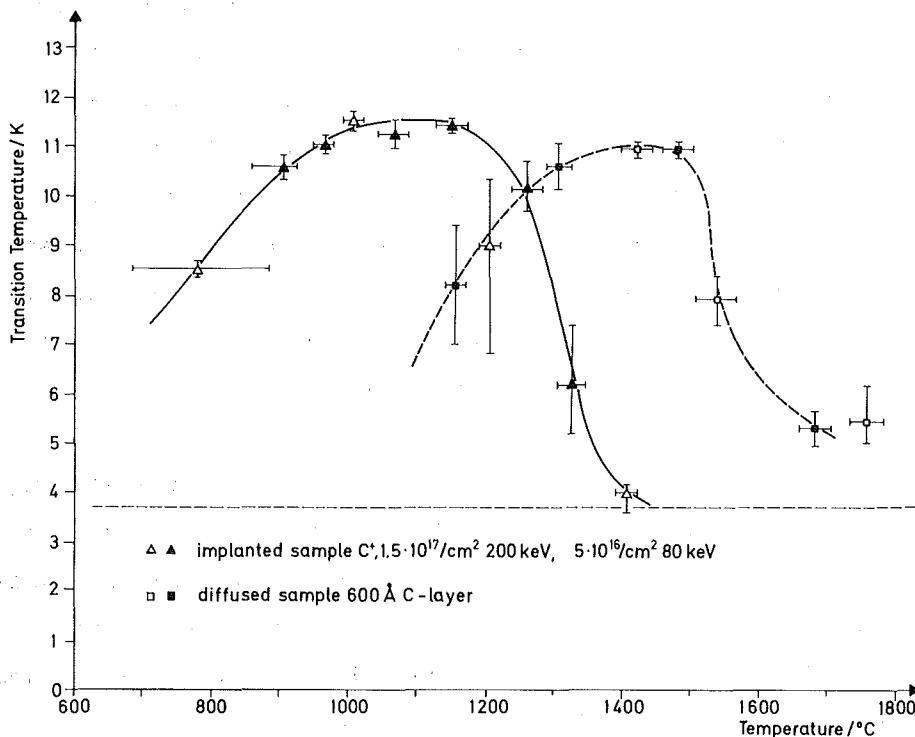


Fig. 1   Full line: Transition temperature of the implanted single crystal versus annealing temperature.

Dashed line: Transition temperature of the carbon diffused single crystals versus diffusion temperature.

The dashed curve in Fig.1 shows $T_c$ values of the carbon diffused single crystals as a function of diffusion temperature. In the temperature range where carbon diffuses out of the implanted layer in this case the diffusion of carbon from the evaporated carbon layer into the bulk is starting thus causing a rapid increase in $T_c$. At diffusion temperatures higher than 1500 $^{\circ}$C the 600 $\overset{\circ}{A}$ carbon layer gets exhausted and $T_c$ decreases rapidly with higher temperature. The maximum transition temperature obtained in the diffusion experiments was 11.0 K, which agrees with the result of Giorgi et al. /1/.

From the $T_c$ results of the implanted and diffused single crystals we conclude that by the use of the implantation technique niobium carbide layers can be produced which are slightly closer to stoichiometry than layers obtained by the diffusion technique.

References

/1/ A. L. Giorgi, E. G. Szklarz, E. K. Storms, Allen L. Bowman, and B. T. Matthias, Phys. Rev. 125, 837 (1962)

/2/ B. W. Roberts, NBS Technical Note 724, U. S. Department of Commerce (1972)

3.2. Nitrogen Implantation into Molybdenum: Superconducting Properties and Compound Formation

M. Kraatz, G. Linker, O. Meyer and R. Smithey

The implantation of several ion species into molybdenum layers leads to an increase of the superconducting transition temperature $T_c$ /1/. This effect has also been observed for nitrogen implantations but in contrast to other ions, compound formation occurs in this system. This compound formation together with the superconducting properties has been studied in dependence of implantation- and subsequent annealing temperature.

Molybdenum layers with thicknesses of 1500 - 3000 $\overset{o}{A}$ were evaporated
onto quartz substrates and implanted to maximum fluences corresponding
to 33 at. % nitrogen. Homogeneous profiles were obtained by implantation
with several different energies; the appropriate energy values and
fluences were selected by inspection of composed profile calculations
with various energy combinations. Implantations were performed at
liquid helium and at room temperature; layers were analysed by back-
scattering of $^4He^+$ ions and by X-ray diffraction.

The $T_c$ increase of the nitrogen implanted molybdenum layers was found
to be a function of fluence starting at lower concentration values
for low temperature implants and having a maximum saturation value for
both low and room temperature implants at a concentration of about
13 at. % nitrogen. A maximum $T_c$ value of about 9 K was observed for low
temperature implants. The phase with this $T_c$ value was stable against
warming up to room temperature; for room temperature implants however
a lower maximum $T_c$ of about 7 K was measured. Annealing of the implanted
samples above room temperature was accompanied by a gradual decrease of
the transition temperature ending with a sharp drop below 1.2 K together
with nitrogen loss from the layers at about 900 $^o$C.

Structural changes and modifications are still a point of investigation
but several characteristic features may already be described. X-ray
photographs from layers implanted at liquid helium temperature and
annealed at room temperature show only few broad reflexions corres-
ponding to the strongest lines of bcc molybdenum indicating a "quasi"
amorphous phase and sometimes, depending on nitrogen concentration,
lines from a fcc phase are observed. In layers which after implantation
at low temperature show only broad reflections a fcc phase is observed
after annealing above 400 $^o$C. In addition molybdenum recrystallizes
during annealing and a second not identified phase appears above
600 $^o$C. For room temperature implants besides lines from bcc molybdenum
the existence of a fcc phase is observed in the as implanted layers. This
phase emerges more distinctly in the annealing procedure and vanishes
parallel to the $T_c$ decrease at about 900 $^o$C and only lines from pure
molybdenum are revealed after annealing above 900 $^o$C.

Pavlov et al. reported the formation of a fcc phase in molybdenum after
implantation of argon /2/; such a phase was not observed in our experiments
with neon implants. Thus we explain the occurence of a fcc phase by $Mo_2N$

formation concluding from the measured lattice constant and from the disappearance of the fcc phase at 900 $^\circ$C coinciding with the decomposition of $Mo_2N$.

From our observations we conclude that there is no direct correlation between variation of the superconducting properties of molybdenum and compound formation with nitrogen implantations. The primary reason for the $T_c$ increase most probably is due to the formation of a quasi amorphous phase which must be stabilized by the chemically active nitrogen. But as the $T_c$ increase obtained with several other ions usually disappears at temperatures of about 400 $^\circ$C it is thought that the higher annealing temperature of 900 $^\circ$C necessary to depress $T_c$ below 1.2 K (the lowest temperature we can attain) in the system molybdenum-nitrogen is due to $Mo_2N$ formation as an additional effect.

Similar experiments are presently being conducted on nitrogen implantation in niobium. In this system also compound formation is observed after room temperature implants accompanied by a $T_c$ depression and no annealing effect so far (800 $^\circ$C) has been observed.

References

/1/ M. Kraatz, O. Meyer, F. Ratzel, R. Smithey; this report
/2/ P. W. Pavlov, D. I. Tetelbaum, A. W. Pavlov, E. I. Zorin;
Dokl. Akad. Nauk, 217, 330 (1974)

3.3. Enhancement of the Superconducting Transition Temperature by Ion Implantation in Molybdenum and Molybdenum-Rhenium Thin Film Alloys

*M. Kraatz, O. Meyer, F. Ratzel and R. Smithey*

Several preparation processes have been described to be suitable to increase the superconducting transition temperature $T_c$ of molybdenum ($T_c$ = 0.9 K) and Mo-based alloys.

$T_c$ is raised:

a)   when the elements Tc, Re, Ru, Os, Rh, Ir, Pd, which have larger
     electron per atom ratios (e/a) than Mo, are dissolved in it and
     form crystalline alloys /1/.

b)   for vapor quenchend Mo thin films and Mo-based alloys which are
     either amorphous or microcrystalline /2/.

c)   for ion beam deposited Mo thin films (produced by sputtering with
     an intense beam of inert gas ions) which are found to be crystalline,
     with a lattice parameter slightly larger than found for bulk Mo /3/.

The physical reason for the $T_c$ increase is not clear and may be different
for the various cases mentioned above.

Ion implantation is thought to be a suitable tool to study the super-
conducting properties in the transition region between the crystalline
and amorphous state of materials and it will be shown that the substrate
temperature during implantation is an important parameter in this respect.

Molybdenum films with thicknesses between 1500 and 4000 Å have been
prepared by electron beam evaporation. The resistance of as evaporated
Mo films has been measured routinely in dependence of the temperature
and no $T_c$ has been observed for temperatures above 1.2 K.

X-ray diffraction patterns from these films showed the Mo bcc-structure
only, with grain sizes larger than 600 Å.

In a systematic study several ion species with different electronegativities
and atomic radii have been implanted in Mo-films at liquid helium tem-
perature. No increase in $T_c$ above 1.7 K has been observed for the
following systems: Mo-Na, Mo-Mg, Mo-Al, Mo-Ga, Mo-Ne, Mo-Xe. This result
is in agreement with earlier measurements on Mo-films implanted at room
temperature where we have shown /4/ that an increase in $T_c$ is found only
for ions having a larger electronegativity value than Mo. An increase in
$T_c$ up to 9.5 K with increasing concentration to about 15 % has been
observed for the systems Mo-N (9.2 K), Mo-C (8.5 K), Mo-S (9.5 K), Mo-P
(9.2 K). These values are several degrees higher than those observed for
similar systems, produced by implantation at room temperature /4/.

For the light ions (N, C, B) the $T_c$ dependence on concentration was found to vary only slightly with ion species, the maximum observed $T_c$-values for all systems was found to be about 9.3 ± 0.2 K and this value corresponds to the maximum $T_c$-value observed for amorphous Mo-Re alloys /2/. Electronegativity and atomic radii are found to have a strong influence on the $T_c$ dependence on concentration as it is shown in Fig. 1 for the systems Mo-N, Mo-P, Mo-As, Mo-Sb. With decreasing electronegativity and increasing atomic radii $T_c^{max}$ decreases and larger concentration values are necessary in order to obtain similar $T_c$ values. In contrast to the linear dependence of $T_c$ on concentration as reported for Mo-based bulk alloys /5/ ion implanted systems reveal a superlinear behaviour. We assume that this steep increase in $T_c$ is due to microscopically distributed impurity atoms which form stable defect-impurity complexes. This complex formation seems to occur preferentially for atoms which have similar or larger electronegativity values than Mo.
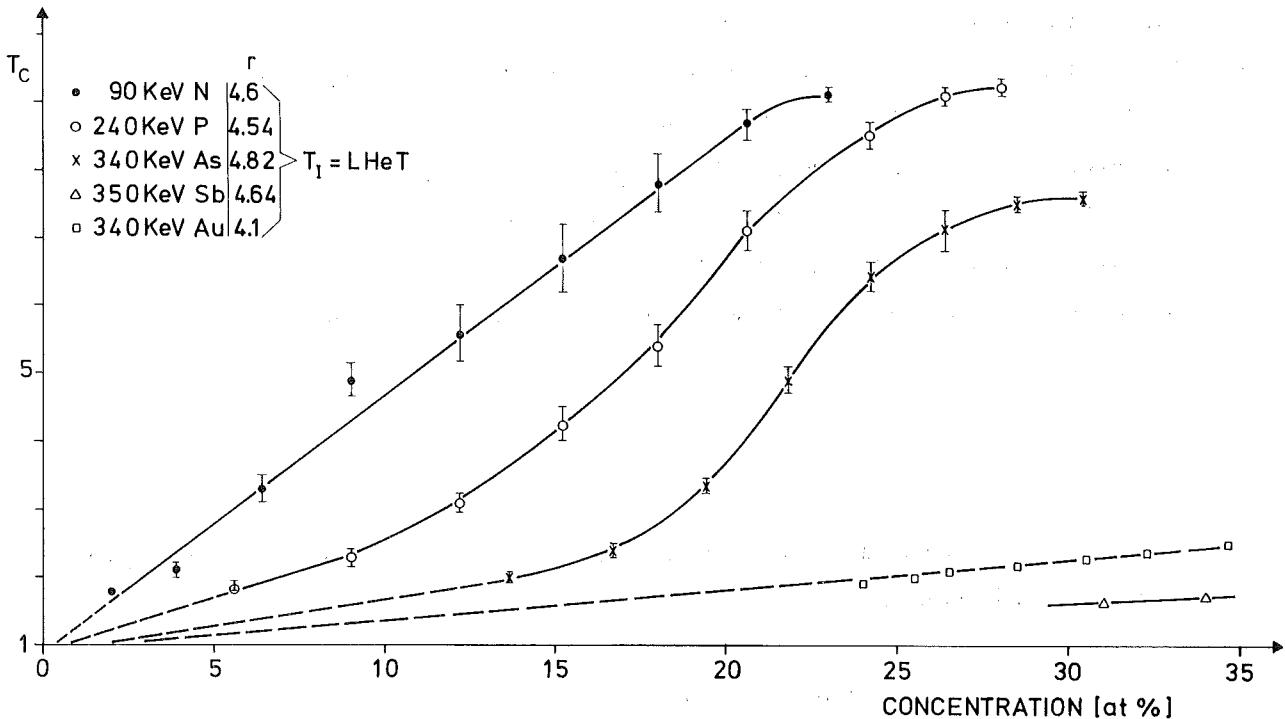


Fig. 1   Dependence of $T_c$ on the concentration for some ion implanted Mo-based systems.

No new phases could be detected in the implanted layers. A single exception to this rule is the system Mo-N, which will be discussed in a separate contribution /6/. Further experiments are underway in order to clarify the metallurgical state of the implanted systems.

Further work has been conducted in order to find out if the $T_c$ of ternary Re-based ion implanted systems could be raised above the value obtained for binary systems. $Mo_x Re_{1-x}$ alloys have been prepared by coevaporation on sapphire- and quartz substrates at room temperature. The layers revealed the bcc structure only and the $T_c$ dependence $(1.2 \le T_c \le 10.5$ K) on the composition $(0.1 \le x \le 0.5)$ was found to agree with the behaviour of bulk alloys. During evaporation on hot substrates $(1000\ ^O C)$ several not yet identified structures have been formed with a $T_c$ of 15 K. Implantation of $N^+$ ions in alloy films with $x \stackrel{<}{\sim} 0.3$ was found to increase $T_c$ up to 9.8 K whereas implantation in alloys films with $x \stackrel{<}{\sim} 0.3$ did not effect $T_c$.

Reference

/1/  B. T.  Matthias, T. H. Geballe  and V. B. Compton,

     Rev. of Modern Physics 35, 1 (1963)

/2/  M. M. Collver and R. H. Hammond,

     Phys. Rev. Letters 30, 92 (1973)

/3/  P. H. Schmidt, R. N. Castellano, H. Barz, A. S. Cooper and

     E. G. Spencer, J. Appl. Phys., 44, 1833 (1973)

/4/  O. Meyer, J. Jap. Soc, Appl. Phys. 44, Suppl. 23 (1975)

/5/  B. T. Matthias, E. A. Wood, E. Corenzwit and V. B. Bala,

     J. Phys. Chem. Solids 1, 188 (1956)

/6/  M. Kraatz, G. Linker, O. Meyer and R. Smithey, this report

3.4.    Superconducting Transition Temperature in Ion Implanted
        Re-Based Systems

M. Kraatz, O. Meyer and R. Smithey

The $T_c$ of Re is known to depend on the metallurgical history of the specimen and in cold worked samples $T_c$ is raised about 1 K above the value of 1.7 K for a pure, strainfree sample /1/. Therefore we expected that radiation damage should increase the $T_c$ of Re.

Re thin films have been produced by evaporation on quartz- and sapphire-substrates. Independent of the substrate temperature and the vacuum conditions during evaporation the Re films always revealed a $T_c$ of 2.7 K, which is 1 degree higher than the bulk value similar to cold worked samples. In contrast to other transition metals such as V, Nb, Ta, and Mo radiation damage, produced by implantation of Ar ions, was found to increase $T_c$ up to 4 K in the Re films.

Alloying effects on $T_c$ have been observed for the following ion implanted Re-based systems: Re-Y (9 K), Re-La (7.8 K), Re-Zr (7.7 K) and Re-Ti (7.4 K). These results are found to be in agreement with Re-based bulk alloys where it is known that the addition of transition elements with smaller e/a values than Re will increase $T_c$ up to 9 K. Implantation of non-transition elements in Re was found to increase $T_c$ up to 8.2 K (Re-Li (7.2 K), Re-Be (7.3 K)). Further results obtained for the systems Re-N (5.5 K), Re-H (3.4 K), Re-Cs (4.3 K), Re-Mg (5.1 K) and specially Re-Ar (3.5 K) are thought to be due to the influence of radiation damage on $T_c$. The differences in $T_c$ ($\sim$ 1 K) between RT and LHeT implants were found to be small and annealing to 800 $^{\circ}$C did not affect $T_c$.

References

/1/ J. K. Hulm, B. B. Goodman, Phys. Rev. 106, 659 (1957)

3.5. Superconducting Transition Temperature of Ion Implanted Al and Pb Thin Films

*M. Kraatz, O. Meyer and R. Smithey*

In our previous work /1/ we have shown that for Al based alloys the dependence of $T_c$ on composition is completely different from what is observed for similar implanted systems produced at RT. The conclusion was, that the implanted ions come to rest in a disturbed local environment and that local stresses might lead to a decrease in density followed by an increase in $T_c$. This work has been continued by ion implantation at LHe temperature in order to see if there are systems, where prevention

from precipitation and annealing will result in a further increase in $T_c$. In contrast to RT implants /1/ the largest increase in $T_c$ has been found for the system Al-Ge (6 K). This $T_c$-value is in agreement with results obtained for vapour quenched Al-Ge systems /2/. After annealing to RT, $T_c$ decreases to 3.5 K. An increase in $T_c$ up to 4.5 K has been observed for vapour-quenched Al in $H_2$-atmosphere /3/ and the authors assumed that this increase of $T_c$ is due to hydrogen coating of granular Al. We implanted hydrogen ions in crystalline Al and observed an increase of $T_c$ up to 5 K. Our result can not be explained by the assumption given above. For the system Al-Ca (3.5 K) $T_c$ was found to be about twice the value observed for RT implants, whereas $T_c$-values for the systems Al-P (2.1 K) and Al-S (21. K) agree with those observed for RT implants. These results only partly fulfill our expectations and work is in progress to study some effects in more detail.

For Pb-films it is known that neither radiation damage nor gaseous impurities during co-evaporation will affect its $T_c$ and this was thought to be a valuable starting condition to study alloying effects in Pb based ion implanted systems. The $T_c$ dependence on the composition for bulk alloys of $Pb_xAs_{1-x}$, $0.97 \leq x \leq 1$ and $Pb_xBi_{1-x}$, $0.8 \leq x \leq 1$ levels off at $T_c$ (max) = 8.4 K for x = 0.97, and 8.8 K for x = 0.8 respectively due to the approach of the solid solubility level /3/.

Ion implantation of As in Pb at liquid helium temperature was not found to affect the $T_c$ of 7.2 K, however after annealing to RT $T_c$ increases up to 8.5 K. We believe that As-defect complexes form after implantation at liquid helium temperature and that this defect complexes anneal out at RT so that the As atom will become substitutional. The implantation temperature seems to be an important parameter which will be subject of further investigations.

## References

/1/ O. Meyer, Ion Implantation in Semiconductors S. Namba ed. Plenum Press N. Y. 1975 p. 301

/2/ A. Fontaine, F. Meunier, Phys. Kondens. Materie 14, 119 (1972)

/3/ G. Deutscher, M. Posternak, Phys. Rev. B10, 4042 (1974)

/4/ R. C. Dynes, J. M. Rowell, Phys. Rev. B11, 1884 (1975)

## 3.6.    Search for High Superconducting Transition Temperature in Nb$_3$Pb

*T. Chakupurakal and O. Meyer*

A Niobium-lead compound with an A15 phase does not form easily /1/ due to an unfavourable atomic size ratio and hence only few studies on this system exist. The present study was intended to investigate whether a Nb$_3$Pb compound does possess an A15 structure with a high transition temperature.

By vacuum evaporation and co-condensation method thin superconducting Nb$_3$Pb films were prepared on quartz and sapphire substrates. The substrate temperature (T$_2$) was varied from room temperature to 800 °C and the film thickness (t) ranged from 1000 Å to 3000 Å. The thickness was measured by a crystal oscillator and controlled by a stylus in- strument. The compositional analysis and layer stoichiometry was determined by high energy $^4$He$^+$ backscattering techniques and structural analysis by X-ray diffraction. The transition temperature (T$_c$) was measured by the standard four probe resistive method, before and after annealing the samples.

In order to prepare thin films of various compositions at a fast rate, we designed and constructed a Four Fold Target Holder (FFTH) with substrate heating facilities. A schematic diagram is given in Fig. 1. Each of the four arms of the FFTH contains four or more substrates (S) mounted on it. By operating a push-pull rotating feed-through (F) the system can be turned 90 ° thereby bringing the adjacent arm in contact with the heating unit. The electron gun (EG) heats the Mo-plate (MP) and the substrate plate (SS) whose temperature is measured with a NiCr-Ni thermocouple, fixed to the arm of the base plate (BP). (MP) and (SS) are brought together by the spring (SP). To avoid friction a ball bearing (BB) is provided. (SS) is thermally well isolated from (BP).

The system has the definite advantage that in each cycle a number of films of the same material can be prepared at various evaporation rates, thicknesses, and substrate temperatures without disturbing the vacuum. Though during evaporation the vacuum in the chamber drops from 10$^{-8}$ to 10$^{-7}$ torr, the heat radiated from the evaporation process and from the
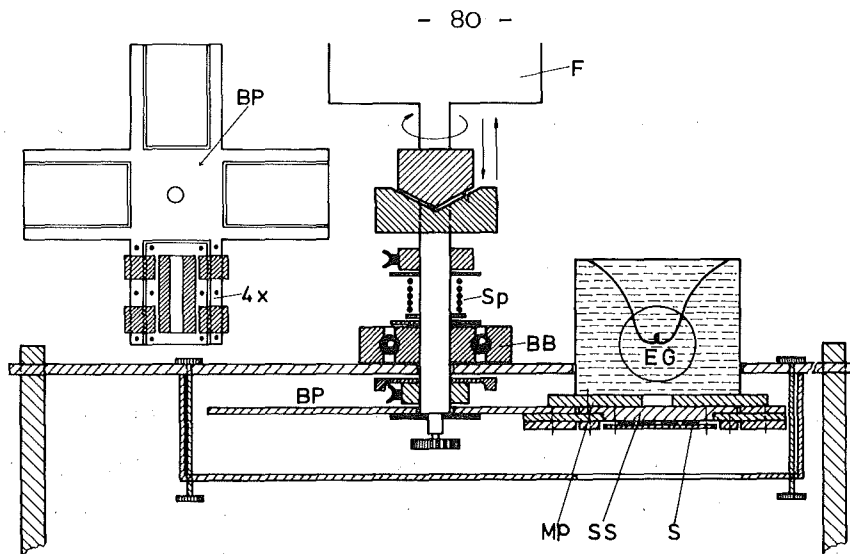
Fig. 1   Four Fold Target Holder (FFTM)

substrate heating unit will bake out the entire system for the subsequent evaporation and the vacuum improves rapidly. Before evaporating $Nb_3Pb$, the chamber was pre-evaporated with Pb /2/ to increase the probability that Pb atoms will stick to the substrate material along with the Nb atoms. While evaporating, the Nb to Pb ratio was maintained 3 : 1 to obtain nearly perfect A15 structure.

The layer composition was analysed with the backscattering technique and it was found that the Nb-Pb films consisted of Nb and Pb, almost in the 3 : 1 ratio. X-ray diffraction showed the existence of an A15 phase in this compound. The lattice constant was determined as 5.41 ± 0.06 Å.

| Sample | rate of evaporation in Å/sec | Substrate temperature °C | Thickness Å | $T_c$ K |
|---|---|---|---|---|
| $Nb_3Pb$ 10375 | Nb 9 - 10 Pb 3 - 4 | 330 | 2100 | 6.1 |
| $Nb_3Pb$ 10475 | Nb 9 - 10 Pb 3 - 4 | 400 | 2600 | 8.0 |
| $Nb_3Pb$ 25375 | Nb 7 - 8 Pb 3 - 4 | 500 | 1500 | 8.1 |
| $Nb_3Pb$ 1475 | Nb 4 - 5 Pb 1 - 2 | 600 | 1660 | 9.3 |

Table  1   Production parameters of the Nb-Pb films and their $T_c$-values.

In $Nb_3Pb$ we observed $T_c$-values ranging from 1.5 K to 9.3 K. We were not able to correlate $T_c$ directly with the A15 phase because in some films additional lines of pure Nb and Pb and even other phases were detected. Contrary to the expectation in literature /3/ we could not obtain the A15 structure with transition temperatures above 10 K. $T_c$ is found to increase with substrate temperature (Table 1), however above 800 °C we could not detect any $T_c$. Annealing the film did not improve $T_c$.

References

/1/  N. Morton, Cryogenics, P. 224, April (1974)

/2/  L. Kammerdiner and H. L. Luo, J. Appl. Phys. 45, 4590 (1974)

/3/  J. M. Leger, Journal of Low Temperature Phys. Vol. 14, No. 3/4
     (1974)

## 3.7.    Properties of Sputtered Vanadium Nitride Thin Films

*B. Hofmann-Kraeft, F. Ratzel and R. Smithey*

For studying the superconducting isotope effect of a refractory nitride
we need samples with a high superconducting critical transition tem-
perature ($T_c$) and a pure cubic phase. Vanadium nitride (VN) has a
reported $T_c$ of 8.5 - 9.2 K for the bulk /1/ and no other phase coexists
in its cubic homogeneity range. So VN is a suitable substance.

We produced thin films of VN by reactive sputtering in an argon-
nitrogen plasma. The substrate temperature $T_s$ at the beginning of the
sputtering process was varied between 20 $^\circ$C and 700 $^\circ$C.

We examined our films applying the following methods:

(1)  stylus instrument measurements for film thicknesses, e.g. deposition
     rates

(2)  the four-point probe resistance technique for the $T_c$ values

(3)  scanning electron microscopy for the topography of the layer surface

(4)  Rutherford backscattering of 2 MeV $^4$He$^+$-ions for the total concen-
     tration ratio Y (number of nitrogen atoms/number of Vanadium atoms)

(5)  X-ray measurements for the lattice constant $a_o$.

The experiments reveal the following properties:
Film thicknesses vary between 2000 and 4000 Å according to the duration
of the sputtering process and the Ar/N ratio in the plasma.
The dependence of $T_c$ on the substrate temperature $T_s$ is shown in Fig. 1.
$T_c$ increases with $T_s$ and saturates for $T_s \geq$ 600 $^\circ$C at 9.0 - 9.2 K, in
agreement with values reported for the bulk /1/. There is no difference

in $T_c$ for layers deposited on quartz and sapphire substrates. For low $T_s$ sputtering in pure nitrogen causes a depression of $T_c$ by about 0.5 - 1 K. This may be caused by the lower deposition rate, which increases the impurity content of the layers. Generally the transition width is about one quarter of a degree.
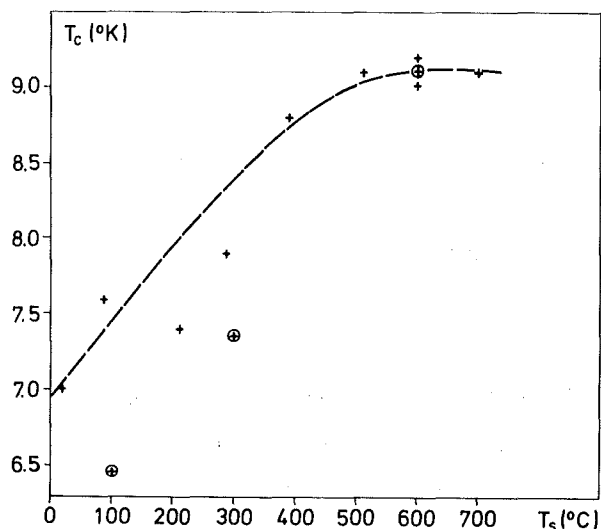


Fig. 1   Critical Temperature **versus**
Substrate Temperature
(Plasma conditions:
+ : $2 \times 10^{-2}$ Torr Argon +
$2 \times 10^{-2}$ Torr Nitrogen;
⊕ no Argon, $\sim 3 \times 10^{-2}$ Torr
Nitrogen).
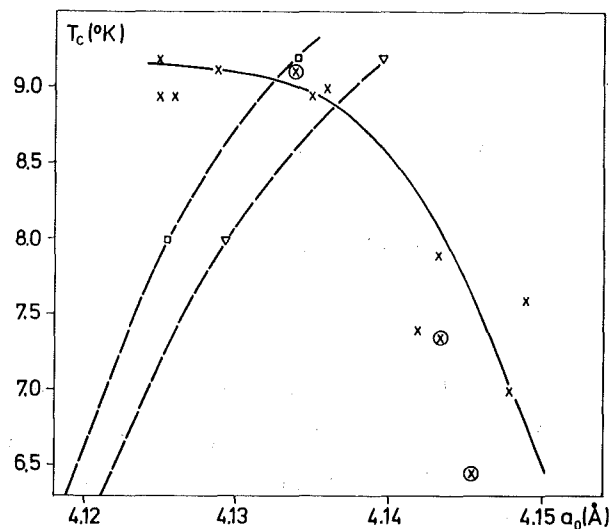
Fig. 2   Critical Temperature
versus Mean Lattice
Constant (x : VN thin
films sputtered in Argon-
Nitrogen, ⊗ : no argon;
☐ : Data from Hahn /3a/
and Toth /2/; ∇ : Data
from Brauer /3b/ and Toth.

The layer surfaces show two different types of topography: For $T_s \leq 300\,^{o}C$ the surface is rough, whereas for $T_s \geq 500\,^{\circ}C$ the surface is smooth but cracked because of the different thermal expansion coefficients of quartz and VN.

In contrast to bulk VN /2/ $T_c$ was found not to depend strongly on Y. This may be due to the fact that the polycrystalline films consist of crystallites of different Y and $T_c$. The resistance technique, however, only yields the highest $T_c$, and from backscattering measurements we get an averaged Y.

The X-ray diffraction scans indicate that all samples have a pure NaCl-structure. The Bragg peaks show a considerable line-broadening, corres-

ponding to a variation in the lattice constant $a_0$ of $\pm$ 0.3 %. For $T_s > 500\ ^{\circ}C$ and $T_c \sim 9$ K the mean lattice constant $a_0$ is in agreement with data reported by Brauer /3b/ for nearly stoichiometric VN. Combining the data for $a_0$ (Y) from Hahn and Brauer /3/ with those for $T_c$ (Y) from Toth /2/, we find, however, a deviating correlation between $T_c$ and $a_0$ (Fig. 2). This supports our assumption that $T_c$ is not constant over the whole layer. For $T_s \leq 300\ ^{\circ}C$ the mean lattice constant $a_0$ is greater than 4.14 Å. This expansion of the lattice is directly correlated with the reduction of $T_c$ and is in contrast to all data reported for the bulk.

For further investigations we intend to apply the induction method for the determination of $T_c$. This will yield better information on the homogeneity of the layers and may allow to relate the different properties of the films more precisely.

## References

/1/  a) Pessal, Hulm, Walker: Westinghouse Research Lab., Final Report AF 3 3(615) - 2729 (1967)

    b) Toth, Wang-Yen, Acta Met. 14, 1403 (1966)

/2/  Toth: Transition Carbides and Nitrides, Academic Press, New York and London, p. 221, Fig. 3

/3/  a) Hahn, Z. Anorg. Allg. Chemie 258 (1949) 58/68, p. 63

    b) Brauer, Schnell, J. Less-Common Metals, 6, 326 (1964)

3.8.    Enhanced Decrease of the Superconducting Transition Temperature in some Heavy Ion Irradiated Transition Metal Layers

*M. Kraatz, G. Linker and R. Smithey*

A decrease of the superconducting transition temperature $T_c$ in transition metal superconductors, especially in niobium, has been already reported for neutron /1/, deuteron /2/ and oxygen /3/ irradiated samples and also

for cold-worked material /4/. The effects observed in these experiments were small and $T_c$-depression did not exceed a few percent. In contrast to these results bombardment with heavy ions in the energy range of several hundred keV leads to an enhanced reduction of $T_c$ the maximum effects being comparable with results obtained for layers condensed onto cryogenic substrates.

The defect production method and first results obtained for heavy ion irradiated vanadium, niobium and tantalum layers have been already described /5/. Further experiments have been performed to correlate $T_c$-reductions with radiation damage and to study whether oxygen con- tamination and/or structural changes occur in bombarded layers. In addition irradiations at low temperatures have been started. Vanadium layers were bombarded with different ions ($He^+$, $Ne^+$, $Ar^+$), and the energies deposited into nuclear collisions on the paths of the penetrating particles were calculated. The fluences for the various ion-energy systems were chosen in such a way that approximately the same energy densities were generated in the layers. The data together with the resulting depression of $T_c$, $-\Delta T_c$ are shown in a table.

| Ion | Vanadium d in Å, Substrate | $E_0$ (keV) | Fluence (Ions/cm²) | Deposited Energy eV/(Åcm²) | $-\Delta T_c$ |
|---|---|---|---|---|---|
| $He^+$ | 2000/Quartz | 70 | $4.7 \cdot 10^{17}$ | $3.5 \cdot 10^{17}$ | 0.95 |
| $Ne^+$ | 1100/Quartz | 180 | $2.0 \cdot 10^{16}$ | $5.4 \cdot 10^{17}$ | 1.15 |
| $Ne^+$ | 2000/Quartz | 320 | $2.9 \cdot 10^{16}$ | $5.0 \cdot 10^{17}$ | 1.30 |
| $Ne^+$ | 2000/SiO₂/Au/V/Au | 320 | $2.7 \cdot 10^{16}$ | $4.9 \cdot 10^{17}$ | 1.20 |
| $Ar^+$ | 1100/Quartz | 320 | $7.8 \cdot 10^{15}$ | $4.6 \cdot 10^{17}$ | 1.10 |

Tab. 1  Properties of the irradiated layers

The scattering in the $\Delta T_c$-values is not greater than that observed for irradiations performed under identical conditions and confirms our conclusion that the observed $T_c$-reduction are due to radiation damage.

It is well known that small amounts of oxygen interstitially dis-
solved in vanadium, niobium and tantalum considerably lower the
transition temperature /6/. We have examined whether knock on oxygen
atoms from oxide surface layers could influence our results. An
estimation of the average transferred energy and the total cross
section e.g. for Ne ions impinging on oxygen indicates that knock
on atoms would be displaced mainly within an oxide layer itself.
In addition, samples were prepared either on quartz substrates
convered with a 100 $\overset{o}{A}$ thick gold layer or on single crystal silicon
to avoid oxygen contamination from the substrates, and on top of
these layers a thin (200 $\overset{o}{A}$) gold protection film was evaporated in
situ and irradiations were performed through this film. Layers
protected in this way did not show oxide surface peaks in backscattering
measurements but $T_c$ depressions after bombardment agreed with results
obtained from unprotected layers. Also XPS spectra were taken from
bombarded and not bombarded samples as a function of depth employing
the sputtering technique for removal of the gold protection films and
parts of the superconducting layers. Though no quantitative analysis
of oxygen content has been performed so far, no increase of the oxygen
peak intensities has been observed in the bombarded layers. Thus we
conclude that knock on oxygen atoms did not influence the $T_c$-depressions.

X-ray diffraction patterns from damaged layers usually showed the V,
Nb or Ta bcc-structure and no distortions of this structure were observed
when compared with measurements from as evaporated layers. Nb-samples
irradiated with very high fluences (> 2 x $10^{17}$ $Ne^+/cm^2$) however showed
structural changes (only the strongest reflexions were observed with
considerable line broadening) together with unusual wide transition
widths. Also backscattering measurements support the argument that
inhomogeneous macroscopic distortions occured in these layers. They
may be due to discontinuous material removal during irradiations.

Preliminary experiments with bombardments of Nb layers with Ne ions
have been performed at liquid helium temperature. The results from
these experiments indicate that $T_c$-depressions are comparable to
those obtained at room temperature and little annealing occurs from
liquid helium to room temperature. Thus it may be concluded that the
$T_c$ reductions are due to defect clusters stable at room temperature.
Further experiments are underway to clarify this issue.

## References

/1/   R. H. Kernohan and S. T. Sekula, J. Appl. Phys. __38__, 4904 (1967)

/2/   H. T. Coffey, E. L. Keller, A. Patterson and S. H. Autler,
      Phys. Rev. __155__, 355 (1967)

/3/   S. Klausmünzer, G. Ischenko and P. Müller, Z. Phys. __268__, 189
      (1974)

/4/   S. J. Thompson  and P. F. J. Flewitt, J. Less-Common Metals, __40__,
      269 (1975)

/5/   G. Linker and O. Meyer, Int. Conf. Ion Impl. Semicond. other
      Materials, OSAKA, Aug. 1974

/6/   W. Desorbo, Phys. Rev. __132__, 107 (1963)

## 3.9.     Electron-Optical Phonon Coupling in Superconductors

*H. Rietschel*

The role of the optical phonons in superconductors with different atomic masses $M_K$ has been investigated. It has been shown that the electron mass enhancement factor $\lambda$ is independent of $M_K$, but depends rather on the inverse force constant matrix. However, when using $\lambda$ to calculate the superconducting transition temperature $T_c$, $\lambda$ must be decomposed into its acoustical and optical contributions, which depend separately on $M_K$. This gives rise to a mass dependence of $T_c$ which is different from the usual BCS-result.

Studying the interference scattering from a light and a heavy mass for a linear diatomic chain and within the free electron approximation, it is shown that a decomposition of $\lambda$ in heavy and light mass contributions is generally impossible. Numerical results are presented for a rocksalt structure crystal with nearest and next nearest neighbour coupling. These results indicate that the optical phonon contribution to $\lambda$ may substantially increase $T_c$. Within the model $T_c$ turns out to be a weakly decreasing function of the decreasing light mass.

3.10.   Preparation of TiC Single Crystals [*]

B. Scheerer, J. Fink and W. Reichardt

Abstract

TiC single crystals were prepared by vertical zone melting for measurements of the phonon dispersion by inelastic neutron scattering. The influence of the starting material and of the growing conditions on the growth of the crystals were studied. The crystals were characterized by chemical methods, EMX and neutron diffraction. It was possible to grow single crystals with a volume of up to 0.6 cm$^3$ and a mosaik spread of less then 0.4 $^{\circ}$.

3.11.   Die Zucht von NiMn-Einkristallen

B. Scheerer

Für Untersuchungen der Spindichteverteilung und Magnonendispersion durch Neutronenstreuung an NiMn-Legierungen werden Einkristalle mit einer Mosaikbreite $\leq$ 0.5 $^{\circ}$ benötigt.
Erster Versuch, Kristalle nach dem Czochralski-Verfahren aus der Schmelze zu ziehen, schlugen fehl. Die erhaltenen Proben waren durchweg polykristallin. Die weiteren Ziehversuche wurden nach dem Bridgman-Verfahren durchgeführt und es gelang,hinreichend große Einkristalle im Konzentrationsbereich 5 - 20 at. % Mn zu züchten.

Die Kristallziehanlage ist mit einem 40 KW, 250 KHz HF-Generator ausgestattet und erlaubt Arbeiten im Vakuum und unter Schutzgas bis 20 atü. Die NiMn-Ziehversuche wurden unter einer Argon-Schutzgasatmosphäre bei 760 Torr vorgenommen. Abb. 1 zeigt die Anordnung im Inneren der Anlage mit HF-Spule, Graphitrohr und wassergekühltem Kupferring. Die NiMn-Probe

| | |
|---|---|
| 4 | Graphitrohr |
| 3 | $Al_2O_3$-Tiegel |
| 2 | $Al_2O_3$-Pulver |
| 1 | NiMn-Probe |
| 5 | Zwischenstück |
| 6 | HF-Spule |
| 7 | Graphitring |
| 8 | BN-Isolierring |
| 9 | wassergekühlter Kupferring |
| 10 | wassergekühlte Tiegelwelle |
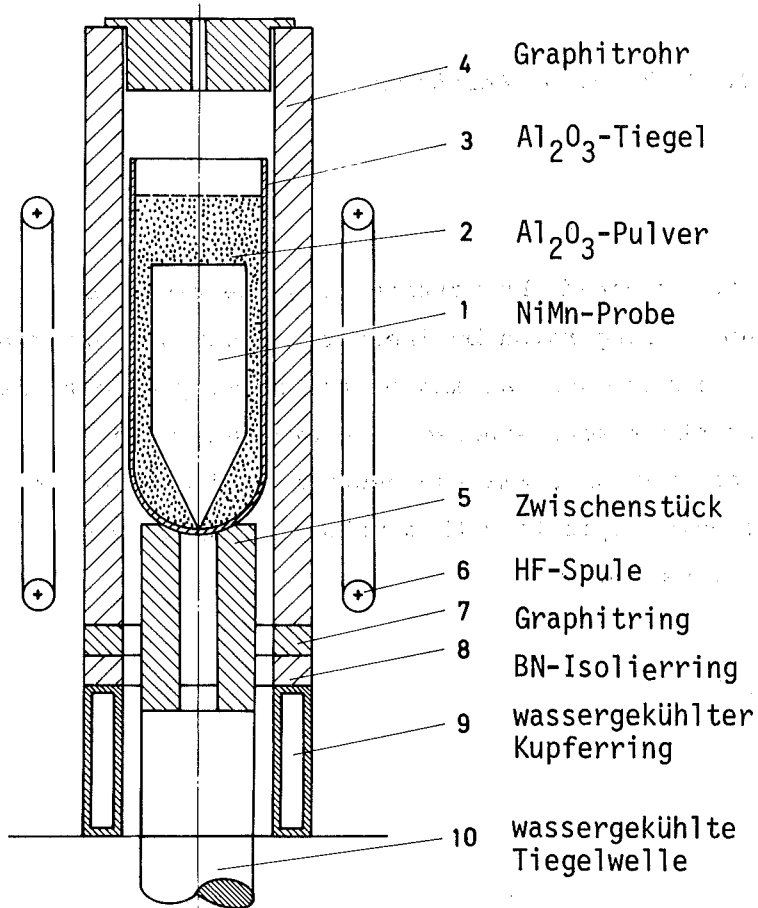
Abb. 1    Aufbau zur NiMn-Kristallzucht
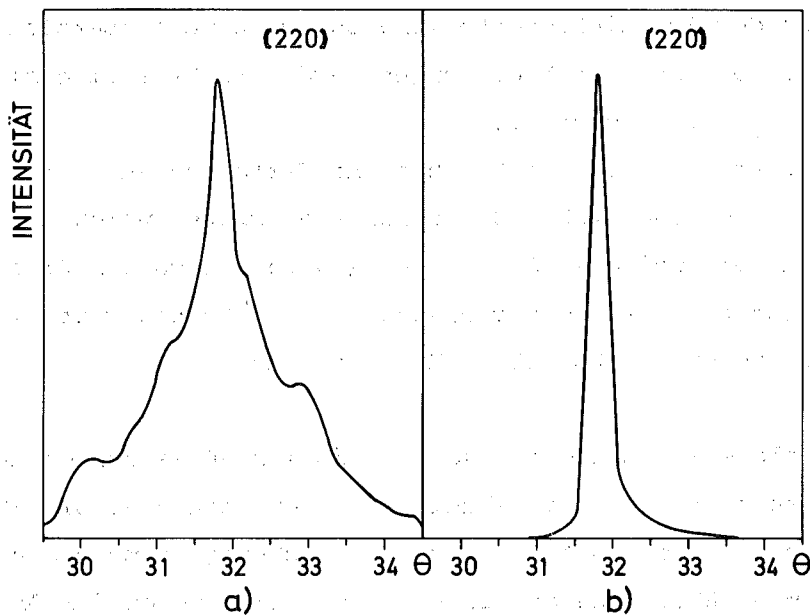


Abb. 2    Rockingkurve des Kristalls, a) vor und b) nach dem Tempern.

wurde im Tiegel in $Al_2O_3$-Pulver eingebettet. Während des Ziehvorgangs war der Tiegel auf der wassergekühlten Tiegelwelle aufgesetzt und wurde mit einem Vorschub von 2 mm/h abgesenkt.

Photographische Aufnahmen des Kristalls im Neutronenstrahl und eine Rockingkurve (Abb. 2a) gaben Aufschluß über die Güte des gezüchteten Kristalls. Die gewonnen Einkristalle hatten üblicherweise eine Mosaikbreite von 2 bis 4 Grad.

Durch Tempern knapp unterhalb des Schmelzpunktes gelang es in den meisten Fällen, die Breite der Mosaikverteilung wesentlich herabzusetzen (Abb. 2b).

Die Kristalle wuchsen mit der Ziehachse vorzugsweise in $[11\bar{1}]$-Richtung. Die chemische Analyse, durchgeführt im Institut für Material- und Festkörperforschung (IMF), zeigte eine unterschiedlich starke Entmischung nahezu aller Kristalle, was entsprechend dem Phasendiagramm /1/ zu erwarten war. Orientierte einkristalline Scheiben wurden durch Funkenerosion aus dem Kristall herausgetrennt.

Die Zucht von NiMn-Einkristallen weiterer Konzentrationsbereiche wird fortgesetzt. Außerdem soll durch geeignete Maßnahmen versucht werden, Kristalle mit einer besseren Mn-Homogenität herzustellen.

References

/1/  M. Hansen, Constit. of Binary Alloys, 2. Ed., 938 (1958)

3.12.     Herstellung von VC-Einkristallen

*B. Scheerer*

Ausgehend von gepreßten Stäben aus VC-Pulver mit einem Kohlenstoffanteil von $C_{gesamt} = 46.75$ at. % und $C_{frei} = 0.21$ at. % ($VC_{.870}$) wurden Einkristalle nach dem tiegelfreien Zonenziehverfahren hergestellt.

Es genügte ein einmaliges vertikales Zonenziehen der Stäbe unter einer Schutzgasatomsphäre von 10 atü Argon. Die geschmolzenen Proben hatten einen Durchmesser von ca. 10 mm und eine Länge von ca. 100 mm. Aus diesen Stäben wurden Einkristalle mit Volumina von ca. 1 cm$^3$ herausgesägt.

Für die Kristalle ergab die chemische Analyse die Werte von $C_{gesamt} = 46.6$ at. % und $C_{frei} < 0.02$ at. % ($VC_{.873}$).

## 3.13. Preparation of the Linear Conductor $(SN)_x$

*L. Pintschovius*

Recently $(SN)_x$ has attracted considerable interest because it represents a new type of quasi one-dimensional conductors. As a first step $S_4N_4$ was synthesized following the method of Arnold, Hugill and Hutson /1/ by passing ammonia into $S_2Cl_2$ in $CHCl_3$ as diluent. $S_4N_4$ was isolated from the reaction mixture and purified by repeated recrystallizations.

In order to convert $S_4N_4$ into $(SN)_x$ we have set up a device similar to that designed by Douillard /2/ (see fig. 1). It is shielded by two plates of plexiglas because of the explosiveness of the intermediate products. $S_4N_4$ is heated to 100 $^{\circ}$C under vacuum and the vapors are passed over silver wool held at a temperature of about 150 $^{\circ}$C. The silver acts as a catalyst for the splitting of $S_4N_4$ into $S_2N_2$. Undecomposed $S_4N_4$ is trapped out at the lower part of a cold finger while at the upper part of the cold finger some $S_2N_2$ is deposited which soon polymerizes to $(SN)_x$. By attaching a substrate to the cold finger it is possible to grow films of $(SN)_x$.

The bulk of $S_2N_2$ is collected in a cold trap at liquid nitrogen temperature. When the cold trap is slowly warmed up small single crystals of $(SN)_x$ grow by condensation and polymerization of $S_2N_2$ vapor.
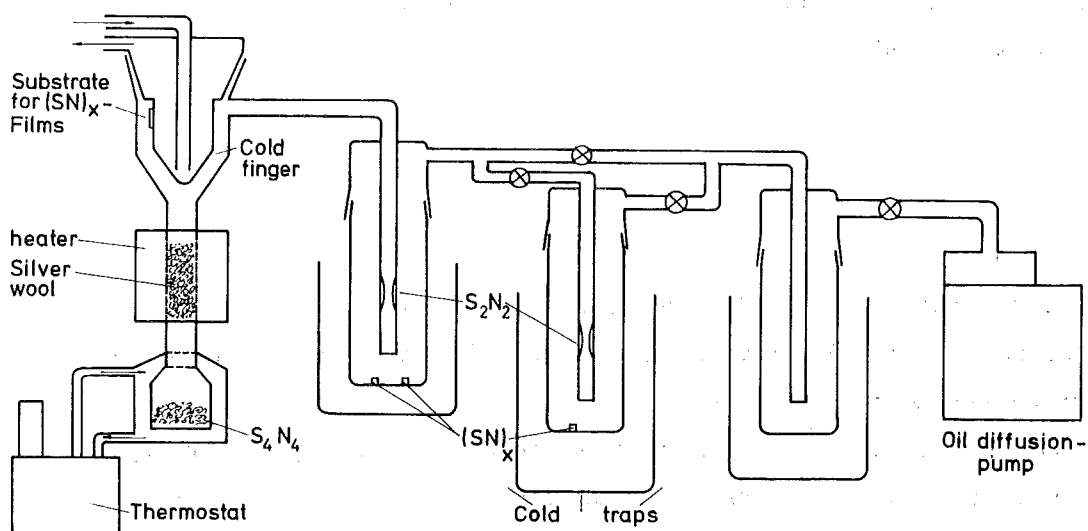
Fig. 1  Apparatus for preparation of $(SN)_x$-crystals

## References

/1/  M. H. M. Arnold, J. A. C. Hugill, J. M. Hutson, J. chem. Soc.
p. 1648 (1936)

/2/  A. Douillard, Thesis, University of Lyon, (1973)

3.14.    Optical Investigations of the Linear Conductor $(SN)_x$

L. Pintschovius

H. P. Geserich and W. Möller, Institut für Angewandte Physik
University of Karlsruhe

Films and single crystals of $(SN)_x$ were grown as described in the
previous chapter. Up to now the crystals were too small ($\sim 1$ mm$^3$)
for neutron investigations but suitable for electrical and optical
measurements. First results are published in a paper with the

following abstract:

Abstract

The optical reflectivity of (SN)$_x$ single crystals was measured in
the visible region and the near infrared with light polarized parallel
and perpendicular to the polymer chain axis. Whereas the reflectivity
for light polarized perpendicular to the chain axis is approximately
constant in this region, the reflectance for light polarized parallel
to the chain axis exhibits a pronounced plasma edge at 2.72 eV. A
simple Drude model was used to analyse the data. Differences between these
results and those of previous film measurements are discussed.

Further optical investigations are in progress in cooperation with the
Institut für Angewandte Physik of the University of Karlsruhe and with
the Max-Planck-Institut für Festkörperforschung at Stuttgart.

# 4.    D A T A   P R O C E S S I N G

## 4.1   An Interactive Computer Graphics Approach for
## Determining the Pairpotential of a Liquid

*W. Abel*

Within the framework of the pair theory the pair potential $v(r)$
is related to the pair correlation function $g(r)$ and the triplet
correlation function $g_3(r,s,t)$ by

$$\frac{\partial}{\partial r}\left[\ln g(r) + \frac{v(r)}{kT}\right] = \frac{\pi\rho}{r^2} \int_0^\infty \frac{1}{kT}\frac{\partial v(s)}{\partial s}\, ds \int_{|r-s|}^{r+s} \frac{g_3(r,s,t)}{g(r)}(t^2 - r^2 - s^2)\, t\, dt \tag{1}$$

where r.s.t are the relative distances between three particles. In
order to determine an "experimental" $v(r)$ by means of eq. (1) it is
necessary to separate $g_3(r,s,t)$ as follows /1/

$$g_3(r,s,t) = g(r)g(s)g(t) - \gamma(r)\gamma(s)\gamma(t) \tag{2}$$

$\gamma(r)$ can be obtained by measuring the pressure derivative of $g(r)$.
Since $v(r)$ is very sensitive to variations in $\gamma(r)$, it is helpful
to use an interactive computer graphic method in studying how the
variations in $\gamma(r)$ (within the experimental error bars) are reflec-
ted in $v(r)$. For this purpose an on-line manual iteration technique
has been developed using interactive graphical computing with an
IBM/2250-1 display unit connected to an IBM/370-168 computer. The
provision of facilities allowing the user to interact with the
program via light pen or function keyboard has the distinct advantage
over the conventional batch-processing computational method that a
user can quickly obtain an insight into the behaviour of the computed
results which are essentially graphic rather than numeric. By modi-
fying the function $\gamma(r)$ on the screen with a light pen the user can
observe the influence of his action on the potential $v(r)$. Further-
more, the user can also investigate how the integrals in eq. (1) are

affected by changing the shape of $\gamma(r)$. Several iteration steps can be compared so that the user can observe whether the process converges or not.

The interactive graphic program will be used to study the pair potential of liquid rubidium /2/.

References

/1/ P. A. Egelstaff et al., J. Phys. C.: Solid State Phys., 4 1453 (1971)

/2/ R. Block, KFK 2054, 35 (1974)

## 4.2 A System of FORTRAN-4-Routines for the Calculation of Phonon Density of States from measured TOF-Spectra of Polycrystals

*J.-B. Suck and W. Reichardt*

Starting from the TOF-spectra or scattering laws given by TIFLIS /1/ a system of programs was written for the determination of the phonon density of states. For coherent scatterers the incoherent approximation is used in the multi-phonon corrections.

In a first step the TOF-spectra or scattering laws are converted to double differential cross-sections, because only these may be added to a full data set, if separate measurements were made in different regions of scattering angles. Before all spectra are summed over the scattering angles $\theta$ to a weighted $(\sin \theta)$ sum-spectrum, some corrections - including the optional removal of the Debye-Waller-factor - may be applied to each of the spectra. From this sum-spectrum $S_o(E)$ a zeroeth order frequency distribution is calculated according to eq. (1)

$$G(\hbar\omega) = S_o(E) \; e^{\alpha\lambda} \; \frac{4\pi}{\sigma} \; \frac{k_o}{k} \; \frac{2M}{\hbar^2} \; \frac{\hbar\omega(e^{\beta}-1)}{\sin\theta_m \; \sin\theta_h \; (k_o^2 + k^2 - 2k_o k \cos\theta_m \cos\theta_h)} \quad (1)$$

$\theta_m = (\theta_{max} + \theta_{min})/2$, $\theta_h = (\theta_{max} - \theta_{min})/2$ while the other symbols have their usual meaning.

In a second step multi-phonon corrections may be applied to the data.

a) MEPHOK:

In the first program the correction is done by a quotient method and numerical integration of the correction factor over all scattering angles. (This routine is based on a program used by Salgado /3/ ).

Starting from eq. (1) as a first approximation the incoherent double differential cross-section is calculated up to the eighth multiphonon term of the phonon expansion (e.g. /4/) for each detector and time-channel of the experiment. These spectra are summed up as was done with the experimental spectra. The correction factor C(E) then is the ratio of the experimental to the calculated sum-spectrum. The one-phonon term of the calculated sum-spectrum is multiplied by the correction factor and a second G(hω) is obtained using this new sum-spectrum $S_1$(E) instead of $S_o$(E) in eq. (1). This is the frequency distribution for the next iteration step.

b) MUPHOCOR:

In the second routine the integration of the cross-section over the range of scattering angles covered by the experiment is calculated analytically including the Debye-Waller-factor. The correction is done by substracting the calculated multi-phonon part of the spectrum from G(hω), which is normalized in each iteration step. Raw data, a weighted sum-spectrum, or a zeroeth G(hω) may be used as input. Compared to MEPHOC the iteration process converges faster in most cases.

The consistency of the two programs was tested with simulated and experimental spectra /5/. The results of the two methods are in excellent agreement.

References:

/1/ W. Abel, J.-B. Suck, KFK-Report 2187 (in press) (1975)

/2/ M. M. Bredov et al. Sov. Phys. Sol. State 9, 214 (1967)

/3/ J. Salgado, KFK-Report 1954 (1974)

/4/   V. F. Turchin, Israel Program for Scientific Translation Ltd.,
      Jerusalem, (1965)

/5/   J.-B. Suck, zur Mehrphononen Korrektur (unpublished) (1975)

## 4.3.    Computer Programs A7-FIT and HCPFIT

*W. Reichardt*

A7-FIT is a least squares fit program to determine the force constants
of a Born von Kármán model for the A7-structure from experimental phonon
frequencies of arbitrary wavevector. Up to the nineth neighbour either
axially symmetric or general forces can be assumed for each shell indivi-
dually. Beyond this limit only axially symmetric forces are possible.

The main problem with the use of such a general program concerns the
correct assignment of the measured frequencies to the six eigenvalues
of the dynamical matrix. So far no foolproof solution to this problem
has been found. By using various input code numbers for each q-value
the eigenvalues of the dynamical matrix are arranged in certain orders
and the input frequencies have to be arranged accordingly. Aspects
according to which this ordering is done are for instance: magnitude
of phonon frequencies - main direction of polarisation - magnitude of
the dynamical  structure factor.

Through minor modifications the program has been adapted to hcp-lattices
(program HCPFIT). In this case the choice between axially symmetric
and tensor forces is restricted to the five nearest neighbours.

## 4.4. Programm zur 3-dimensionalen Darstellung von Vektoren

*R. Moser*

Um das Magnetfeld einer spiralförmigen Spule anschaulich darstellen zu können, wurde ein Programm erstellt, das jeden Vektor $\vec{p}$ des Magnetfeldes auf die x, y-Ebene projiziert.

Die Spule soll zu induktiven $T_c$-Messungen benutzt werden. An Hand der Darstellung des Magnetfeldes soll bestimmt werden, welcher Bereich der Spule für die Messung ausgenutzt werden kann.

Die Aufpunkte der Vektoren waren in Polarkoordinaten $P(r_p, \phi)$, die Endpunkte in kartesischen Koordinaten $P_1(\xi, \eta, \zeta)$ bezüglich des Aufpunktes gegeben.

Das Programm rechnet zunächst unter Berücksichtigung eines gegebenen Blickwinkels $\beta$ die Polarkoordinaten in kartesische Koordinaten um:

$$P(r_p, \phi) \rightarrow P'(x', y') \text{ mit } x' = r_p \cdot \cos\phi, \; y' = r_p \cdot \sin\phi \cdot \cos\beta$$

Anschließend werden die Koordinaten des Endpunktes in x, y-Koordinaten bezüglich des Nullpunktes der Ebene konvertiert:

$$P_1(\xi, \eta, \zeta) \rightarrow P_1'(x_1', y_1') \text{ mit } x_1' = x' + \xi$$
$$y_1' = y' + \eta \cdot \cos\beta + \zeta \cdot \sin\beta$$

Jeder Vektor $\vec{p} = \overrightarrow{PP_1}$ des Magnetfeldes wird nun als Verbindungslinie $\overrightarrow{P'P_1}$ geplottet.
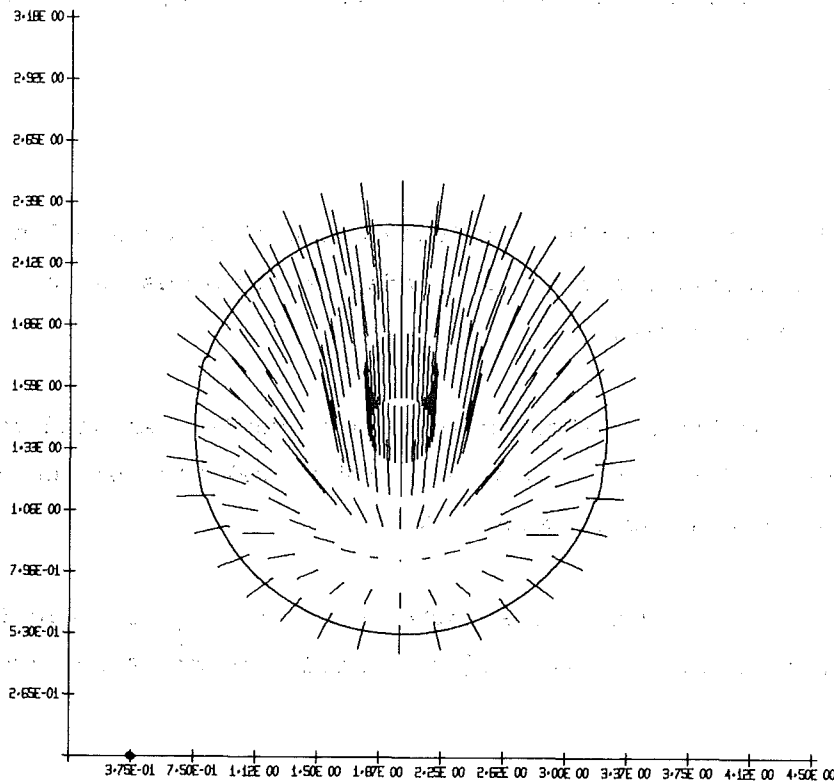
Fig. 1   Magnetfeld einer spiralförmigen Spule


## 4.5.   Zeichnungserstellung von Leiterbahnen für elektronische Schaltungen

*R. Moser*


Multiwire ist ein Verdrahtungskonzept, das es ermöglicht, schnell vom Entwurf ohne Umwege über eine Druckvorlage zu Fertigungsmustern zu gelangen. Da mit isoliertem Draht auf beschichtetes Basismaterial "geschrieben" wird, sind Leiter-Kreuzungen zulässig. Zur Herstellung von Multiwire-Schaltungen wird eine Rasterskizze bzw. eine Netzliste benötigt, aus der die Punkte hervorgehen, die miteinander verbunden werden sollen.

Zur Erstellung des Layout wurde ein Programm entwickelt, das für vorgesehene Anfangs- und Endpunkte die zugehörigen Leiterbahnenführungen sucht.

Das Programm arbeitet mit 2 Matrizen des Typs Integer·2. Die erste Matrix
dient zum Auffinden von möglichen Wegen, in die zweite werden die endgül-
tigen, gegebenenfalls abgekürzten Wege eingetragen. In der Ausgabe treten
nur die endgültigen Wege in Form einer Liste der Koordinaten von Anfangs-
und Endpunkten sowie aller Knickpunkte auf.

Zunächst wird geprüft, ob alle vorgesehenen Positionen für die ge-
wünschten IC-Gruppen frei sind.
Beim Aufsuchen der Verbindungslinien versucht das Programm, eine Linie
möglichst lang in eine Richtung zu ziehen. Bei einer Richtungsänderung
werden die Koordinaten des Knickpunktes festgehalten. Daraus ergibt sich
jeder Weg als eine Serie von Knickpunktkoordinaten. Wurde ein gültiger
Weg gefunden, so wird untersucht, ob dieser bezüglich der Knickpunkte
optimiert werden kann, Umwege werden durch Streichen überflüssiger
Koordinaten abgekürzt.

Die Koordinaten des endgültigen Weges werden punktweise geplottet und
durch gerade Linien verbunden. Außerdem wird eine Druckerliste mit allen
Knickpunkten erstellt. Des weiteren ist vorgesehen, die Liste der Koordi-
naten auf NC-Lochstreifen auszugeben.


4.6.    A Universal Microprogrammed Interface for "Spectra-"
        and "List"-Experiments with Memory-Switch for the NOVA2

        *G. Ehret and H. Hanak*


The 32 K memory limit of the minicomputers is a serious problem for multi-
detector multichannel experiments. Within this memory frame only 16 K -
20 K may be used for spectra totalization. More elaborate operating systems
further decrease the available space down to less than 5 K. This is often
untolerably small.

Commercially available memory switching units have an absolute upper limit
of 32 K, which was decided to be too small and too fixed. Therefore we had

to design a memory switch ourselves. This memory switch is able to have the program running in 32 K memory space and to assign automatically data buffer (including spectra totalization) in additional memory space. At present 64 K for data buffer is a threshold given by the 16 bit paths and the size of a computer frame. The memory switch is able implicitely to be shared by several data channel devices, like magnetic tape, display, digital input etc. The digital input may be working in list mode or in spectra (add "1") mode.

We decided to combine a digital interface plus memory switch on one standard 15 x 15 NOVA-card.

Optimizing in electronic components, microprogramming and pin assignment leads to the following interface for the experimenter:

a)  Spectra (add "1") Mode:

3 separate input each with its own hardware range checking. The number of inputs and their range limits are selectable by the software. Each input may have 16 bits. The size of the memory limits the total number of bits.

b)  List Mode:

96 data bits as input, selectable in various combinations of 16 and 32 bits by the software.

The two modes of operation are also selectable under program control and are mutually exclusive. One NOVA2 may house two different interface cards with full software support under BASIC.

4.7.  "Scaler" Experiments with a NOVA2 Computer

H. Hanak and G. Ehret

The central processing unit (CPU) of the NOVA2 Computer has been modified in order to install an additional mode of direct memory access (DMA). By reorganization and extension of the internal micro-program the CPU now

manages besides the three standard DMA-modes

1.  Input to memory
2.  Output from memory }          List mode

3.  Increment memory (add one)            Multichannelanalyser mode, an

additional DMA mode:

4.  Add to memory (add any 16 bit quantity)   Multicounter
                                              Multiscaler      } mode

This new mode allows the NOVA2 to be used in "counter" experiments. From
the point of view of data acquisition "counter" experiments are those ex-
periments whose counting rates are too high for the add-one mode. With
the new DMA-mode external precounters may be read-out with DMA-speed,
either periodically or triggered by an external signal.

4.8.        M I D A S  II  at  the  FR2  is  Working

G. Ehret, H. Hanak and H. Richelsen

The first stage of the new central data handling system MIDAS II   at
the reactor FR2 is operational. A NOVA2 system with 5 MByte disc space
has been coupled with the ASSTRO-System using the 4038 multicomputer-
communication-adapter. The software of the ASSTRO-NOVA-Computer has been
upgraded to a three-user-configuration. These users are the old CDC-MIDAS,
the RING-I/O-system and the new MIDAS II (Fig. 1). Depending on the
expected load of the system the operation program may be reconfigured
to run in an 8 K or 16 K memory environment.

The new MIDAS II is running under the REAL Time Disk Operation System
(RDOS) of Data General. User programming is done in the Extended
BASIC-Language with file capability. There exists on the discs one
common library read-accessible to all users, and several specific
libraries, one for each user. The libraries may be used for storing
programs and spectra.

Visualisation of the spectra directly read from the ASSTRO System or
evaluated during data reduction processes will be shortly possible
with TV-Display. The driver has been incorporated into RDOS.
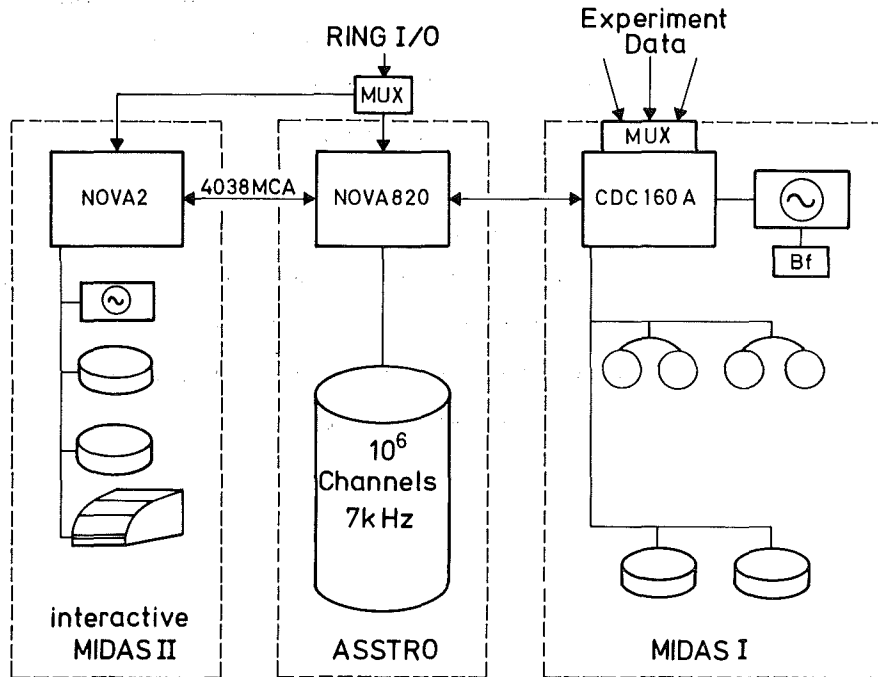


Fig. 1    MIDAS Configuration 1975

# 5. DEVELOPMENT OF MEASURING DEVICES AND TECHNIQUES

## 5.1. Steuereinheit für Spektrometer

*N. Nücker*

Für das Drehkristallspektrometer IN4 am HFR Grenoble und für zwei Dreiachsenspektrometer am FR2 Karlsruhe wurden Steuereinheiten zum Antrieb von Motoren, Auslesen von Kodierern, Zählern etc. erstellt. Bei allen drei Geräten waren ähnliche Voraussetzungen zu erfüllen: sie sollten zunächst ohne Rechner zum Einsatz kommen, aber bereits alle Elemente zum Rechneranschluß besitzen. Die Geräte enthalten:

1. Eingabeeinheit mit digitalen Vorwahlschaltern, Adressenabhandlung und einem Binär zu BCD Wandler für 16 bit Datenwörter von einem Rechner.

2. Bis zu 12 Schrittmotorantriebe. Alle Schrittmotore werden langsam angefahren, um ein Verschlucken von Schritten zu vermeiden. Bei Teilen mit großem Trägheitsmoment, wie z.B. einem Analysatorarm, werden die Schrittmotore außerdem vor dem Anhalten langsam abgebremst.

3. Positionsregister für die Drehgeber mit Codewandlern. Wir haben an die Schrittmotore Winkelgeber mit $3.6^{\circ}$ Auflösung angeflanscht und erzielen durch die nachfolgende mechanische Untersetzung eine Winkelauflösung von $0.01^{\circ}$.

4. Eine Phasenregelung für den phasenstarren Antrieb zweier Synchronmotore (nur für IN4) /1/.

5. 7-stellige Zähler, wovon einer mit Pulszahlvorwahl betrieben werden kann.

6. Multiplexer für den Anschluß externer Geräte, wie z.B. Digital-
   voltmeter und Leser von Endschalterstellungen.

7. Ausgabeneinheit mit Ziffernanzeige, Adressenabhandlung und einem
   BCD zu Binär-Wandler.

Die Leistungsstufen für die Schrittmotoransteuerungen befinden sich
mit dem dazu nötigen Netzteil (ca. 70 A bei 12 V) in einem gesonder-
ten Gehäuse. Um die Erwärmung der Schrittmotore gering zu halten,
werden sie mit geringerer Spannung versorgt,solange sie nicht laufen.

References

/1/ N. Nücker, Progress Report, KFK 2054, 92 (1974)

5.2.      F e r m i  -  C h o p p e r  f ü r  h o h e  D r e h z a h l e n

        *K. Weber*

Zur Untersuchung der elastisch diffusen Neutronenstreuung wurde ein
Fermi-Chopper mit relativ schlechter Zeitauflösung und kurzem Puls-
abstand benötigt, um den größten Teil der an der Probe unelastisch
gestreuten Neutronen sowie die in höherer Ordnung vom Monochromator
reflektierten Neutronen separieren zu können.

Die bisher von uns gebauten Chopper hatten eine höchstzulässige Dreh-
zahl von 15000 $min^{-1}$. Der weiterentwickelte Chopper (Abb. 1) läuft im
Dauerbetrieb mit 24000 $min^{-1}$. Dieses Ergebnis wurde durch folgende
Verbesserungen erreicht:

Rotor, Antriebsläufer, Stator und Lüfter sind nach dem Baukastenprin-
zip zusammengesteckt und verschraubt. Dadurch entsteht eine service-
freundliche Kompaktversion mit minimalen Bauteilen. Durch die Einsparung
von zwei Motorkugellagern, einer elastischen Kupplung und des motor-
eigenen Lüfters konnte die Verlustleistung sehr stark reduziert werden.
Aus diesem Grunde reichte auch die bisher verwendete Motoransteuerein-
heit mit 3 x 200 VA für diese hohen Drehzahlen aus.

Daten: Fermi-Chopper
_____

System:                    Mehrfachschlitzsystem mit geraden Schlitzen

eff. Strahlfläche:         Höhe 7,9 cm x Breite 3.97 cm = 31.4 cm$^2$

Kollimatoreinsatz:         34 beiseitig vernickelte und verkadmete $Al_{99.5}$-
                           Bleche mit Araldit zu einem Paket zusammenge-
                           klebt.

Kollimatorblechgröße:      Höhe 85 mm, Länge 9.12 mm, Dicke ges. 1.14 mm
                           (1 mm Al, 2 x 0.01 Ni, 2 x 0.06 Cd)

Winkeldivergenz:           6.5 $^{\circ}$

Pulshalbwertsbreite:       44.44 µs

Pulsabstand:               1.24 ms

Drehzahl:                  24 000 U/min

Rotordurchmesser:          7.5 cm

Rotorlänge:                10.5 cm

Rotormaterial:             St. 60, mit 0.4 mm starkem Gadoliniumblech aus-
                           gekleidet

Rotorlagerung:             je 1 Schleifspindel-Kugellager S 6002 Hg TB
                           und S 6004 HgTB, (Fa. Müller, Nürnberg)

Kugellagerölung:           Balgöler (Eigenbau)

Chopperantrieb:            An den Chopperrotor direkt angeschraubter Läufer
                           aus V2A mit der Hülse eines Elinco-Hysteresis-
                           Synchronmotors. Stator auf ein Polpaar umgewickelt.

Motoransteuereinheit:      3 Verstärker à 200 VA (Fa. Elgar)
                           Spannung 56 V, max. Motorstrom 3.6 A

Motorkühlung:              Durch angeflanschten Axiallüfter (Fa. Papst)

Motorkühlung

Hysteresis-Synchron-Motor

Stator

Läufer

Chopper Rotor

Kollimatoreinsatz

Neutronen Eingang

Neutronen Ausgang gepulst

Magn. Nullzeitgeber
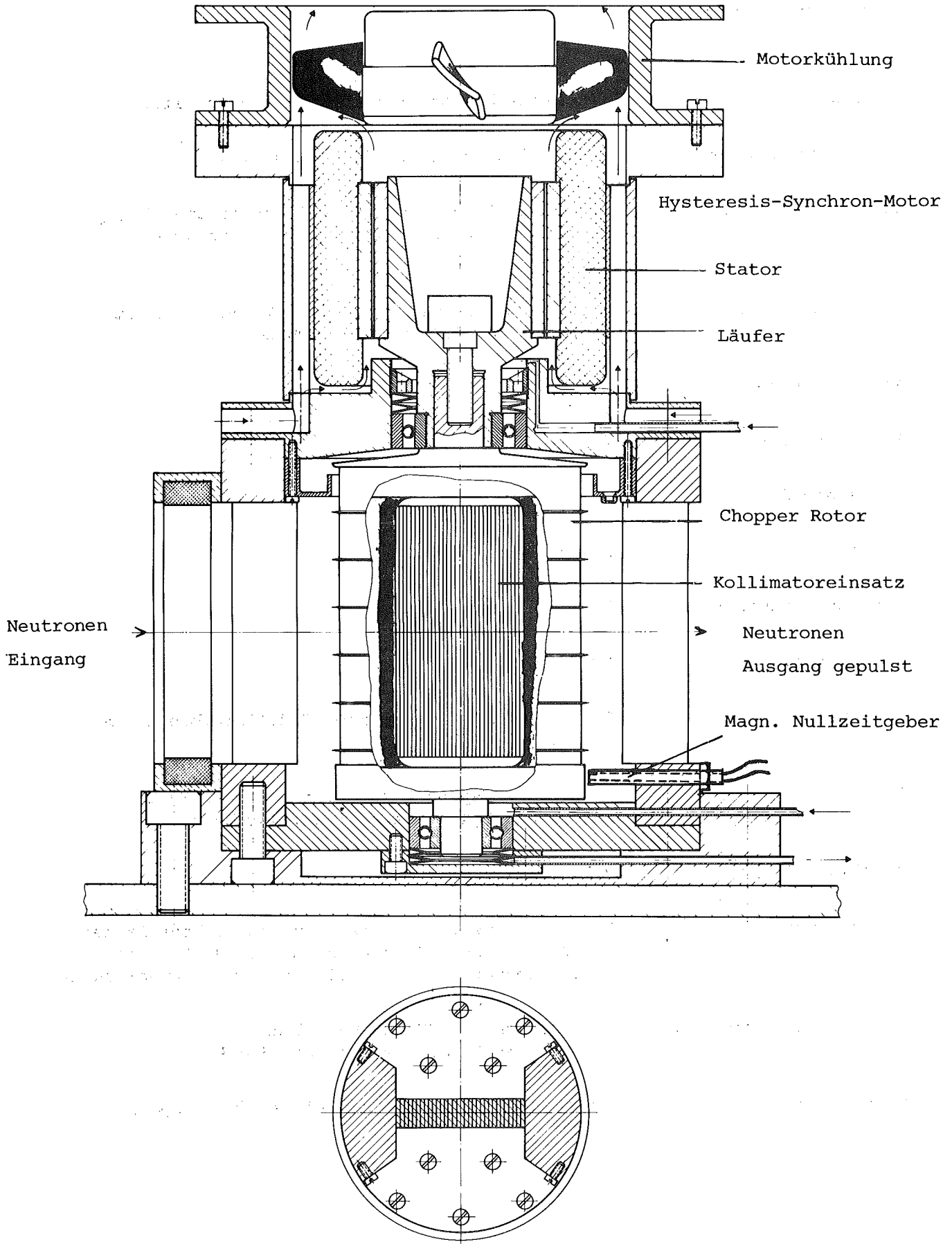
Fig. 1  Fermi-Chopper für hohe Drehzahlen

## 5.3.   Development of Electronic Implements

*H. Klann*

### Zero-Time trigger

This unit serves as a zero-time transmitter of signals from rotating crystals or choppers needed to   trigger time-of-flight units. Magnetic record playback heads and pick-up's are presently in use. They are used in a current source mode. First incoming signals are analysed with respect to their shape and sequence, then output pulses are generated after zero cross detection. Ripple and noise ratio may rise up to 0.5 of the signal. It is also possible to use photo-diodes and -transistors instead of magnetic pick-up's. Then the treshold is automatically set at half the hight of the signal.

### Trigger doubler

This unit generates a second trigger pulse with a phase displacement angle of 180 $^{\circ}$. It is used for choppers or rotating crystals producing two bursts of neutrons per one magnetic pick-up signal. The resolution error is 100 ns. This device is also suitable for all those applications in which frequency doubling up to 5 Mc is desired.

## 5.4.   Kleingoniometer

*K. Weber*

Messungen  der Phononendispersion scheitern of an zu kleinen Einkristall-proben. Es wurde daher ein Gerät benötigt, das es ermöglicht, mehrere kleine Einkristalle zu einer für die Messung notwendigen Probengröße zu-sammenzusetzen. Hierbei wird die Forderung gestellt, daß jeder Kristall individuell über zwei Kippbewegungen und eine Drehbewegung genau justier-bar ist.

Bei der hier beschriebenen Vorrichtung werden die Kippbewegungen durch Kleingoniometer realisiert, die durch Kugellager spielfrei an einer Grundplatte befestigt sind (Abb. 1). Diese Grundplatte wird auf einen großen Goniometerkopf aufgesetzt, mit dem der zentrale Kristall justiert werden kann. Das Kleingoniometer besteht aus zwei um 90 $^{\circ}$ verdreht übereinandergesetzten Kippeinrichtungen mit je ± 5 $^{\circ}$ Kippbereich. Zusätzliche Kreuztische ermöglichen eine optimale Probenplazierung.
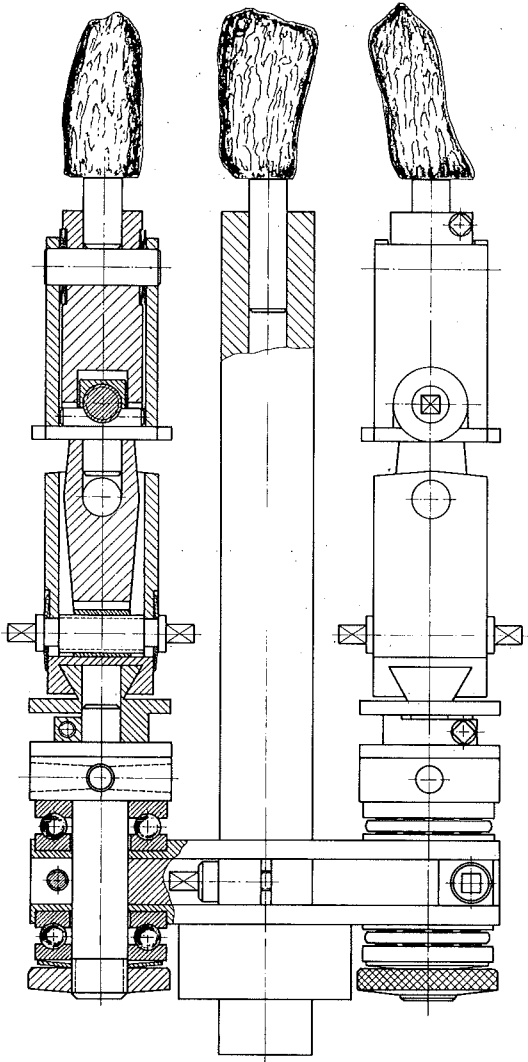


Fig. 1  Kleingoniometer
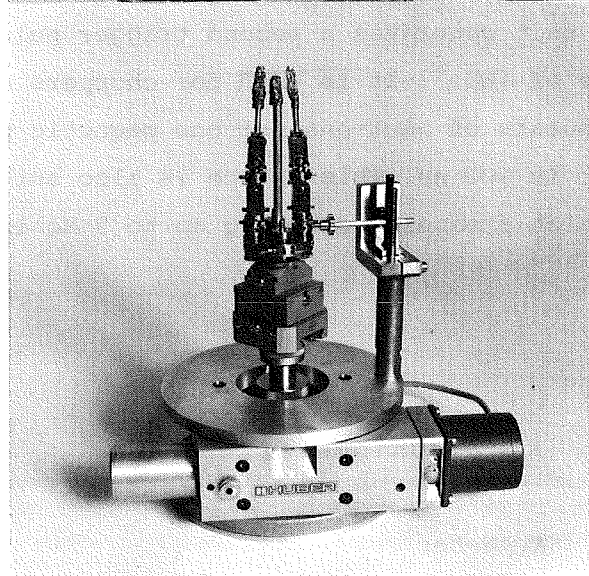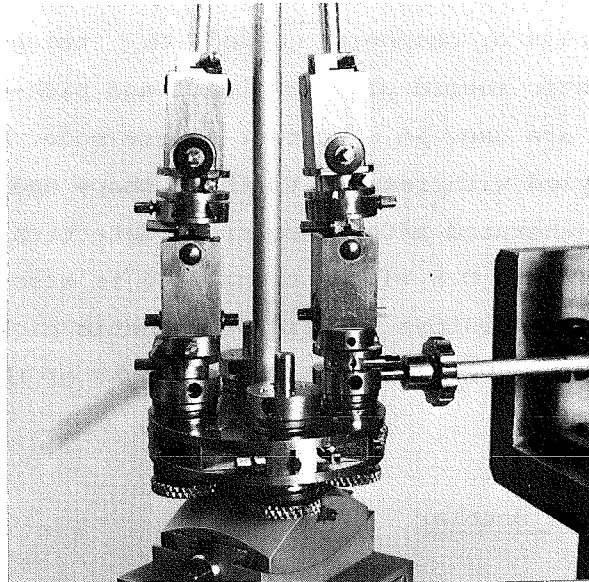
Fig. 2 a, b  Kleingoniometer mit Drehtisch

Die Drehbewegung wird von einem Präzisionsdrehtisch (Genauigkeit 1/100 Grad) durch eine Mitnahmestange auf das Kleingoniometer übertragen (Abb. 2a und b). Nach der Justierung wird das Kleingoniometer durch eine Klemmvorrichtung an der Grundplatte arretiert und die Mitnahmestange entfernt.

Da die Meßprobleme sehr unterschiedlich sind, wurde auf große Variations-
möglichkeit des Gerätes geachtet (Baukastenprinzip). Die in den Abbildungen
gezeigte Version gestattet die unabhängige Justierung von maximal 5 Kristallen.


## 5.5 Einsatz eines CLOSED CYCLE REFRIGERATORS für Neutronen-beugungsmessungen an Einkristallen bei tiefen Temperaturen

*G. Heger*

*S. Massing, RBT/FR2*

Um bei tiefen Temperaturen Neutronenbeugungsmessungen an Einkristallen durch-
führen zu können, wurde ein Displex Split-Cycle Refrigerator (Modell CS-1003)
/1/ in die große Eulerwiege (Innen-⌀ 56 cm) des Vierkreisdiffraktometers
P32/FR2 eingebaut (Abb. 1). Es wurde gezeigt, daß bei diesen kalten Messungen
der zu untersuchende Kristall alle Orientierungen einnehmen kann; seine Küh-
lung ist unabhängig von den verschiedenen Orientierungen gewährleistet. Es
wurde eine minimale Temperatur von 31 ± 1 K erreicht. Der problemlose Langzeit-
einsatz des Kühlsystems konnte bisher durch drei komplette Strukturbestimmungen
gezeigt werden ($K_2 | Pt(CN)_4 | Br_{.3} \cdot 3D_2O$ bei 31.5 und 73.5 K und $(CH_3NH_3)_2MnCl_4$ bei 190 K).

References

/1/ Fa. Air-Products and Chemicals, Deutsche Vertretung: H. Erben GmbH, Düsseldorf
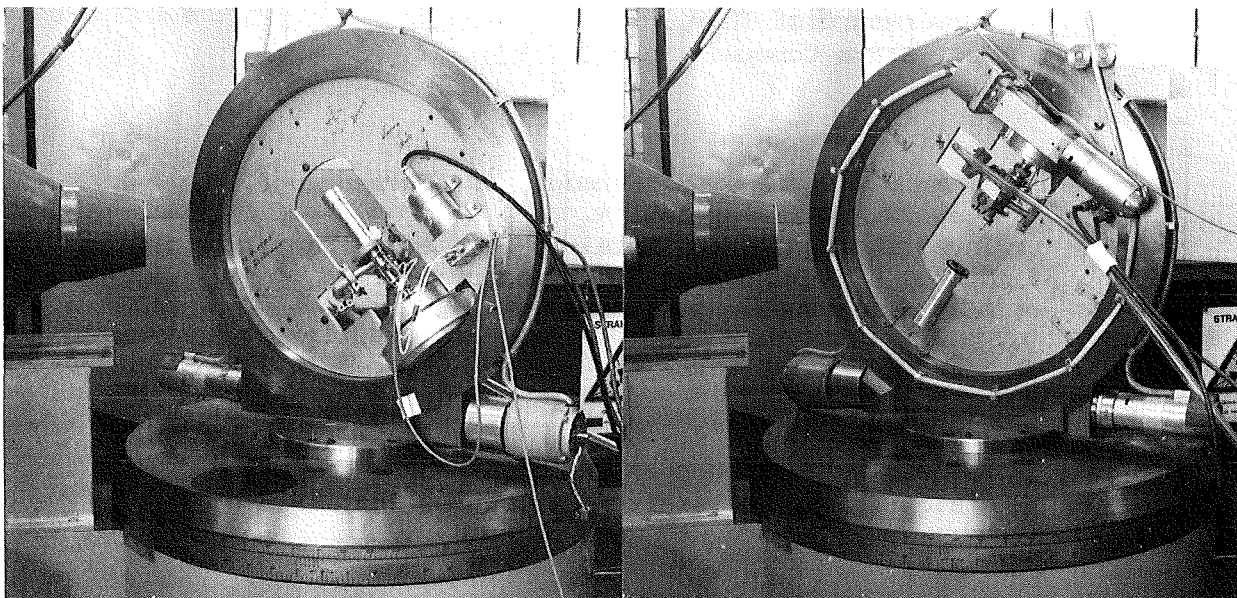


Abb. 1  Vierkreisdiffraktometer P32:FR2 mit eingebautem Kühlsystem

(a) Ansicht des betriebsbereiten Aufbaus  Diffraktometerwinkel: $\omega_a$; $\chi_a$; $\rho_a$

(b) Ansicht mit geöffnetem Probenraum
Diffraktometerwinkel: $\omega_b \cong \omega_a + 180°$; $\chi_b \cong \chi_a + 90°$; $\rho_b \cong \rho_a$

# 6. PUBLICATIONS, CONFERENCE CONTRIBUTIONS AND SEMINARS

## 6.1. PUBLICATIONS

*Block, R.; Schommers, W.*
Triplet Correlations in Disordered Systems: A Study
for Liquid Rubidium
J. Phys. C8, 1997 (1975

*Comés, R.; Renker, B.; Pintschovius, L.;*
*Currat, R.; Gläser, W.; Scheiber, G.*
Inelastic Neutron Scattering Study of the $2k_F$
Instability in $K_2Pt(CN)_4Br_{.30} - x\ D_2O$
Phys. Stat. Sol. (b) 71, Sept. 1, (1975)

*Czjzek, G.; Fink, J.; Schmidt, H.; Krill, G.;*
*Gautier, F.; Lapierre, M.F.; Robert, C.*
Investigation of Magnetic Structures and Phase
Transitions in $NiS_2$ by $^{61}$Ni-Mössbauer Spectroscopy
Journal de Phys. 35 C6, 603 (1974)

*Dietrich, M.; Grey, W.; Rietschel, H.; Satterthwaite, C.B.*
Pressure Dependence of the Superconducting Transition
Temperature of $Th_4H_{15}$
Sol. State Commun. 15, 941 (1974)

*Fink, J.; Czjzek, G.; Schmidt, H.; Ruebenbauer, K.;*
*Coey, J.M.D.; Brusetti, R.*
Investigation of the Metal-to-Semimetal Transition in
NiS by $^{61}$Ni-Mössbauer Spectroscopy
Journal de Phys. 35 C6, 681 (1974)

*Geerk, J.*
Tunneluntersuchungen an supraleitenden Niobkarbid
Dissertation, Universität Karlsruhe, Juni 1975

*Gautier, F.; Krill, G.; Lapierre, M.F.; Panissod, P.;*
*Robert, C.; Czjzek, G.; Fink, J.; Schmidt, H.*
Existence of an Antiferromagnetic Metallic Phase (AFM)
in the $NiS_{2-x}Se_x$ System with Pyrite Structure
Phys. Lett. 53A, 31 (1975)

*Heger, G.; Renker, B.; Deiseroth, H.J.; Schulz, M.; Scheiber, G.*
On the Water Distribution in $K_2(Pt(CN)_4)Br_{.3} \cdot 3D_2O$. A Single
Crystal Neutron Diffraction Structure Analysis
Mat. Res. Bull. <u>10</u>, 217 (1975)


*Hellner, E.; Heger, G.; Mullen, D.; Treutmann, W.*
On the Crystal Structures of the Intermetallic System
$Cr_{1+\delta}Sb$ - $Fe_{1+\delta}Sb$: A Combined Single Crystal X-Ray and
Neutron Diffraction Study
Mat. Res. Bull. <u>10</u>, 91 (1975)


*Knorr, K.; Jahn, I.R.; Heger, G.*
Birefrigence, X-Ray and Neutron Diffraction Measurements
on the Structural Phase Transitions of $(CH_3NH_3)_2MnCl_4$ and
$(CH_3NH_3)_2FeCl_4$
Sol. State Commun. <u>15</u>, 231 (1974)


*Linker, G.; Meyer, O.*
The Influence of Heavy Ion- Bombardment on the Superconducting
Transition Temperature in Thin Films in Ion Implantation in
Semiconductors
S. Namba, ed. Plenum Press, New York  1975


*Mehringer, W.*
Model Calculation of Dispersion of Phonon-Like Excitations
in Liquid Argon
Phys. Lett. <u>49A</u>, 27 (1974)


*Mehringer, W.*
An Approach by Classical Statistics to the Dynamics of
Atomic Motion in Solids
Phys. Lett. <u>53A</u>, 197 (1975)


*Meyer, O.*
Enhancement of the Superconducting Transition Temperature
by Ion Implantation in Aluminium
S. Namba ed. Plenum Press, New York (1975)


*Meyer, O.*
Enhancement of the Superconducting Transition Temperature
by Ion Implantation
J. Japan. Soc. of Appl. Phys. <u>44</u> (Suppl.), 23 (1975)

Pintschovius, L.; Geserich, H.P.; Möller, W.
Optical Reflectivity of $(SN)_x$ - Single Crystals
Solid State Commun. 17, 477 (1975)


Renker, B.; Comès, R.
X-Ray and Neutron Diffraction Studies of the
Peierls Instability
Low Dimensional Cooperative Phenomena, Nato
Advanced Study Institutes, Ser. B7, Physics, P. 235


Renker, B.; Pintschovius, L.; Gläser. W.; Rietschel, H.;
Comès, R.
Neutron Scattering Studies of Lattice Dynamics and
Structural Changes in the One-Dimensional Conductor
$K_2Pt(CH)_4Br_{.3} \cdot 3D_2O$
Lecture Notes in Phys. 34, One Dimensional Conductors p. 53


Rieder, K.M.; Migoni, R.; Renker, B.
Lattice Dynamics of Strontium Oxide
Phys. Rev., in press


Rietschel, H.
Electron-Optical Phonon Coupling in Superconductors
Zeitschrift für Physik., in press


Schommers, W.
The Velocity Autocorrelation Function and the Effect
of the Long-Range Interaction in Liquid Rubidium
Solid State Commun. 16, 45 (1975)

## 6.2. CONFERENCE CONTRIBUTIONS AND SEMINARS

*Blanckenhagen, P. von; Platen, Chr. von*
Nahordnung in ungeordneten ferromagnetischen
Ni-Mn-Legierungen
Verhandlungen der DPG (VI) <u>10</u>, 486 (1975)


*Blanckenhagen, P. von; Platen, Chr. von;*
*Happel, H.; Knorr, K.*
Inelastische Neutronenstreuung zur Kristallfeld-
spektroskopie an $ErAl_2$ im paramagnetischen Bereich
Verhandlungen der DPG (VI) <u>10</u>, 634 (1975)


*Block, R.; Schommers, W.*
Untersuchungen zu den Dreiteilchenortskorrelationen
in flüssigem Rubidium
Verhandlungen der DPG (VI) <u>10</u>, 499 (1975)


*Czjzek, G.; Fink, J.; Schmidt, H.; Krill, G.;*
*Lapierre, M.F.; Robert, C.; Gautier, F.*
Untersuchung von $NiS_2$ mit Hilfe der Mössbauer-
spektroskopie an $^{61}Ni$
Verhandlungen der DPG (VI) <u>10</u>, 473 (1975)


*Deiseroth, H.J.; Schulz, H.; Heger, G.; Renker, B.*
Ordnung und Unordnung in der Kristallstruktur von
KCP $(K_2Pt(CH)_4 Br(O.3) \cdot 3H_2O)$
Verhandlungen der DPG (VI) <u>10</u>, 355 (1975)


*Ehret, G.*
Applications of Digital Computers in Physical Experiments
and Process Control at Karlsruhe
Pakistani Institute of Nuclear Science on Technology,
Oktober 1974


*Geller, R.; Heger, G.;*
Untersuchung der magnetischen Eigenschaften des Weberits
$Na_2NiFeF_7$ mit Mößbauereffekt, Neutronenbeugung und Sus-
zeptibilitätsmessungen
15. Diskussionstagung der Arbeitsgemeinschaft Kristallo-
graphie, Erlangen, September 1974

*Gompf, F.; Geerk, J.; Reichardt, W.*
Vergleich der Phononenzustandsdichte und Tunneldichte
von Niobkarbid
Verhandlungen der DPG (VI) 10, 616 (1975)


*Heger, G.; Fink, J.; Czjzek, G.;  Schmidt, H.;*
*Morariu, M.; Geller, R.*
Magnetische Untersuchungen an Weberiten
Verhandlungen der DPG (VI) 10, 470 (1975)


*Hofmann, B.*
Phonondispersion in Wismut-Antimon Legierungen
Verhandlungen der DPG (VI) 10, 648 (1975)


*Hofmann-Kraeft, B.; Meyer, O.*
Herstellung und Untersuchung gesputterter VN-Schichten
Verhandlungen der DPG (VI) 10, 648 (1975)


*Linker, G.*
Einfluß von Strahlenschäden auf die supraleitende Über-
gangstemperatur dünner V-, Nb- und Ta-Schichten
Verhandlungen der DPG (VI) 10, 639 (1975)


*Linker, G.; Meyer, O.*
The Influence of Heavy Ion Bombardment on the Supercon-
ducting Transition Temperature of Thin Films
4. Internat. Conf. on Ionimplantation in Semiconductors
and other Materials, Osaka, August 1974


*Meyer, O.*
Enhancement of the Superconducting Transition Temperature
by Ion Implantation in Aluminium Thin Films
4. Internat. Conf. on Ionimplantation in Semiconductors
and other Materials, Osaka, August 1974


*Meyer, O.; Phrilingos, E.*
$T_c$-Enhancement by Ion Implantation in Molybdenum and
Aluminium Layers
4. Internat. Conf. on Ionimplantation in Semiconductors
and other Materials, Osaka, August 1974

*Meyer, O.; Phrilingos, E.;*
Änderung der supraleitenden Übergangstemperatur durch
Ionenimplantation in Molybdän-Schichten
Verhandlungen der DPG (VI) 10, 633 (1975)


*Meyer, O.*
Analysis of Superconducting Thin Films
Ion Beam Anaysis of Near Surface
Regions, Catania, Juni 1974


*Pintschovius, L.; Renker, B.*
Temperature Dependence of the Giant Kohn Anomaly in
the One-Dimensional Conductor KCP
Symposium on Low Dimensional Cooperative Phenomena and
the Possibility of High-Temperature Superconductivity,
Starnberg, September 1974


*Reichardt, W.*
Untersuchungen zur Dynamik von Festkörpern und
Flüssigkeiten am Karlsruher Reaktor FR2
Physikalisches Kolloquium, Universität Frankfurt, Juni 1974


*Reichardt, W.; Wagner, V.; Kress, W.*
Gitterschwingungen in NiO
Verhandlungen der DPG (VI) 10, 393 (1975)


*Reichardt, W.*
Arbeiten zur Gitterdynamik in Karlsruhe
Arbeitstreffen des Verbands Nukleare Festkörperforschung,
Königstein, Januar 1975


*Renker, B.*
Elektronische Eigenschaften von 1D-Systemen
Inst. für Kernphysik der Universität Frankfurt, Juni 1974


*Renker, B.*
Kohn-Anomalien
Spezielle Phononen, Inst. für Kernphysik der Universität
Frankfurt, Sommerschule Riezlern, August 1974

Renker, B.; Pintschovius, L.; Gläser, W.
Untersuchung zur Temperaturabhängigkeit der Gitter-
dynamik von $K_2Pt(CN_4)Br_3 \cdot 3D_2O$ im Bereich der
$2k_F$ - Anomlie
Verhandlungen der DPG (VI) 10, 618 (1975)


Schweiss, P.; Schneider, E.; Nücker, N.; Reichardt, W.
Temperaturabhängigkeit der Phononenzustandsdichten
einiger A-15-Verbindungen
Verhandlungen der DPG (VI) 10, 615 (1975)


Suck, J.-B.
Frequency Moments of Liquid Rubidium
Workshop on Liquid Dynamics, Grenoble, March 11-12,
1975


Suck, J-B.
Frequenzmomente und Hochfrequenzdispersion in
flüssigem Rubidium
Verhandlungen der DPG (VI) 10, 499 (1975)

7.  L I S T   O F   T H E   N E U T R O N   S P E C T R O-
    M E T E R S   A T   T H E   F R 2   A T   K A R L S R U H E


DIF 1 :        Four circle diffractometer, $\lambda = 1.035$ Å

DIF 2 :        Two circle diffractometer, $1$ Å $\leq \lambda < 2.6$ Å

DIF 3 :        Powder diffractometer, $\lambda = 1.28$ Å or $1.09$ Å

DIF 4 :        Two circle diffractometer, $\lambda \geq 4$ Å (cold neutrons)


TAS 1 :        Three-axis spectrometer, $13$ meV $\leq E_o \leq 120$ meV

TAS 2 :        Three-axis spectrometer,  $8$ meV $\leq E_o < 65$ meV


TOF 1 :        Time of-flight spectrometer with Fermi-Chopper,
               100 detectors, thermal neutrons

TOF 2 :        Time of-flight spectrometer with rotating crystal,
               100 detectors, cold neutrons

TOF 3 :        Time of-flight spectrometer with Fermi-Chopper,
               10 detectors, thermal neutrons

TOF 4 :        Time of-flight spectrometer with rotating crystal.
               6 detectors, cold neutrons


MAG 1 :        Spectrometer for diffuse scattering, 20 detectors,
               thermal neutrons

MAG 2 :        Multipurpose spectrometer, 20 detectors, cold
               neutrons.

# 8. STAFF MEMBERS

Head of Institute: Prof. Dr. W. Gläser[+]

## Professional Staff

| | | |
|---|---|---|
| Blanckenhagen, P. von | Mehringer, W. | Schneider, E. |
| Czjzek, G. | Meyer, O. | Schmidt, H. |
| Fink, J. | Nücker, N. | Schommers, W. |
| Geerk, J. | Pintschovius, L. | Schweiß, P. |
| Gompf, F. | Reichardt, W. | Suck, J.-B. |
| Heger, G. | Renker, B. | |
| Linker, G. | Rietschel, H. | |

## Technical Staff

| | | | |
|---|---|---|---|
| Abel, W.[++] | Klann, H. | Richelsen, H.[++] | Weber, K. |
| Ehret, G.[++] | Kraatz, M. | Scheerer, B. | |
| Hanak, H.[++] | Ratzel, F. | Smithey, R. | |

## Visiting Scientiests

Chakupurakal, T. India

Ruebenbauer, K., Guest from Institute of Physics, Krakow

## Research Students

Block, R., Universität Karlsruhe

Hofmann, B., Universität Karlsruhe

Hofmann-Kraeft, B., Universität Karlsruhe

Langguth, K.-G.,Universität Karlsruhe

Ziemann, P., Universität Karlsruhe

[+] now at Universität Munich

[++] Member of infrastructure